Investigations into the antiviral activities and functions of the *Aedes aegypti* Ago2 protein

Krittika Dummunee, BSc. MSc.

xxxxxxxx

Submitted in fulfilment of the requirements for the Degree of
Doctor of Philosophy in Virology

School of Infection and Immunity
College of Medical, Veterinary and Life Sciences
University of Glasgow

Abstract

Arboviruses represent a significant and growing threat to global public health, causing diseases such as dengue, chikungunya, and Zika. These viruses are transmitted by arthropod vectors, primarily mosquitoes, which support viral replication while remaining largely asymptomatic. A key determinant of this ability is the insect antiviral immune system, particularly RNA interference (RNAi). The exogenous small interfering RNA (exo-siRNA) pathway represents the primary antiviral defence mechanism in insects, recognising viral double-stranded RNA intermediates generated during replication and directing sequence-specific degradation of viral RNA. Central to this process is Argonaute-2 (Ago2), the catalytic component of the RNA-induced silencing complex (RISC), which uses virus-derived small interfering RNAs (vsiRNAs) to guide cleavage of complementary viral RNA targets. While the antiviral role of RNAi has been extensively characterised in *Drosophila melanogaster*, the molecular mechanisms governing Ago2-mediated antiviral defence in mosquito vectors remain incompletely understood.

This thesis aimed to investigate the role of Ago2 catalytic activity in antiviral RNAi and to identify host proteins that interact with Ago2 and may influence antiviral responses in mosquito cells. Using *Aedes aegypti*–derived cell lines, including an Ago2 knockout line (AF525) and RNAi-competent AF5 cells, a series of molecular and virological approaches were employed to dissect the contribution of Ago2 to antiviral defence against Semliki Forest virus (SFV), a model alphavirus. Recombinant cell lines expressing either wild-type Ago2 or catalytic mutants targeting the conserved PIWI-domain catalytic tetrad were generated to assess the requirement of Ago2 slicing activity during infection.

Functional analyses demonstrated that mutation of the Ago2 catalytic tetrad significantly impaired antiviral RNAi activity, resulting in enhanced viral replication compared with cells expressing wild-type Ago2. These findings confirm that Ago2 endonucleolytic activity is essential for efficient suppression of SFV replication and highlight the importance of RISC-mediated cleavage of viral RNA in antiviral defence. The results further support a model in which Dicer-2-mediated production of vsiRNAs alone is insufficient to control viral infection, and that effective antiviral activity requires functional Ago2-mediated target cleavage.

To further explore the regulation of Ago2 activity, immunoprecipitation coupled with mass spectrometry was used to identify proteins associated with Ago2 in mosquito cells under both infected and uninfected conditions. This analysis revealed a diverse Ago2 interactome containing RNA-binding proteins, RNA processing factors, and proteins of previously unknown function. Functional screening of selected candidate interactors identified the DEAD-box RNA helicase AAEL014414-PA (AAIP12) as a potential antiviral factor. Knockdown of AAIP12 resulted in increased viral replication, suggesting that this helicase contributes to host antiviral defence, potentially through modulation of RNA metabolism or RNAi-related processes.

Together, the findings presented in this thesis provide new insight into the molecular mechanisms underlying Ago2-mediated antiviral immunity in mosquito cells. By demonstrating the importance of Ago2 catalytic activity and identifying candidate host factors associated with Ago2 function, this work advances current understanding of RNAi-based antiviral defence in mosquito vectors. These findings contribute to a broader understanding of virus–vector interactions and provide a foundation for future studies exploring how host RNA regulatory pathways influence arbovirus replication and transmission.

Table of Contents

List of Tables

List of Figures

Acknowledgements

First of all, I would like to thank my supervisor, Dr. Benjamin Brennan. I truly appreciate your constant support and incredible patience throughout this journey. It has been a sincere pleasure being a part of your research group. To my secondary supervisor, Dr. Melanie McFarlane, thank you for your dedicated guidance in the lab. I have always felt your genuine care and kindness, and I am deeply grateful for everything you have done for me.

I also want to express my gratitude to Prof. Alain Kohl, my former supervisor. Thank you for supporting me from my very first year until now. I am deeply grateful for your constant motivation and support. Your guidance and insightful advice were essential in helping me navigate this journey and successfully complete my thesis.

To the Brennan Group, the former Kohl Group and the Pondeville group (Igor, Rose, Selim, Andy, Alex, Alma, Marine, Mazigh, Kelsey, James, David, Emilie and JP) thank you all for the scientific discussions and the great chats in the office. I especially appreciate the tips and suggestions you shared during my lab presentations. To people on HWB L3 and L4, Yubing, Divya, Ju Eun, Zulma, Jocelyn, Alice, Laura, and Mihah, a big thank you for the great times we shared when I first joined the CVR. To Thai people in the CVR, Palm and Aeh, I am so glad to have met you here and have had such wonderful conversations with you.

To my Thai friends in Glasgow, Taow, my bestie and flatmate; I am so happy we met. It is not easy to find someone so similar to myself who understands me so well. I will never forget all the fun things we did together. To the people I came to consider family here at the Thai restaurants, Thai Siam and Ting Thai: Ann, Lek, Yai, Nim, Sin, Fon, and Eve, thank you for being my ‘home away from home’ and for always providing such a warm environment. You made my time here special.

To my family (Mum, Dad, Grandpa, and Grandmas), I am so grateful to you for your loving encouragement. Your words always uplifted me during the difficult times. To my wonderful twin sister, Krittiya, I am always amazed by how you seem to know exactly when I am not okay. Even without knowing the details, your messages always came at the right time to give me the best advice and help me relax. To my

husband, Wuttisak, thank you for making our long-distance relationship seem easy. Thank you for always being by my side and understanding me so deeply.

Finally, I would like to thank my sponsor, the Ministry of Higher Education, Science, Research and Innovation (Royal Thai Government Scholarship), for their support and guidance throughout my PhD. I also want to thank my home institute, Princess of Naradhiwas University, for allowing me to take this next step in my career. I am truly thankful for the incredible opportunity to gain such life-changing experiences in the UK and across Europe.

Khob Khun Ka.

Author's Declaration

I, Krittika Dummunee, declare that, except where reference is made to the contribution of others, that this thesis is the result of my own work and has not been submitted for any other degree at the University of Glasgow or any other institution.

Printed Name: KRITTIKA DUMMUNEE

Signature:

Publications

The following first author publications have arisen from the works contained within this thesis:

1. Dummunee K, Parry RH, Redecke L, Varjak M, Brennan B, Kohl A, McFarlane M.
   The catalytic tetrad of Aedes aegypti argonaute 2 is critical for the antiviral activity of the exogenous siRNA pathway.
   J Biol Chem. 2025 Apr;301(4):108332.
   DOI: 10.1016/j.jbc.2025.108332.

Author contributions

Writing–review & editing: R. H. P., L. R., M. V., B. B., A. K., M. M., and K. D.
Writing–original draft: R. H. P., L. R., M. V., B. B., A. K., M. M., and K. D.
Visualisation: R. H. P., L. R., M. M., and K. D.
Validation: R. H. P., L. R., M. M., and K. D.
Methodology: R. H. P., L. R., M. V., A. K., M. M., and K. D.
Investigation: R. H. P., L. R., M. M., and K. D.
(The AlphaFold3 prediction and structural analysis of *Ae. aegypti* Ago2wt, including the DEDH catalytic domain and associated residues, was performed by Prof. Lars Redecke and is therefore outside the scope of this thesis.)
Formal analysis: R. H. P., L. R., M. M., and K. D.
Data curation: R. H. P., B. B., A. K., M. M., and K. D.
Conceptualisation: R. H. P., B. B., A. K., M. M., and K. D.
Resources: M. V., B. B., and A. K.
Supervision: A. K. and M. M.
Project administration: A. K. and M. M.
Funding acquisition: A. K. and K. D.

Definitions/Abbreviations

Abbreviation	Definition
AAIP12	*Aedes aegypti* interacting protein 12 (AAEL014414-PA)
Aag2	*Aedes aegypti* cell line
AF5	RNAi-competent *Aedes aegypti* cell line derived from Aag2
AF525	Ago2 knockout *Aedes aegypti* cell line derived from AF5
Ago	Argonaute protein
Ago1	Argonaute-1
Ago2	Argonaute-2
Ago3	Argonaute-3
Amp	Ampicillin
Ars2	Arsenic resistance protein 2
ATP	Adenosine triphosphate
Aub	Aubergine protein
BHK-21	Baby hamster kidney cells (clone 21)
bp	Base pairs
C3PO	Component 3 Promoter of RISC
Cas9	CRISPR-associated protein 9
CRISPR	Clustered regularly interspaced short palindromic repeats
CPE	Cytopathic effect
Dcr	Dicer
Dcr1	Dicer-1
Dcr2	Dicer-2
DDA	Data-dependent acquisition
DEAD	Asp-Glu-Ala-Asp helicase motif
DEDH	Asp-Glu-Asp-His catalytic tetrad
DExD/H	Asp-Glu-any-Asp/His helicase domain
DH5α	*Escherichia coli* cloning strain
DIA	Data-independent acquisition
DNA	Deoxyribonucleic acid
dsRNA	Double-stranded RNA
dFXR	*Drosophila* fragile X mental retardation protein
eGFP	Enhanced green fluorescent protein
exo-siRNA	Exogenous small interfering RNA
FBS	Foetal bovine serum
FFLuc	Firefly luciferase
GMEM	Glasgow modified Eagle’s medium
h.p.i.	Hours post infection

h.p.t.	Hours post transfection
Hsp90	Heat shock protein 90
IP	Immunoprecipitation
LB	Luria-Bertani medium
LFQ	Label-free quantification
L-15	Leibovitz's L-15 medium
MID	Middle domain of Argonaute proteins
miRNA	MicroRNA
miRISC	microRNA-induced silencing complex
MOI	Multiplicity of infection
mRNA	Messenger RNA
nLC-MS/MS	Nano-liquid chromatography tandem mass spectrometry
NP-40	Nonidet P-40 detergent
nt	Nucleotides
PAZ	PIWI–Argonaute–Zwille domain
PAMP	Pathogen-associated molecular pattern
PBS	Phosphate buffered saline
PBS-T	Phosphate buffered saline with Tween-20
PCR	Polymerase chain reaction
PFU	Plaque forming units
PIWI	P-element induced wimpy testis protein family
piRNA	PIWI-interacting RNA
PRR	Pattern recognition receptor
qPCR	Quantitative polymerase chain reaction
R2D2	Double-stranded RNA binding protein cofactor of Dcr2
RISC	RNA-induced silencing complex
RNA	Ribonucleic acid
RNAi	RNA interference
RLuc	*Renilla* luciferase
RT	Reverse transcription
RT-qPCR	Reverse transcription quantitative PCR
SDS	Sodium dodecyl sulphate
siRNA	Small interfering RNA
siRISC	siRNA-induced silencing complex
SFV	Semliki Forest virus
SOC	Super optimal broth with catabolite repression
SP3	Single-pot solid-phase enhanced sample preparation
TE	Transposable element
TEAB	Triethylammonium bicarbonate
TPB	Tryptose phosphate broth
UV	Ultraviolet
VIG	Vasa intronic gene

vsiRNA	Virus-derived small interfering RNA
vpiRNA	Virus-derived PIWI-interacting RNA
WT	Wild type

Chapter 1:
General Introduction

Chapter 1 General Introduction

1.1 Arboviruses

1.1.1 Overview

Arboviruses are viruses transmitted by blood-feeding arthropods such as mosquitoes, ticks, midges, and sandflies. Transmission occurs when infected vectors take a blood meal from susceptible vertebrate hosts. A defining feature of arboviruses is their ability to replicate in both vertebrate and invertebrate hosts, requiring them to overcome distinct cellular environments and immune responses in each to maintain their transmission cycle.

Arboviruses are responsible for a substantial global burden of infectious disease, causing a range of clinical manifestations including encephalitis, haemorrhagic fever, and acute febrile illness (Weaver and Reisen, 2010, Blair, 2011, Weaver *et al.*, 2018, Pierson and Diamond, 2020, Varjak *et al.*, 2020). Several arboviral families contain medically important pathogens, including members of the *Flaviviridae*, *Togaviridae*, and the order Bunyavirales. Notable examples include dengue virus (DENV), Zika virus (ZIKV), and yellow fever virus (YFV) within the *Flaviviridae*; chikungunya virus (CHIKV) within the *Togaviridae*; and viruses such as Rift Valley fever virus and Crimean–Congo haemorrhagic fever virus within the order Bunyavirales (Brown *et al.*, 2024). Many of these viruses have caused major epidemics and continue to pose significant threats to human and animal health.

CHIKV, an alphavirus transmitted primarily by *Aedes* mosquitoes, has emerged as a major public health concern in recent decades. Large outbreaks have occurred across Africa, Asia, the Indian Ocean region, and the Americas, often causing debilitating febrile illness accompanied by severe arthralgia that can persist for months or years in some patients. The rapid global spread of CHIKV highlights the capacity of arboviruses to expand into new geographic regions when ecological conditions favour vector transmission (Zhang *et al.*, 2026).

Although vaccines exist for some arboviral infections in humans and animals, many important arboviruses still lack widely available or highly effective vaccines. Vaccine candidates against viruses such as DENV, CHIKV, and ZIKV remain under active

development (Metz and Pijlman, 2011, Pereira *et al.*, 2025). Increasingly, arboviruses represent a growing global health challenge driven by factors including international travel and trade, climate change, urbanisation, population growth, and the ability of vectors to adapt to new habitats. The emergence and spread of arboviral diseases are therefore shaped by a complex interplay between viral evolution, vector ecology, and environmental conditions that collectively influence vector competence and transmission dynamics.

1.2 Medical and Veterinary Important Arboviral Families

1.2.1 Class *Bunyaviricites*

The class *Bunyaviricites* comprises a diverse group of enveloped viruses with segmented, single-stranded negative-sense RNA genomes that infect a wide range of vertebrate, invertebrate, and plant hosts. Members of this class are organised within the order *Bunyavirales*, which includes several medically important arboviruses responsible for significant human and veterinary disease. Notable families within *Bunyavirales* include *Peribunyaviridae*, *Phenuiviridae*, and *Nairoviridae*, which contain viruses such as Oropouche virus (OROV), Rift Valley fever virus (RVFV), Severe fever with thrombocytopenia syndrome virus (SFTSV), and Crimean–Congo haemorrhagic fever virus (CCHFV). These viruses are transmitted by diverse arthropod vectors including mosquitoes, ticks, and sandflies, and can cause disease ranging from mild febrile illness to severe haemorrhagic fever and encephalitis (Hartman and Myler, 2023).

Viruses within the order *Bunyavirales* typically possess a tripartite genome composed of large (L), medium (M), and small (S) RNA segments. The L segment encodes the viral RNA-dependent RNA polymerase (RdRP), which mediates transcription and replication of the viral genome. The M segment encodes a glycoprotein precursor that is post-translationally processed into the envelope glycoproteins responsible for host-cell attachment and membrane fusion. The S segment encodes the nucleoprotein (N), which encapsidates viral RNA to form ribonucleoprotein complexes required for genome replication. Many bunyaviruses also encode non-structural proteins that contribute to viral replication and modulate host antiviral responses, facilitating immune evasion (Hartman and Myler, 2023).

Arboviruses within *Bunyavirales* are widely distributed and increasingly recognised as emerging or re-emerging pathogens. For example, Oropouche virus is a major cause of febrile illness in South America, while Rift Valley fever virus and Crimean–Congo haemorrhagic fever virus cause severe zoonotic outbreaks affecting both humans and livestock. The emergence of viruses such as SFTSV in Asia further highlights the public health importance of this viral group and its capacity for geographic expansion and cross-species transmission (Hartman and Myler, 2023).

1.2.2 Family *Flaviviridae*

The family *Flaviviridae* comprises more than 70 viruses classified into three genera: *Flavivirus*, *Hepacivirus*, and *Pestivirus*. Among these, the genus *Flavivirus* is the largest and the only one that contains arboviruses. Members of this genus are transmitted either by mosquitoes, including YFV, DENV, West Nile virus (WNV), and Japanese encephalitis virus (JEV), or by ticks, such as tick-borne encephalitis virus (TBEV) (Schweitzer *et al.*, 2009, Rust, 2012). The diversity and global distribution of flaviviruses make them valuable systems for studying the evolution and emergence of vector-borne viral diseases (Pierson and Diamond, 2020).

Flaviviruses are enveloped viruses possessing a single-stranded, positive-sense, non-segmented RNA genome of approximately 11 kb (Lindenbach and Rice, 2003, Harris *et al.*, 2006, Pierson and Diamond, 2020). The genomic RNA contains a 5′ cap but lacks a polyadenylated [poly(A)] tail at the 3′ end. Viral translation occurs as a single polyprotein that is flanked by 5′ and 3′ untranslated regions (UTRs), which form complex secondary structures involved in regulating translation, genome replication, and RNA stability (Charlier *et al.*, 2002, Gritsun *et al.*, 2006). This polyprotein is cleaved co- and post-translationally by both viral and host proteases to generate three structural proteins: the capsid protein (C), precursor membrane protein (prM), and envelope glycoprotein (E), as well as seven non-structural proteins (NS1, NS2A, NS2B, NS3, NS4A, NS4B, and NS5). Among these, NS5 is the most conserved protein and encodes the viral RNA-dependent RNA polymerase (RdRP) (Mandl *et al.*, 1989). Together with other viral proteins and host factors, NS5 forms the replication complex responsible for viral RNA synthesis. The capsid protein mediates assembly of the icosahedral nucleocapsid that packages the viral

genome (Mukhopadhyay *et al.*, 2005). This nucleocapsid is surrounded by a host-derived lipid envelope containing the E glycoprotein, which is the primary surface protein and a major target of neutralising antibodies (Sánchez *et al.*, 2005, VanBlargan *et al.*, 2013).

Mosquito-borne flaviviruses are among the most significant emerging and re-emerging pathogens worldwide (Mackenzie *et al.*, 2004, Pierson and Diamond, 2020). They are broadly divided into viruses transmitted predominantly by *Culex* species, such as WNV and JEV, and those transmitted mainly by *Aedes* species, including DENV and YFV. This distinction also broadly reflects differences in disease manifestations, with *Culex*-associated viruses more frequently linked to encephalitic disease, whereas *Aedes*-associated viruses are commonly associated with haemorrhagic or febrile illness (Gaunt *et al.*, 2001). Among these pathogens, DENV imposes the greatest global disease burden. DENV is the causative agent of dengue fever as well as the more severe dengue haemorrhagic fever and dengue shock syndrome. Four serotypes of DENV (DENV-1 to DENV-4) are widely recognised (Zanotto *et al.*, 1996), although a potential fifth serotype was reported following a 2007 outbreak in Malaysia (Normile, 2013).

1.2.3 Family *Togaviridae*

The family *Togaviridae* is divided into two genera, *Alphavirus* and *Rubivirus* (Contigiani and Diaz, 2016, Chase, 2022). The genus *Rubivirus* contains a single species, rubella virus, which causes a common childhood infection but is not transmitted by arthropod vectors. In contrast, the genus *Alphavirus* comprises numerous arboviruses, with approximately 31 recognised species capable of infecting humans and animals (Contigiani and Diaz, 2016). These viruses infect a range of hosts and can broadly be divided into those associated with terrestrial vertebrates, such as mammals and birds, and those infecting aquatic species.

Aquatic alphaviruses include salmon pancreatic disease virus and sleeping disease virus, which infect salmonid fish such as salmon and trout. Although sea lice have been shown to harbour these viruses, their role as biological transmission vectors remains unclear (McLoughlin and Graham, 2007, Forrester *et al.*, 2012). Most

alphaviruses are maintained in transmission cycles involving mosquito vectors and vertebrate hosts, although transmission by ticks and lice has also been reported for some species. Clinically, alphavirus infections are associated with a range of symptoms including fever, rash, arthritis, arthralgia, and, in some cases, severe neurological disease such as encephalitis (Zacks and Paessler, 2010).

1.2.3.1 Genus *Alphavirus*

Semliki Forest virus (SFV) is an alphavirus originating from sub-Saharan Africa and transmitted primarily by *Aedes* mosquitoes (Fazakerley, 2002). The virus was first identified in 1942 from female *Ae. abnormalis* mosquitoes collected in the Semliki Forest of Uganda (Smithburn and Haddow, 1944). Human infections reported in the Central African Republic were associated with mild febrile illness characterised by fever, myalgia, arthralgia, and severe persistent headaches (Mathiot *et al.*, 1990). Although SFV has been detected in humans, primates, equines, and small mammals, the natural vertebrate reservoir remains unknown.

Alongside Sindbis virus (SINV), SFV is widely used as a model alphavirus due to its experimental versatility. Its genome is highly amenable to manipulation, allowing the introduction of targeted mutations or the insertion of foreign reporter genes such as luciferase or fluorescent proteins. This property has also led to its development as a vector for gene delivery in vaccine and therapeutic applications (Hoffmann *et al.*, 2001, Lundstrom, 2003). Reporter genes can be inserted at several genomic locations, resulting in distinct outcomes in terms of expression and stability. For example, insertion within the replicase provides an indirect marker of viral replication, whereas insertion before, within, or after the structural open reading frame enables expression of the encoded protein in progeny virions (Fragkoudis *et al.*, 2007, Kiiver *et al.*, 2008). Expression levels can be further enhanced through duplication of the subgenomic promoter (Tamberg *et al.*, 2007).

Several laboratory strains of SFV have been developed, including the molecular clone of the prototype strain SFV4. These strains exhibit differing levels of virulence in adult mice (Seamer *et al.*, 1967, Fazakerley, 2002, Fazakerley, 2004). SFV has also been used to infect a range of additional animal models, including rats, rabbits,

guinea pigs, and voles, as well as numerous vertebrate and invertebrate cell lines (Leake *et al.*, 1980, Atkins *et al.*, 1990). Because SFV is closely related to CHIKV but displays substantially lower pathogenicity, it provides a useful and safer surrogate for studying alphavirus replication and infectivity. Its rapid replication cycle and ease of propagation further enhance its utility as an experimental system in arbovirus research.

SFV infection also exhibits clear differences between vertebrate and invertebrate cells. In mammalian cells, infection typically results in rapid cytotoxicity and a pronounced cytopathic effect (CPE), whereas mosquito and tick cells do not display this response (Leake *et al.*, 1980, Brown, 1984). Instead, infection in mosquito cells is characterised by an initial burst of viral replication followed by a decline to a stable, low-level persistent infection (Fragkoudis *et al.*, 2008). These features have made SFV an important model for investigating antiviral and innate immune responses in mosquito vectors (Fragkoudis *et al.*, 2008, Rodriguez-Andres *et al.*, 2012).

1.2.3.2 Alphavirus replication cycles

Replication of alphaviruses occurs entirely within the cytoplasm of infected cells and begins following receptor-mediated endocytosis of the virion. Viral entry is initiated through interactions between the E2 glycoprotein and host cell surface receptors, followed by internalisation and membrane fusion within the endosomal compartment, which releases the nucleocapsid into the cytoplasm (Voss *et al.*, 2010). Disassembly of the nucleocapsid allows the genomic RNA to function directly as messenger RNA, enabling immediate translation of the non-structural polyprotein nsP1234 by host ribosomes (Strauss and Strauss, 1994). Proteolytic processing of this polyprotein generates the four non-structural proteins that assemble into membrane-associated replication complexes. These complexes first synthesise a complementary negative-strand RNA intermediate, which serves as the template for production of new genomic RNA and the shorter subgenomic RNA. The subgenomic RNA directs high-level translation of the structural polyprotein, which is subsequently processed to generate the capsid protein and viral envelope glycoproteins (Strauss and Strauss, 1994). Newly formed nucleocapsids then interact with glycoproteins trafficked to the plasma membrane through the secretory

pathway, where budding gives rise to mature enveloped virions (Strauss and Strauss, 1994, Kiiver *et al.*, 2008). The speed and tractability of this replication cycle have contributed to the widespread use of SFV as a model for studying alphavirus biology. A cartoon schematic of the SFV life cycle can be found in Figure 1-1.

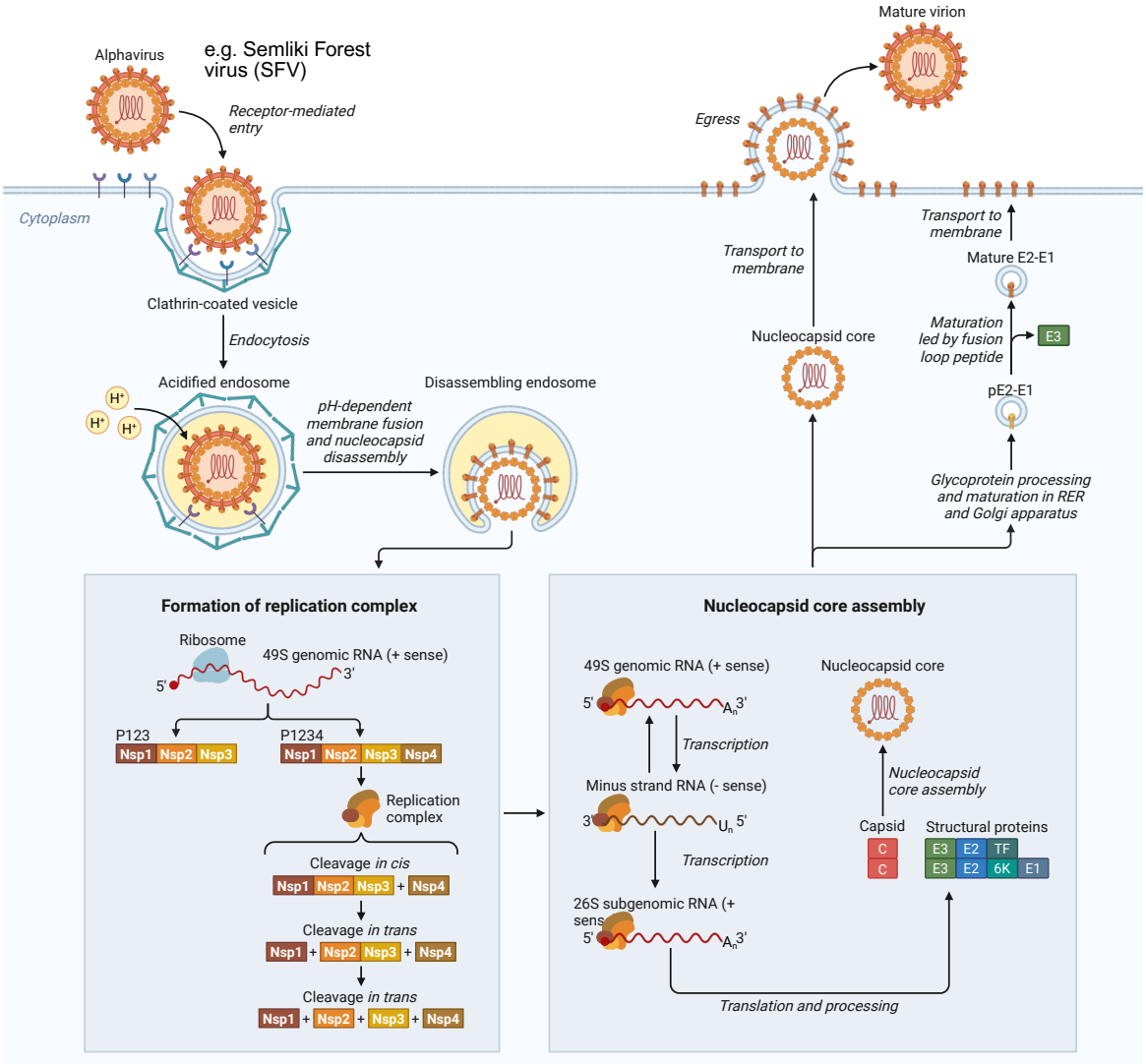

Figure 1-1 Replication cycle of an alphavirus (example: SFV).

Schematic representation of the alphavirus replication cycle. Virus entry occurs via receptor-mediated endocytosis followed by clathrin-mediated internalisation. Acidification of the endosome triggers pH-dependent membrane fusion and nucleocapsid disassembly, releasing the positive-sense genomic RNA into the cytoplasm. The genomic RNA is translated to produce the non-structural polyprotein (P1234), which is proteolytically processed to form the viral replication complex responsible for synthesis of negative-strand RNA intermediates and new genomic RNA. Transcription of a 26S subgenomic RNA drives expression of the structural polyprotein, which is processed to generate capsid and envelope glycoproteins. Capsid proteins assemble with genomic RNA to form nucleocapsids, while envelope glycoproteins are processed through the endoplasmic reticulum and Golgi apparatus before transport to the plasma membrane. Interaction between nucleocapsids and envelope glycoproteins drives budding and release of mature virions from the cell surface. Adapted from (Zimmerman et al., 2023).

1.2.3.3 Spread and Geographic Distribution

The geographic distribution of arboviruses is strongly influenced by ecological factors that determine the presence, abundance, and competence of their arthropod vectors. Recent analyses indicate that climatic and ecological suitability for arboviral transmission is increasingly overlapping on a global scale. The recent expansion of CHIKV and ZIKV has occurred largely in regions that are already environmentally favourable for dengue transmission. Current estimates suggest that approximately 5.66 billion people live in areas suitable for transmission of DENV, CHIKV, and ZIKV, while around 1.54 billion people reside in regions suitable for YFV circulation (Lim *et al.*, 2025). However, substantial variation exists in arbovirus surveillance capacity both between and within countries. Wealthier and more accessible regions are generally more likely to detect, confirm, and report infections, which may contribute to an inflated perception of risk in areas such as the United States and Europe where diagnostic and reporting systems are more robust (Lim *et al.*, 2025).

Climate change is expected to further influence the distribution and transmission dynamics of arboviruses through several mechanisms. Rising temperatures may enable mosquito vectors to establish populations in previously unsuitable regions, facilitating the emergence of arboviral diseases in new geographic areas. Changes in climatic conditions can also alter the timing and duration of transmission seasons, thereby extending periods of viral circulation. In addition, environmental changes may influence vector abundance, viral replication within vectors, and host–vector contact rates, ultimately affecting the magnitude and frequency of outbreaks in both endemic and outbreak-prone regions (Dorigatti *et al.*, 2025).

Understanding these ecological and epidemiological drivers of arbovirus spread provides important context for interpreting the biological characteristics of these viruses, including the genomic features that underpin their replication, transmission, and host adaptation.

1.2.3.4 Alphavirus Genome Organisation

Alphaviruses possess a single-stranded, positive-sense RNA (ssRNA(+)) genome enclosed within an enveloped virion. The genome is approximately 11.5 kb in length and is capped at the 5′ end and polyadenylated at the 3′ end, enabling it to function similarly to cellular mRNA. This structure allows the viral RNA to be directly translated by host ribosomes while also contributing to RNA stability within the cytoplasm (Strauss *et al.*, 1983). The genome contains two open reading frames (ORFs) that encode a total of nine viral proteins (Strauss and Strauss, 1994). The larger 5′ ORF, comprising roughly two-thirds of the genome, encodes four non-structural proteins (nsP1–nsP4) as part of the nsP1234 polyprotein. The remaining third of the genome encodes a structural polyprotein that gives rise to five structural proteins, including the capsid protein (C), the 6 kDa protein (6K), and three envelope glycoproteins (E1, E2, and E3), whose expression is regulated by an internal subgenomic (26S) promoter (Kääriäinen *et al.*, 1987). During processing, E2 and E3 are initially produced as a precursor protein, p62, which is subsequently cleaved to yield the mature glycoproteins (Strauss and Strauss, 1994, Kääriäinen and Ahola, 2002). A cartoon representing the generic alphavirus genomic organisation can be found in Figure 1-2.

Alphavirus particles are approximately 70 nm in diameter and exhibit a spherical morphology. The viral envelope consists of a lipid bilayer derived from the host cell plasma membrane. Embedded within this membrane are 80 trimeric surface spikes, each composed of three E1–E2 heterodimers, which surround the nucleocapsid core (Ziemiecki and Garoff, 1978, Vaux *et al.*, 1988). The nucleocapsid displays T = 4 icosahedral symmetry and is formed from 240 copies of the capsid (C) protein that encapsidate the viral genomic RNA (Coombs and Brown, 1987, Paredes *et al.*, 1993).

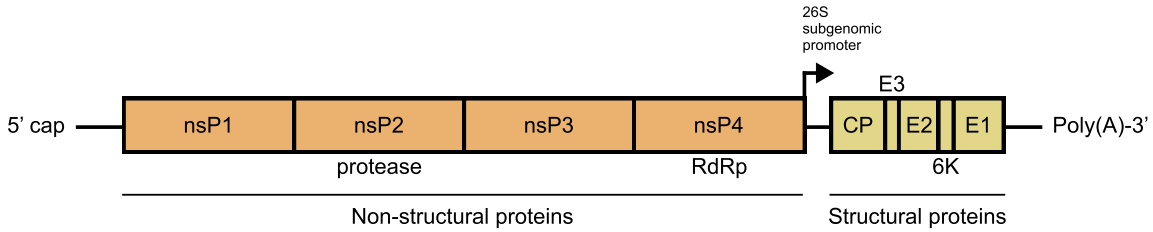

Figure 1-2 Genome organisation of alphaviruses.

Schematic representation of the alphavirus positive-sense RNA genome (~11.5 kb). The genome contains a 5′ cap and a 3′ poly(A) tail and encodes two open reading frames. The 5′ region encodes the non-structural polyprotein (nsP1–nsP4), which is processed to generate proteins required for viral RNA replication, including the RNA-dependent RNA polymerase (RdRp). The 3′ region is expressed from the internal 26S subgenomic promoter and encodes the structural polyprotein that is processed into the capsid protein (CP), envelope glycoproteins (E3, E2, and E1), and the 6K protein. Figure adapted from (Skidmore and Bradfute, 2023).

1.3 Mosquitoes as arbovirus vectors

Mosquitoes are among the most important vectors of human and animal pathogens worldwide and play a central role in the transmission of numerous arboviruses. *Ae. aegypti* is one of several mosquito species responsible for transmitting arboviruses to humans, although many additional mosquito species act as vectors for a wide range of viruses and parasites. Understanding mosquito biology and vector competence is therefore essential for understanding the transmission dynamics of vector-borne pathogens.

Following ingestion of an infectious blood meal, arboviruses initially infect and replicate within the epithelial cells of the mosquito midgut. After this primary replication stage, viruses escape the midgut barrier and disseminate into the haemolymph, allowing infection of secondary tissues throughout the mosquito body. Subsequent viral replication in these tissues ultimately leads to infection of the salivary glands, from which progeny virions can be transmitted to new vertebrate hosts during subsequent blood feeding (Franz *et al.*, 2015, Liu *et al.*, 2019).

The distribution and diversity of mosquito species are strongly influenced by environmental factors such as climate, rainfall, and temperature. Temperature in particular plays a critical role in shaping arbovirus transmission dynamics, as it influences both mosquito development and viral replication and dissemination within the vector (Huang *et al.*, 2019). Consequently, ongoing climate change is expected to alter the geographic range of mosquito populations, enabling expansion into previously unsuitable regions while potentially reducing suitability in others. These ecological shifts are likely to increase the number of human populations at risk of mosquito-borne viral diseases.

1.3.1 Important Vectors of Disease Transmission

Mosquitoes are members of the family *Culicidae* within the order *Diptera*. This family is divided into two subfamilies and comprises more than 3,500 recognised species. Among these, species within the genus *Aedes* are particularly important vectors of

arboviruses affecting human health. Given their global epidemiological significance, this section focuses on two major vectors: *Ae. aegypti* and *Ae. albopictus*.

Species belonging to the genera *Aedes* and *Culex* are among the most widely distributed mosquitoes globally (Figure 1-3A). The yellow fever mosquito, *Ae. (Stegomyia) aegypti*, originated in Africa and is a major vector of human arboviruses, particularly DENV and YFV. Its spread beyond Africa is largely attributed to human transportation, especially during the transatlantic slave trade, and the species is now established across tropical, subtropical, and some temperate regions worldwide (Soumahoro *et al.*, 2010, Powell and Tabachnick, 2013). Highly anthropophilic, *Ae. aegypti* has adapted to human environments and typically lays eggs in artificial containers such as water storage vessels and discarded tyres. Its preference for feeding on humans and relatively limited flight range, generally less than 100 m, facilitate the maintenance of urban transmission cycles for arboviruses (Powell and Tabachnick, 2013). The transmission dynamics of arboviruses by *Ae. aegypti* are fundamentally structured around distinct ecological cycles, primarily the sylvatic and urban cycles (Gubler, 1998). Historically, many significant viruses, such as YFV and DENV, originated in a sylvatic (or jungle) cycle. In this ancestral environment, the virus circulates between non-human primates and specialised tree-hole breeding mosquitoes, such as *Ae. africanus* in Africa or members of the Sabethes and Haemagogus genera in the Americas (Braack *et al*., 2018). Within this cycle, humans are typically considered accidental hosts, infected only through encroachment into forested areas.

The transition to an urban transmission cycle was facilitated by the evolutionary adaptation of *Ae. aegypti* to human-dominated landscapes (Powell and Tabachnick, 2013). As the species became highly domesticated and anthropophilic, it acted as a bridge vector, facilitating viral spillover from forest reservoirs into human populations. Unlike the sylvatic cycle, the urban cycle is sustained entirely through a human-mosquito-human transmission chain, requiring no animal reservoir for its persistence (Weaver and Barrett, 2004). This cycle is particularly explosive in densely populated urban centres where *Ae. aegypti* thrives in artificial water containers. Understanding the interplay between these cycles is essential, as the continued existence of sylvatic reservoirs poses a permanent risk of viral re-emergence, complicating global eradication efforts (Braack *et al*., 2018).

Consequently, control of this species has long been a central focus of public health efforts to prevent urban epidemics of DENV and YFV, particularly given the limited availability of vaccines for many arboviral diseases. Eradication campaigns historically eliminated *Ae. aegypti* from parts of the Americas (Soper, 1967, Kouri *et al.*, 1989), while coordinated vector control programmes in parts of southern Asia substantially reduced disease incidence (Pant *et al.*, 1971, Bang and Pant, 1972, Ooi *et al.*, 2006). However, many of these programmes proved difficult to sustain, and following their decline, *Ae. aegypti* has re-established populations in many previously controlled regions. In numerous endemic areas, larvae are now detected in more than half of surveyed households (Nathan and Knudsen, 1991). In addition, widespread resistance to multiple classes of insecticides has emerged, further complicating control efforts and highlighting the need for alternative vector control strategies (Hemingway *et al.*, 2004).

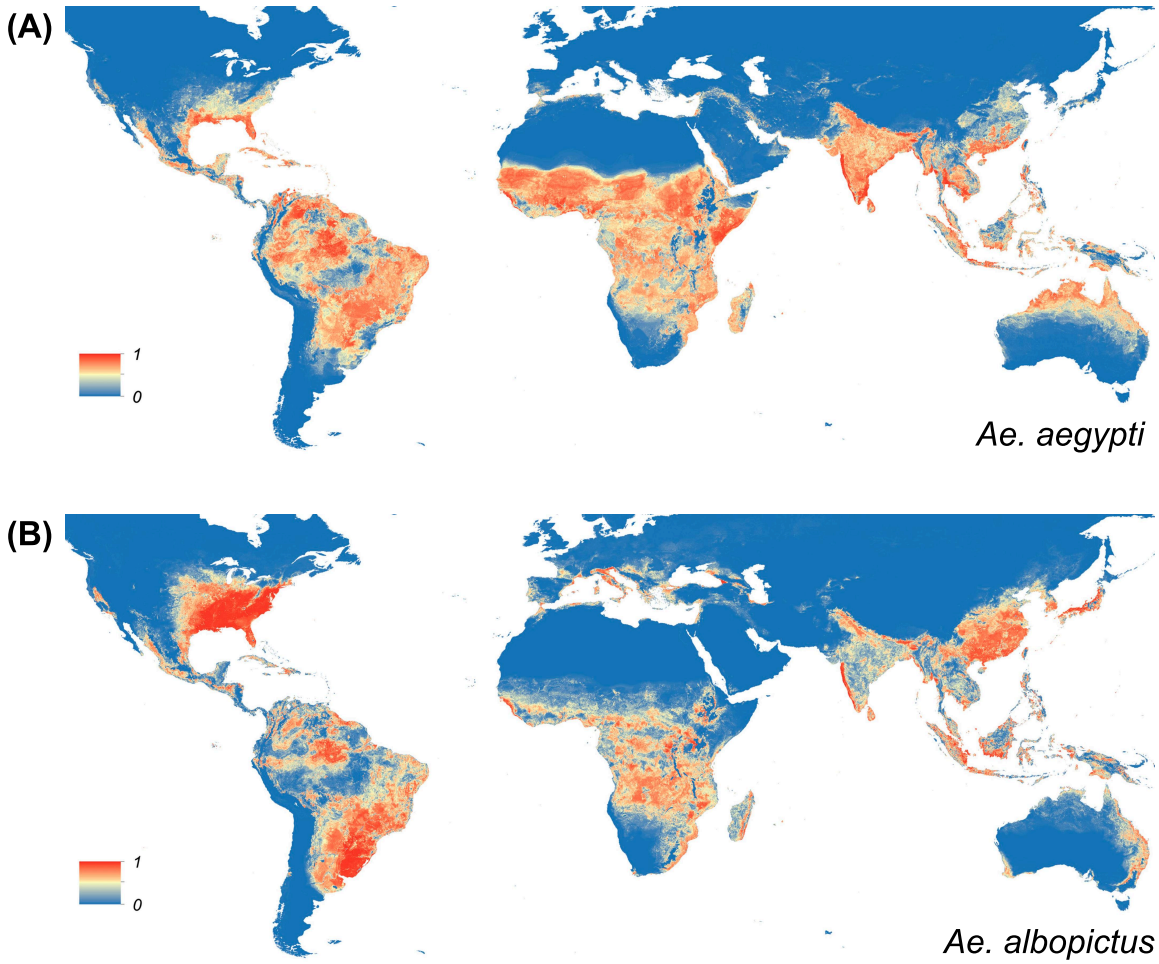

Figure 1-3 Global predicted distribution of *Ae. aegypti* and *Ae. albopictus*.

Global maps showing the predicted probability of occurrence for (A) *Ae. aegypti* and (B) *Ae. albopictus*. Colour gradients represent the estimated probability of species occurrence, ranging from low probability (blue, 0) to high probability (red, 1), at a spatial resolution of 5 km × 5 km. These models highlight the extensive global distribution of both species and illustrate regions with high environmental suitability for their establishment, particularly across tropical and subtropical regions (Kraemer et al., 2015).

Ae. (Stegomyia) albopictus, commonly known as the Asian tiger mosquito, is a highly invasive species that has expanded far beyond its native forests of Southeast Asia (Smith, 1956) (Figure 1-3B). The species is now widely established in Africa (Savage *et al.*, 1992, Fontenille and Toto, 2001, Coffinet *et al.*, 2007), the Americas (Moore, 1999, Braks *et al.*, 2003), Europe (Dalla Pozza and Majori, 1992, Knudsen *et al.*, 1996, Adhami and Reiter, 1998, Schaffner *et al.*, 2004, Klobučar *et al.*, 2006, Medlock *et al.*, 2012, Roiz *et al.*, 2014), and across various islands in the Indian and Pacific Oceans (Bagny *et al.*, 2009, Guillaumot *et al.*, 2012). Compared with *Ae. aegypti*, this species shows greater tolerance to temperate climates, as its eggs can enter diapause during cold periods, allowing survival in more northern regions (Tran *et al.*, 2013, Liu-Helmersson *et al.*, 2014). Its rapid global spread has been strongly associated with international trade in used tyres and bamboo products, which can transport dormant eggs in small volumes of trapped rainwater (Benedict *et al.*, 2007). *Ae. albopictus* exhibits considerable ecological plasticity and is thought to have shifted from predominantly zoophilic feeding behaviour in its native forest habitats to a more anthropophilic lifestyle in human-modified environments, including rural, suburban, and urban settings (Paupy *et al.*, 2009). Although it was initially regarded primarily as a “bridge vector” transmitting viruses between animal reservoirs and humans, it is now recognised as an important arbovirus vector in its own right (Gratz, 2004, Paupy *et al.*, 2009).

Table 1-1 Key biological and epidemiological differences between *Ae. aegypti* and *Ae. albopictus*.

Characteristic	*Ae. aegypti*	*Ae. albopictus*
Common name	Yellow fever mosquito	Asian tiger mosquito
Native range	Africa	Southeast Asia
Current distribution	Tropical and subtropical regions worldwide	Global, including temperate regions
Habitat preference	Highly adapted to urban environments	Urban, suburban, and rural environments
Egg deposition	Artificial containers (e.g., water storage containers, tyres)	Natural and artificial containers
Climate tolerance	Less tolerant of colder climates	More tolerant of temperate climates due to egg diapause
Host feeding preference	Strongly anthropophilic	Opportunistic; feeds on humans and animals
Flight range	Typically, <100 m	Often greater than *Ae. aegypti*
Major arboviruses transmitted	DENV, YFV, ZIKV, CHIKV	DENV, CHIKV, ZIKV
Epidemiological role	Primary urban vector of dengue and yellow fever	Important secondary vector and bridge vector

As *Ae. aegypti* and *Ae. albopictus* continue to expand their geographic ranges, interspecific competition may lead to displacement of native mosquito species, potentially altering local vector–virus dynamics and influencing disease incidence (Chevillon *et al.*, 2008). Both species represent major public health concerns, particularly as vectors of DENV and CHIKV (Gratz, 2004, Manore *et al.*, 2014). While DENV transmission is primarily driven by *Ae. aegypti*, which dominates in most endemic regions, *Ae. albopictus* acts as an important secondary vector. While DENV transmission is primarily driven by Ae. aegypti, which dominates in most endemic regions, Ae. albopictus acts as an important secondary vector. Nevertheless, exceptions to this pattern have been reported. In Gabon, Ae. albopictus was identified as the principal vector during concurrent chikungunya and dengue outbreaks following its recent invasion and establishment in the region (Pagès et al., 2009, Leroy *et al*., 2009). Historically, it has been responsible for dengue epidemics in Japan (1942–1945) (Hotta, 1998, Kuno, 2007), Hawaii (2001–2002) (Effler *et al.*, 2005), and several Indian Ocean islands, including La Réunion (1977–1978) (Coulanges *et al.*, 1979, Paupy *et al.*, 2001). Similarly, *Ae. albopictus* contributed to chikungunya outbreaks in Central Africa in 2007 (Peyrefitte *et al.*, 2007, Leroy *et al.*, 2009, Paupy *et al.*, 2010).

The 2005–2006 chikungunya epidemic on La Réunion affected nearly 40% of the island's population (Enserink, 2007a) and was associated with a single point mutation (A226V) in the viral E1 glycoprotein. This mutation enhanced viral infectivity in *Ae. albopictus* relative to *Ae. aegypti*, resulting in the former becoming the primary vector during the epidemic (Reiter *et al.*, 2006, Vazeille *et al.*, 2007, Arias-Goeta *et al.*, 2014). Consequently, viral dissemination within mosquitoes accelerated from approximately 7–15 days to 2–6 days, while viral loads in the salivary glands increased substantially, facilitating wider geographical spread in regions inhabited by *Ae. albopictus* (Paupy *et al.*, 2010).

The first European chikungunya outbreak occurred in Italy in 2007 and originated from a viraemic traveller returning from India who introduced the virus to local *Ae. albopictus* populations (Enserink, 2007b, Rezza *et al.*, 2007, Angelini *et al.*, 2008). The species has since been implicated in autochthonous transmission of CHIKV and DENV in southern France and continues to contribute to emerging outbreaks in Central Africa (Gould *et al.*, 2010, Grandadam *et al.*, 2011, Vega-Rua *et al.*, 2013).

More recently, the re-emergence of CHIKV on La Réunion Island in 2024 and the subsequent detection of travel-associated cases in mainland France further highlighted the risk of broader regional and international spread (Frumence *et al.*, 2025).

Changes in the geographic distribution of mosquito vectors and the composition of dominant local mosquito populations are likely to influence patterns of arbovirus emergence and transmission. Consequently, understanding the ecological and biological factors that determine vector competence and virus transmission is essential for developing effective strategies for the control and prevention of arboviral diseases.

1.4 Current Biological Strategies for Arbovirus Vector Control

Traditional mosquito control strategies, including insecticide application and elimination of breeding sites, have been widely used to reduce arbovirus transmission. However, these approaches face increasing challenges due to the development of insecticide resistance, operational costs, and difficulties in maintaining long-term control programmes. As a result, alternative strategies aimed at reducing mosquito vector competence have gained considerable attention (Achee *et al.*, 2015, Benelli and Mehlhorn, 2016, Hemingway *et al.*, 2016, Wilson *et al.*, 2020). One promising approach involves the use of microbial symbionts to interfere with viral replication within mosquitoes.

1.4.1 Targeting of immune pathways

In addition to microbial symbiont-based strategies, another emerging approach to limiting arbovirus transmission involves targeting the mosquito's innate immune pathways. Mosquitoes possess several antiviral defence mechanisms that restrict viral replication and dissemination within the vector. These include pathways such as RNA interference (RNAi), Toll, immune deficiency (Imd), and the Janus kinase–signal transducer and activator of transcription (JAK–STAT) pathway, which

together contribute to antiviral immunity in insects (Blair, 2011, Silver *et al.*, 2021). Manipulation of these pathways has therefore been proposed as a potential strategy to reduce vector competence and interrupt arbovirus transmission.

Among these mechanisms, RNAi is considered the major antiviral pathway in mosquitoes and plays a key role in controlling arbovirus replication. Experimental disruption of components of this pathway can lead to increased viral replication and dissemination in mosquito cells, highlighting its importance in limiting infection (Blair and Olson, 2015, Olson and Blair, 2015). Other immune pathways, including Toll, Imd, and JAK–STAT signalling, also contribute to antiviral responses by regulating immune gene expression and cellular defence mechanisms (Blair, 2011). Together, these pathways form a complex antiviral network that influences the ability of mosquitoes to acquire and transmit viruses.

Understanding how these immune mechanisms regulate arbovirus infection is therefore important for identifying new strategies to control virus transmission. Experimental systems such as mosquito-derived cell lines have become valuable tools for investigating host–virus interactions and the molecular mechanisms that determine vector competence.

1.4.2 *Wolbachia* symbiosis

Among the biological strategies developed for arbovirus vector control, the use of *Wolbachia* has emerged as one of the most successful and widely implemented approaches for reducing mosquito vector competence and suppressing arbovirus transmission. *Wolbachia* are maternally inherited, intracellular endosymbiotic bacteria that naturally infect a wide range of arthropods. Although *Wolbachia* are not naturally present in *Ae. aegypti*, they can be artificially introduced into mosquito populations, where they spread through a reproductive mechanism known as cytoplasmic incompatibility. In this process, mating between *Wolbachia*-infected males and uninfected females results in inviable offspring, whereas infected females produce viable progeny regardless of the infection status of the male. As a result, infected females gain a reproductive advantage, allowing the symbiont to spread rapidly through mosquito populations (Turelli and Hoffmann, 1995, Minwuyelet *et*

al., 2023). This property enables *Wolbachia*-infected mosquitoes to establish and persist in wild populations following field releases (Hoffmann *et al.*, 2011, Hoffmann *et al.*, 2014, Utarini *et al.*, 2021).

A key feature of this strategy is the phenomenon known as virus blocking, whereby *Wolbachia*-infected mosquitoes show a reduced capacity to support viral replication and dissemination to the salivary glands. Experimental studies have demonstrated that *Wolbachia* infection can significantly reduce the replication of arboviruses such as DENV and delay the appearance of infectious virus in mosquito saliva, thereby decreasing transmission potential (Moreira *et al.*, 2009, Ye *et al.*, 2015). These biological properties underpin an operational strategy referred to as population replacement, in which wild mosquito populations are gradually replaced by *Wolbachia*-infected mosquitoes with reduced vector competence.

Although this approach offers several advantages, including species specificity and reduced risk to non-target organisms, its long-term success may be influenced by ecological and climatic conditions that affect mosquito population dynamics and *Wolbachia* transmission. In addition, maintaining high infection frequencies within mosquito populations remains a key operational challenge. Continued surveillance is therefore necessary to monitor potential changes in mosquito population structure or viral evolution that could influence the effectiveness of this strategy (Hoffmann *et al.*, 2015).

1.5 Mosquito Cell Lines

Mosquito cell lines are valuable experimental tools for studying mosquito immune responses and host–virus interactions, providing important insights into the molecular mechanisms that influence arbovirus transmission. Several mosquito cell lines have been established and are widely used because they provide sensitive, reproducible, and relatively homogeneous experimental systems compared with *in vivo* mosquito studies (Barletta *et al.*, 2012, Walker *et al.*, 2014).

The C6/36 cell line was derived from larvae of *Ae. albopictus* (Walker *et al.*, 2014). These cells are commonly used for the propagation and study of arboviruses;

however, they possess a dysfunctional exogenous small interfering RNA (exo-siRNA) pathway, which is normally associated with antiviral responses in mosquitoes. As a result, C6/36 cells are often considered a limited model for studying mosquito–arbovirus immune interactions (Brackney *et al.*, 2010).

In contrast, the Aag2 cell line, derived from embryos of *Ae. aegypti*, retains functional antiviral immune pathways and is therefore widely used to investigate mosquito antiviral responses (Barletta *et al.*, 2012, Walker *et al.*, 2014). Aag2 cells possess active RNAi pathways, providing advantages for the study of mosquito innate immunity and antiviral defence mechanisms. This cell line has been extensively characterised for investigating RNAi-mediated antiviral responses during bacterial and viral infections (McFarlane *et al.*, 2014, Dietrich *et al.*, 2017, McFarlane *et al.*, 2020, Russell *et al.*, 2021).

The Aag2-AF5 (AF5) cell line is a single-cell clonal derivative of the *Ae. aegypti* Aag2 mosquito cell line and is widely used as an *in vitro* model for studying arbovirus–mosquito interactions and mosquito antiviral immunity. AF5 cells are considered immunocompetent, retaining functional antiviral pathways including the exo-siRNA pathway, the piRNA pathway, and NF-κB signalling. These properties make AF5 cells useful for mechanistic investigations of mosquito innate immune responses. Due to their susceptibility to multiple arboviruses, including DENV and ZIKV, AF5 cells also serve as an important platform for virus propagation and infection experiments relevant to vector biology (Varjak *et al.*, 2017a, Fredericks *et al.*, 2019).

To investigate RNAi-mediated antiviral defence, genetically modified derivatives of AF5 have been developed. The Aag2-AF319 (AF319) cell line is a Dicer-2 knockout (Dcr2 KO) clone derived of the AF5 cell line. Since Dcr2 is a central enzyme required to produce 21-nt virus-derived small interfering RNAs (vsiRNAs) in the mosquito exo-siRNA pathway, AF319 cells provide a valuable loss-of-function system for studying the role of Dcr2 in restricting arbovirus infection (Varjak *et al.*, 2017b, Fredericks *et al.*, 2019, Varjak *et al.*, 2020).

In addition, the Aag2-AF525 (AF525) cell line is an Argonaute-2 knockout (Ago2 KO) derivative of the AF5 cell line. Because Ago2 is the key effector protein responsible for loading siRNAs into the RNA-induced silencing complex (RISC) for

viral RNA degradation, AF525 cells enable targeted investigation of Ago2-dependent RNAi mechanisms during arbovirus replication and persistence in mosquito cells (Scherer *et al.*, 2021).

Together, AF5, AF319, and AF525 constitute a powerful experimental system of related *Ae. aegypti* cell models that allow comparison between wild-type antiviral competence (AF5) and impaired RNAi antiviral responses (Dcr2 in AF319 and Ago2 in AF525). These cell lines therefore provide a valuable framework for investigating mosquito vector competence and the molecular basis of arbovirus transmission (Scherer *et al.*, 2021, Altinli *et al.*, 2022).

1.6 Vector Control of Arboviruses

1.6.1 RNA interference

Several RNAi pathways operate in insects and play important roles in regulating gene expression and antiviral defence. Among these pathways, the small interfering RNA (siRNA) pathway is considered the primary antiviral mechanism of the insect innate immune system.

1.6.2 Small interfering RNAs (siRNAs)

Small interfering RNAs (siRNAs) can be broadly classified into two types based on their origin within the siRNA pathway: endogenous siRNAs (endo-siRNAs) and exo-siRNAs. Endogenous siRNAs are generated from cellular RNA sources, including retrotransposons, regions of convergent transcription, overlapping transcripts, or structured genomic RNAs such as inverted repeats and hairpin structures. These RNA structures are distinguished from microRNA (miRNA) precursors by their more limited stem lengths (Figure 1-4).

Endo-siRNAs play an important role in maintaining genome stability by repressing transposable elements and other aberrant mobile transcripts. In addition, they contribute to the regulation of heterochromatin formation and genome integrity

within the cell (Chung *et al.*, 2008, Czech *et al.*, 2008, Ghildiyal *et al.*, 2008, Watanabe *et al.*, 2008, Fagegaltier *et al.*, 2009).

In contrast, the exo-siRNA pathway is induced by long, non-cellular double-stranded RNA (dsRNA) molecules, typically produced during RNA virus replication or through overlapping transcriptional complexes of DNA viruses (Bronkhorst *et al.*, 2012). These dsRNA molecules are recognised as pathogen-associated molecular patterns (PAMPs) rather than 'self' RNA and are processed into short duplex fragments known as exo-siRNAs or virus-derived small interfering RNAs (vsiRNAs), which function to restrict viral infections (Figure 1-5). Notably, vsiRNAs show no nucleotide bias at the first position, indicating that Dcr-2 cleaves dsRNA in a largely sequence-independent manner (Galiana-Arnoux *et al.*, 2006, Wang *et al.*, 2006). Both the endo- and exo-siRNA pathways are thought to operate similarly in *D. melanogaster* and utilise the same core protein machinery, with the exception of the Loquacious isoform PD (Loqs-PD), which is specific to the endo-siRNA pathway (Hartig *et al.*, 2009, Marques *et al.*, 2013).

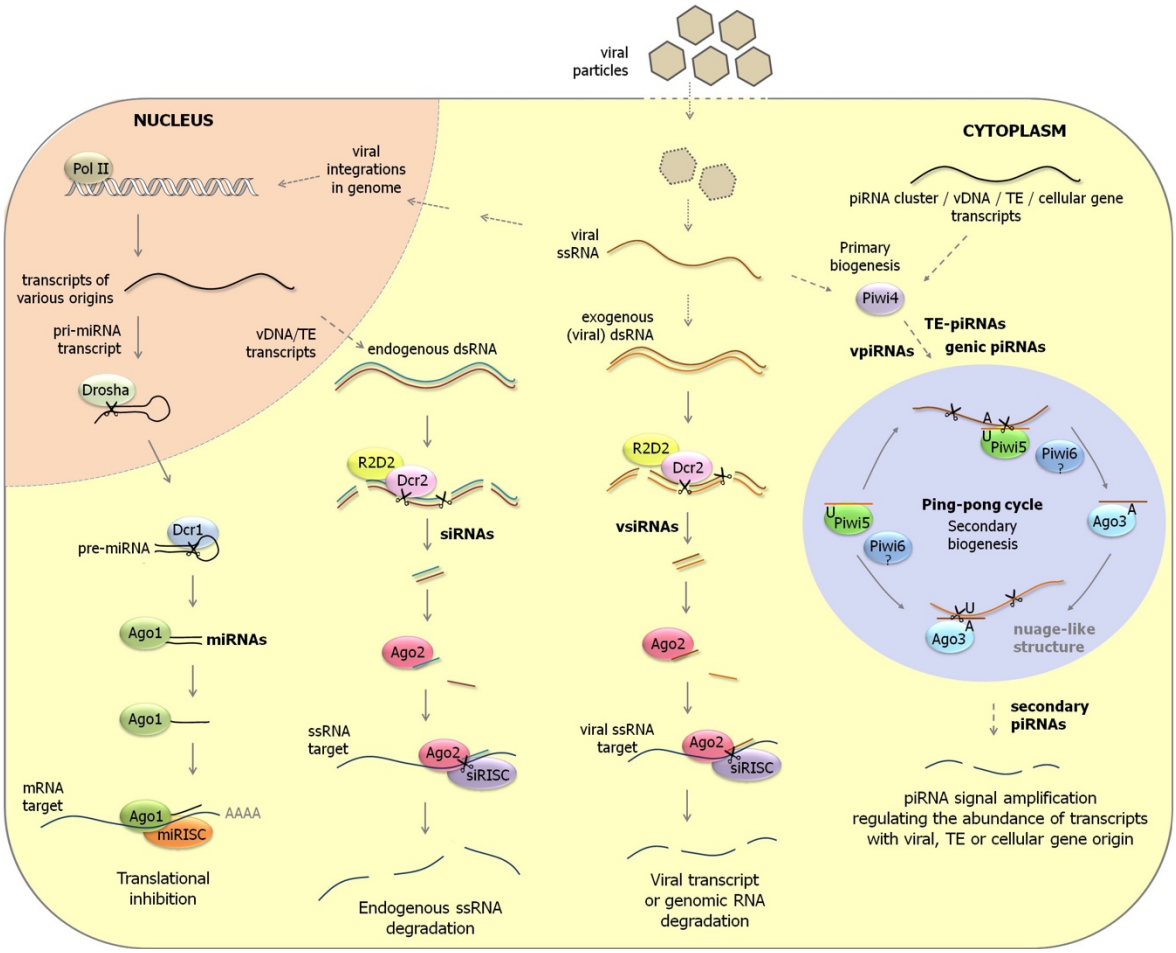

Figure 1-4 Overview of the three major RNAi pathways in mosquitoes.

Schematic representation of the microRNA (miRNA), small interfering RNA (siRNA), and PIWI-interacting RNA (piRNA) pathways that regulate gene expression and antiviral defence in mosquito cells. In the miRNA pathway (left), primary miRNA transcripts (pri-miRNAs) are processed in the nucleus by Drosha to form precursor miRNAs (pre-miRNAs), which are exported to the cytoplasm and further cleaved by Dicer-1 (Dcr1) to generate mature miRNAs. These are loaded into Argonaute-1 (Ago1) to form the miRNA-induced silencing complex (miRISC), which mediates translational repression or degradation of target mRNAs. In the small interfering RNA (siRNA) pathway (centre), endogenous or virus-derived double-stranded RNA (dsRNA) is cleaved by Dcr2 in association with the cofactor R2D2 to generate 21-nt siRNAs. These siRNAs are incorporated into Argonaute-2 (Ago2) within the siRNA-induced silencing complex (siRISC), which directs sequence-specific cleavage of complementary RNA targets, including viral RNA during infection. In the PIWI-interacting RNA (piRNA) pathway (right), long single-stranded precursor transcripts derived from genomic piRNA clusters, transposable elements, or viral sequences are processed into primary piRNAs that associate with PIWI proteins such as Piwi4, Piwi5, Piwi6, and Ago3. Secondary piRNAs are generated through the ping-pong amplification cycle, contributing to the regulation of transposable elements and viral RNA (Liu et al., 2019).

Detection of dsRNA trigger molecules is mediated by the RNase III enzyme Dcr-2 (Bernstein *et al.*, 2001, Kim *et al.*, 2006, Aliyari and Ding, 2009, Kemp and Imler, 2009), which functions in association with the dsRNA-binding protein R2D2, named for its two dsRNA-binding domains (R2) and its interaction with Dcr-2 (D2). Dcr-2 therefore acts as a cellular pattern recognition receptor (PRR) capable of recognising viral dsRNA (Takeuchi and Akira, 2008). The resulting siRNAs, or virus-derived siRNAs (vsiRNAs), are loaded into the RNA-induced silencing complex (RISC), a ribonucleoprotein assembly containing several components, most notably Argonaute-2 (Ago2), which possesses catalytic "slicer" activity that directly mediates gene silencing (Hammond *et al.*, 2001, Meister *et al.*, 2004, Okamura *et al.*, 2004, Kawamura *et al.*, 2008).

While much of the fundamental understanding of the Ago2 interactome is derived from studies in *D. melanogaster,* orthologous proteins have been identified in *Ae. aegypti*, as summarised in Table 1-2. However, the functional conversation of these factors during viral infection in mosquitoes remains an area of active investigation, highlighting the necessity of the proteomics approach used in this thesis.

Table 1-2 Comparison of Ago2-associated factors and RISC assembly components between *D. melanogaster* and *Ae. aegypti.*

Protein	Role in RNAi pathway	*D. melanogaster*	*Ae. aegypti*
VIG (Vasa intronic gene)	Part of the active RISC; RNA binding	Identified as Ago2-associated and linked with active RISC formation (Caudy *et al*., 2002)	Orthologue identified in mosquitoes; proposed involvement in RNAi, although less extensively characterised (Campbell *et al.,* 2008)
dFXR/FXRP	Fragile X protein orthologue; RISC assembly	Identified as an Ago2-associated factor important for RNA silencing complexes (Caudy *et al.,* 2002)	Orthologue identified in mosquitoes; possible role in antiviral RNAi not yet fully characterised
C3PO (Trax/Translin)	Endonuclease that promotes RISC loading by degrading the passenger strand	Well-characterised as a RISC activator facilitating siRNA unwinding (Liu *et al.,* 2009)	Core components conserved in mosquitoes; presumed involvement in RNAi based on conserved RISC activation mechanisms
Aubergine (Aub)	Piwi-family protein; involvement in small RNA biogenesis	Associated with transposon silencing and interaction with RNA silencing factors (Specchia *et al.,* 2008)	Mainly linked to the piRNA pathway in mosquitoes and germline antiviral defence (Morazzani *et al.,* 2012)
Hsp90	Chaperone; facilitates ATP-dependent loading of small RNA onto Ago2	Essential for RISC assembly and stability (Miyoshi *et al.*, 2005)	Hsp90 is conserved in mosquitoes, although its direct involvement in RISC assembly remains unclear.

Once the siRNA or vsiRNA duplex is loaded into active RISC, it is unwound, with the passenger strand being degraded and the guide strand retained. Ago2 then uses the guide strand to recognise and cleave complementary target mRNAs. This results in the degradation of cytoplasmic mRNAs with high sequence similarity to the RISC-bound siRNA, making RNAi a highly sequence-specific, siRNA-dependent process (Ender and Meister, 2010). For viruses, this leads to inhibition of gene expression and reduced viral progeny production.

Dcr-2 plays a central role in the antiviral immune response of insects, and in principle its activity alone can limit viral infections. Notably, it belongs to the same DExD/H box helicase family as mammalian RIG-I-like pattern recognition receptors (Deddouche *et al.*, 2008). Structurally, Dcr-2 comprises, from the N- to C-terminus: (1) a DExH/D (DEAD) box helicase ATPase domain, (2) a dsRNA-binding domain, (3) a Piwi/Argonaute/Zwille (PAZ) domain, and (4) two tandem RNase III domains (Aliyari *et al.*, 2008, Welker *et al.*, 2011, Morazzani *et al.*, 2012). The PAZ domain binds dsRNA, while the RNase III domains are responsible for processing it into siRNAs or vsiRNAs (Blaszczyk *et al.*, 2001, Lee *et al.*, 2004, Flynt *et al.*, 2009).

This cleavage generates vsiRNAs with characteristic 5′ monophosphate and two-nucleotide 3′ overhangs, immediately reducing the pool of viral RNA available for replication. The 21-nucleotide length of Dcr-2-derived siRNAs is determined by the spacing between the PAZ and RNase III domains (Zhang *et al.*, 2004, Macrae *et al.*, 2006). The ATPase domain provides the energy required for RNA processing. In *D. melanogaster*, additional factors such as Loqs-PD and Arsenic resistance protein 2 (Ars2) enhance Dcr-2 binding affinity for dsRNA, promoting efficient cleavage (Sabin *et al.*, 2009, Zhou *et al.*, 2009, Marques *et al.*, 2010, Gestuveo *et al.*, 2022a).

In *D. melanogaster*, Ago2 was the first RNAi pathway protein identified to possess antiviral activity in higher eukaryotes (Li *et al.*, 2002). Like Dcr-2, Ago2 contains both a PAZ domain and a PIWI-like domain (Lingel *et al.*, 2003, Kim *et al.*, 2009). The PAZ domain binds the guide strand of the siRNA via its two-nucleotide 3′ overhang within a hydrophobic cleft, while the PIWI-like domain possesses endonucleolytic activity that cleaves the phosphodiester bond of the passenger strand between the ninth and tenth nucleotides from the 5′ end (Lingel *et al.*, 2003, Lingel *et al.*, 2004, Ma *et al.*, 2004, Okamura *et al.*, 2004, Rand *et al.*, 2004, Matranga *et al.*, 2005,

Miyoshi *et al.*, 2005, Rand *et al.*, 2005). The resulting 9- and 12-nucleotide fragments are subsequently degraded by C3PO, which exhibits exonuclease activity (Liu *et al.*, 2009).

Guide strand selection depends on the internal thermodynamic stability of the siRNA duplex, with the strand exhibiting lower 5′ stability being preferentially incorporated into RISC (Khvorova *et al.*, 2003, Schwarz *et al.*, 2003). The rapid evolution of antiviral RNAi genes such as *dcr2*, *r2d2*, and *ago2*, compared with non-immune genes such as *dcr1*, *r3d1*, and *ago1* in *D. melanogaster*, reflects an ongoing evolutionary arms race between viruses and their hosts (Obbard *et al.*, 2006, Obbard *et al.*, 2009). Interestingly, studies in *Ae. aegypti* suggest that, unlike in *D. melanogaster*, genes involved in both the miRNA and exo-siRNA pathways show accelerated evolution, highlighting species-specific differences in RNAi-mediated immunity (Bernhardt *et al.*, 2012).

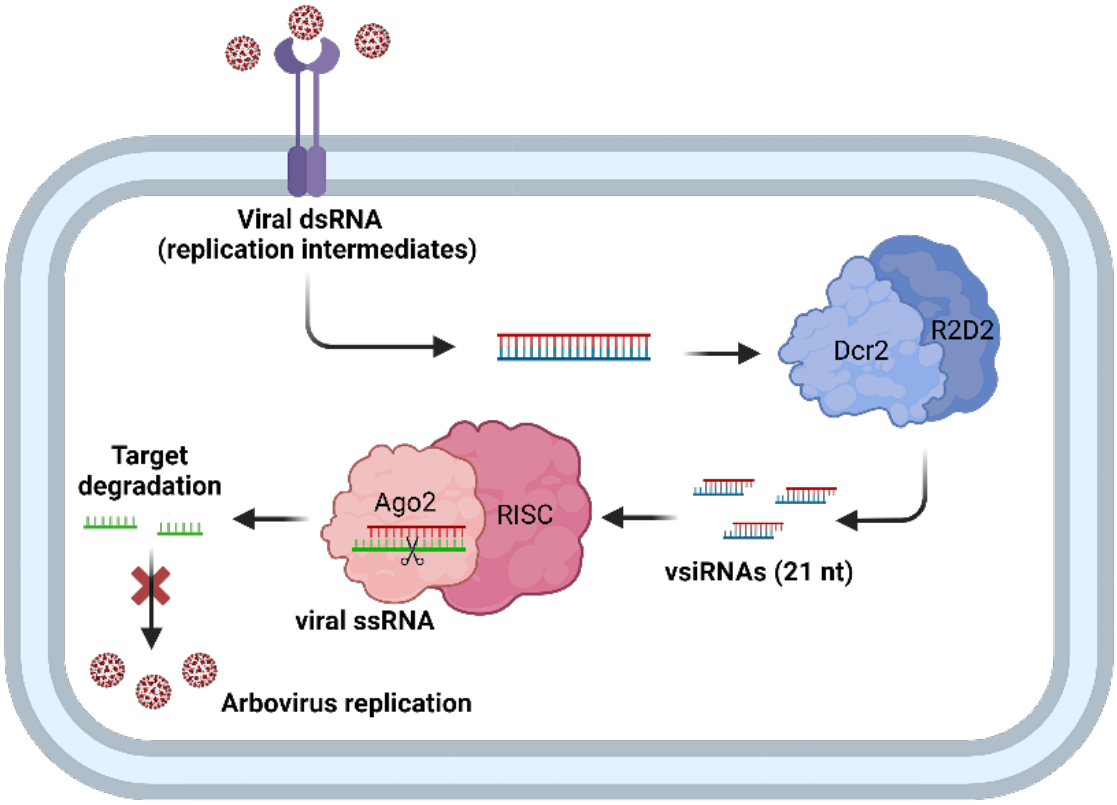

Figure 1-5 The exo-siRNA antiviral pathway in mosquito cells.

Schematic representation of the exogenous siRNA pathway activated during arbovirus infection in mosquitoes. Viral replication generates double-stranded RNA (dsRNA) intermediates that are recognised and cleaved by the RNase III enzyme Dcr2 in association with the cofactor R2D2. This processing produces ~21-nucleotide virus-derived small interfering RNAs (vsiRNAs), which are subsequently incorporated into the RNA-induced silencing complex (RISC) containing Argonaute-2 (Ago2). The guide strand of the vsiRNA directs RISC to complementary viral single-stranded RNA (ssRNA), resulting in sequence-specific cleavage and degradation of viral RNA. This process suppresses viral gene expression and limits arbovirus replication in infected mosquito cells.

1.6.3 MicroRNAs (miRNA)

MicroRNAs (miRNAs) are a conserved class of endogenous small non-coding RNAs (~22 nucleotides) that regulate gene expression primarily through post-transcriptional repression of target mRNAs. In *D. melanogaster*, miRNA biogenesis begins in the nucleus, where primary miRNA transcripts (pri-miRNAs) are processed into precursor miRNAs (pre-miRNAs) by the Drosha–Pasha complex. These pre-miRNAs are exported to the cytoplasm and further cleaved by Dicer-1 (Dcr-1) in association with the dsRNA-binding protein Loquacious, generating mature miRNA duplexes that are preferentially loaded into Argonaute-1 (Ago1) to form the miRNA-induced silencing complex (miRISC) (Saito *et al.*, 2005, Czech *et al.*, 2008). Once incorporated into Ago1, miRNAs typically guide sequence-specific gene regulation by repressing translation and/or promoting mRNA destabilisation, supporting essential biological processes such as development and cell differentiation (Forstemann *et al.*, 2007, Pressman *et al.*, 2012).

In mosquitoes, including *Ae. aegypti*, the miRNA pathway is also conserved and follows a comparable core biogenesis framework involving Drosha, Dcr-1, and Ago1. However, mosquito miRNAs have gained attention due to their roles in physiological adaptation and host–pathogen interactions. Several studies have shown that miRNA expression changes in response to factors such as blood feeding, development, and arbovirus infection, suggesting that miRNAs contribute to regulating gene networks relevant to vector competence (Hussain *et al.*, 2013, Feng *et al.*, 2018).

Additionally, evidence suggests that mosquito miRNA pathway genes may experience stronger evolutionary pressures than those in *D. melanogaster*, reflecting host–pathogen-driven adaptation in vector species (Bernhardt *et al.*, 2012). Beyond their endogenous regulatory roles, mosquito miRNAs may also participate in responses to microbial symbionts. For example, *Wolbachia* infection can alter host miRNA expression and influence mosquito gene regulation, supporting bacterial maintenance and potentially affecting pathogen transmission outcomes (Hussain *et al.*, 2011, Zhang *et al.*, 2013). Overall, studies in both *D. melanogaster* and mosquitoes highlight miRNAs as central regulators of gene expression, while mosquito-focused work emphasises their potential contribution to

traits linked to arbovirus transmission and vector control applications (Feng *et al.*, 2018, Ramos-Nino *et al.*, 2022).

1.6.4 Piwi-interacting RNAs (piRNAs)

PIWI-interacting RNAs (piRNAs) are a distinct class of small non-coding RNAs, typically ~24–30 nucleotides in length, that associate with PIWI-clade Argonaute proteins. In *D. melanogaster*, the piRNA pathway is best known for its essential role in maintaining genome integrity by suppressing transposable elements (TEs), particularly within the germline. Most *Drosophila* piRNAs originate from specialised genomic regions known as piRNA clusters, which contain large numbers of fragmented transposon sequences that serve as templates for producing antisense piRNAs (Brennecke *et al.*, 2007, Handler *et al.*, 2013). These piRNAs are typically loaded into PIWI proteins such as Piwi and Aubergine (Aub), which are enriched in antisense piRNAs, whereas Ago3 complexes are more frequently associated with sense-oriented piRNAs, enabling efficient transposon targeting (Brennecke *et al.*, 2007).

A defining feature of *Drosophila* piRNA biogenesis is the “ping-pong” amplification cycle, in which reciprocal cleavage events between Aub- and Ago3-bound piRNAs generate new piRNAs and reinforce silencing of active transposon transcripts. This cycle produces characteristic sequence signatures such as a strong 1U bias and a 10-nucleotide overlap between complementary piRNAs, reflecting endonucleolytic slicing during amplification (Brennecke *et al.*, 2007). In addition to post-transcriptional repression, nuclear Piwi can contribute to transcriptional silencing of transposons through chromatin-associated mechanisms, supporting long-term transposon control (Wang and Elgin, 2011, Rozhkov *et al.*, 2013).

In mosquitoes, piRNA biology is broadly conserved but exhibits several notable differences compared with *D. melanogaster*. In particular, the PIWI gene family has undergone expansion in several mosquito vectors, including *Ae. aegypti*, suggesting diversification of piRNA-related functions in these species (Miesen *et al.*, 2016). Unlike the largely germline-restricted role of piRNAs in *D. melanogaster*, mosquitoes also possess a prominent somatic piRNA pathway, and accumulating evidence

indicates that virus-derived piRNAs (vpiRNAs) are generated during arbovirus infection (Miesen *et al.*, 2016).

For example, studies in *Ae. aegypti* have identified somatic PIWI proteins, including Piwi5 and Ago3, that participate in the production of small RNAs with ping-pong-like characteristics, implying that piRNA-related mechanisms may contribute to antiviral responses in vector mosquitoes (Miesen *et al.*, 2016). Additional evidence for functional specialisation comes from the study of Piwi4, a non-canonical PIWI protein in *Ae. aegypti* that has been linked to antiviral activity. Piwi4 interacts with both piRNA-associated proteins and components of the exo-siRNA pathway, suggesting cross-talk between distinct small RNA pathways in mosquito antiviral immunity (Varjak *et al.*, 2017b).

Overall, work in *D. melanogaster* has established the piRNA pathway as a core defence system against transposable elements, while mosquito studies indicate that piRNA-mediated regulation has expanded in complexity and may also influence antiviral responses (Brennecke *et al.*, 2007, Miesen *et al.*, 2016, Varjak *et al.*, 2017a).

1.7 Argonaute (Ago) proteins

1.7.1 Introduction to Argonaute proteins

Argonaute (Ago) proteins are highly conserved and broadly expressed across nearly all organisms. Eukaryotic Argonautes are classified into three major clades based on their structure and functional mechanisms: AGO, PIWI (P-element-induced wimpy testis), and WAGO (worm-specific Argonautes). Ago proteins comprise four structural domains: the N-terminal domain, PAZ (PIWI-Argonaute-Zwille), MID (middle), and PIWI domains. The PIWI domain contains the catalytic active site and adopts an RNase H-like fold, which is essential for endonuclease activity and the cleavage of target RNA.

1.7.2 Ago2

Argonaute proteins are core components of RNAi, acting as the principal effector proteins that use small RNAs to recognise and silence complementary target RNAs. In *D. melanogaster*, Argonaute-2 (Ago2) is best known for its role in the exo-siRNA pathway, where it binds ~21-nucleotide siRNAs and mediates antiviral defence as well as the silencing of foreign RNA molecules. Ago2 contributes directly to gene silencing by forming the RNA-induced silencing complex (RISC), which recognises RNA targets through guide-siRNA complementarity (Iwakawa and Tomari, 2022).

A defining feature of Ago2 is its ability to function as a “slicer” endonuclease, enabling cleavage of target RNAs that exhibit extensive complementarity to the guide strand. This catalytic activity resides within the PIWI domain, which adopts an RNase H-like fold and depends on a conserved DEDH catalytic tetrad (Asp–Glu–Asp–His). These residues coordinate metal ions required for cleavage and are essential for efficient RNA cutting during RNAi-mediated silencing (Müller *et al.*, 2020, Nakanishi, 2023).

In *D. melanogaster*, functional evidence for Argonaute slicing has been supported by studies demonstrating slicer activity across Argonaute proteins, with Ago2 playing a central role in siRNA-guided cleavage reactions in insect systems (Miyoshi *et al.*, 2005). Mechanistically, Ago2-mediated slicing contributes to strong target suppression and supports effective RNAi-based antiviral responses.

1.8 Objectives

Arboviruses establish persistent infections in mosquito vectors, enabling their transmission between vertebrate hosts without causing overt pathology in the insect. The outcome of infection in mosquito cells is therefore shaped by intrinsic antiviral mechanisms that restrict viral replication while maintaining cellular viability. Among these mechanisms, the RNAi pathway represents the primary antiviral defence in mosquitoes, with the exo-siRNA pathway playing a central role in detecting and degrading viral RNA.

Argonaute-2 (Ago2) is the catalytic effector of the RNA-induced silencing complex (RISC) and is responsible for mediating sequence-specific cleavage of viral RNA guided by virus-derived siRNAs. Although Ago2 is recognised as a key antiviral factor in insects, several aspects of its function in mosquito antiviral immunity remain incompletely understood. In particular, the importance of its catalytic “slicer” activity during antiviral responses and the identity of host factors that interact with Ago2 to regulate RNAi-mediated defence are not fully defined.

The overall aim of this thesis was therefore to investigate the molecular mechanisms by which Ago2 contributes to antiviral RNAi responses in mosquito cells.

To address this aim, the thesis was structured around three major objectives:

1.8.1 To characterise the role of Ago2 catalytic activity in the antiviral RNAi response of mosquito cells.

This objective aimed to determine whether the endonucleolytic “slicer” activity of Ago2 is required for effective RNAi-mediated silencing and antiviral defence in mosquito-derived cell systems.

1.8.2 To determine how Ago2 catalytic activity influences arbovirus replication in mosquito cells.

This objective investigated the functional consequences of disrupting Ago2 catalytic activity on arbovirus replication dynamics, providing insight into the mechanistic contribution of Ago2-mediated RNA cleavage to antiviral immunity.

1.8.3 To define the Ago2 protein interaction network and identify host factors associated with antiviral RNAi responses.

This objective aimed to characterise the Ago2 interactome using proteomic approaches to identify cellular proteins that interact with Ago2 and may contribute to the regulation of RNAi-mediated antiviral activity in mosquito cells.

Together, these objectives aim to advance understanding of the molecular mechanisms that underpin RNAi-mediated antiviral defence in mosquito vectors and to clarify how Ago2 function contributes to the restriction of arbovirus infection.

The following chapters address these objectives by first examining the functional importance of Ago2 catalytic activity in antiviral RNAi responses in mosquito cells. This is followed by a detailed investigation of the Ago2 protein interaction network to identify host factors associated with antiviral RNAi activity. Together, these studies provide mechanistic insight into how Ago2 contributes to antiviral defence in mosquito vectors and improve understanding of the molecular processes that influence arbovirus infection and persistence in vector cells.

Chapter 2:
Materials and Methods

Chapter 2 Materials and Methods

2.1 Materials

2.1.1 Cell culture

AF525 cells, an Argonaute-2 (*Ago2*) knockout cell line derived from Aag2-AF5 cells using CRISPR/Cas9 (Fredericks *et al.*, 2019, Scherer *et al.*, 2021), and RNAi-competent AF5 cells, previously confirmed to behave similarly to the parental Aag2 cell line (Varjak *et al.*, 2017b), were used in this study.

Both mosquito cell lines were maintained in Leibovitz's L-15 medium supplemented with 10% foetal bovine serum (FBS; Gibco), 10% tryptose phosphate broth (TPB; Gibco), and 1% penicillin–streptomycin (100 U/mL penicillin and 100 µg/mL streptomycin; Gibco) at 28°C.

Baby hamster kidney cells (BHK-21) were cultured in Glasgow modified Eagle's medium (GMEM; Gibco) supplemented with 10% FBS, 10% tryptose phosphate broth (TPB; Gibco), and 1% penicillin–streptomycin (Gibco). Cells were maintained at 37°C in a humidified incubator with 5% CO_2.

2.1.2 Viruses

SFV4 expressing firefly luciferase (SFV4(3H)-FFLuc; titre 4.5×10^8 PFU/mL) and wild-type SFV4 (titre 2.5×10^9 PFU/mL) were used in this study. Viral stocks were generated from infectious cDNA clones as described below.

2.1.3 Plasmids

The following plasmids were used in this study: pCMV-SFV4(3H)-FFLuc (Rodriguez-Andres *et al.*, 2012, Varjak *et al.*, 2018), pCMV-SFV4 (Ülper *et al.*, 2008), pPUb-Zeo-2A2A-V5-eGFP (Varjak *et al.*, 2017a), pPUb-Zeo-2A2A-V5-Ago2wt (Varjak *et al.*, 2017b), pGL3-Pub (Anderson *et al.*, 2010), pPUb-RLuc (Alexander *et al.*, 2023), and pPUb-myc-eGFP (Varjak *et al.*, 2017b).

2.1.4 Primer sequences

Table 2-1 Sequences of primers used in this study.

All primer sequences are shown reading from 5' to 3'. Bases in underline indicate overhangs homologous to the destination vector and bases in bold indicate the T7 promoter sequences.

Primer	Sequence 5'-3'	Use
Ago2 mutant F	GAGGCGATATGAGCACCATCAGCAATATTTGGCTC	Generation of Ago2mut construct
Ago2 mutant R	CTCCTTGGTCAGGTTGTTCATGTTCAGAGGACGATC	
Ago2 linearisation F	AACCTGACCAAGGAGTACGAG	
Ago2 linearisation R	TGCTCATATCGCCTCGTTTC	
PUb start FOR	ATCTTTACATGTAGCTTGTG	Plasmid sequencing for pPUb-Zeo-2A2A-V5-Ago2wt
Margus Pub F	GGCGACTATTGAGCTTTGAG	
Ago2 F1	GTCGAGGAGAATCCTGGACCT	
Ago2 F2	GCAACAACAGGGACAGTCATG	
Ago2 F3	GTGGAGGTCAACTACATCC	
Ago2 F4	CAACGGCAGCACGCTCGATAAG	
Ago2 R1	CGTGAAGATCTCTGCTCATCC	
Ago2 R2	GAGCATTGTTGTAGCCGATCTG	
Ago2 R3	CTGTAGTTGGACACCCTGC	
Ago2 R4	CGACGTACATCACCGTTTTGC	
SV40 late REV	CCACATTTGTAGAGGTTTTAC	
T7-eGFP F	**GTAATACGACTCACTATAGGG**GGCGTGCAGTGCTTCAGCCGC	dsRNA
T7-eGFP R	**GTAATACGACTCACTATAGGG**GTGGTTGTCGGGCAGCAGCAC	
T7-FFLuc F	**GTAATACGACTCACTATAGGG**ACTTACGCTGAGTACTTC	
T7-FFLuc R	**GTAATACGACTCACTATAGGG**GAAATCCCTGGTAATCCG	
T7-1 F	**GTAATACGACTCACTATAGGG**GCTGGGTTCTTCTCGCAGATTG	
T7-1 R	**GTAATACGACTCACTATAGGG**CAATGCATCTCACGAATCAATG	
T7-2 F	**GTAATACGACTCACTATAGGG**CGAACTATTGGACGAAATCCTG	
T7-2 R	**GTAATACGACTCACTATAGGG**GACGATCTTATCGTTGATACC	
T7-3 F	**GTAATACGACTCACTATAGGG**GCAGCATTTCGTTCGAGTTG	
T7-3 R	**GTAATACGACTCACTATAGGG**GACGATAGGTCCGAATGCTTC	
T7-4 F	**GTAATACGACTCACTATAGGG**CTCCGTGCATGTTGACGAACG	
T7-4 R	**GTAATACGACTCACTATAGGG**GTACTCATGCTCGAAGGATCC	
T7-5 F	**GTAATACGACTCACTATAGGG**GTGAGGGAGCTATGCAAAGTGC	
T7-5 R	**GTAATACGACTCACTATAGGG**GTGTTGCGTGTTTCCAGTGATC	
T7-6 F	**GTAATACGACTCACTATAGGG**CCACCTACCTGTATATTCC	
T7-6 R	**GTAATACGACTCACTATAGGG**CCGACGATGGTAACTTTACGC	
T7-7 F	**GTAATACGACTCACTATAGGG**GGACAAATGCAAAAAGTGC	
T7-7 R	**GTAATACGACTCACTATAGGG**CTTGTATTGGGGCATGCCCTC	
T7-8 F	**GTAATACGACTCACTATAGGG**GAACAGATGAAGAAGGCTGCC	
T7-8 R	**GTAATACGACTCACTATAGGG**CTGTGGCAACTGGAGCAGTG	
T7-9 F	**GTAATACGACTCACTATAGGG**GAGAACCCCTCGAAGGGAGAAC	
T7-9 R	**GTAATACGACTCACTATAGGG**GACAGCCGCACAATACCTCCAC	
T7-10 F	**GTAATACGACTCACTATAGGG**CTGACCAGCAGGCAGTAAGTG	
T7-10 R	**GTAATACGACTCACTATAGGG**CATCTTCTTGCGTATCGCCACG	
T7-11 F	**GTAATACGACTCACTATAGGG**GACTATCAACCCAGAGTACATC	
T7-11 R	**GTAATACGACTCACTATAGGG**GCGATATCGCTCAGTTTGTTC	
T7-12 F	**GTAATACGACTCACTATAGGG**GAAGATGCGGGAGGCCAACTTC	
T7-12 R	**GTAATACGACTCACTATAGGG**GACCGATACGATGGATGTAC	
T7-13 F	**GTAATACGACTCACTATAGGG**CAGAATCTGGACGGGTACGTG	
T7-13 R	**GTAATACGACTCACTATAGGG**CATCATACCGTTGAGTTCAC	
T7-14 F	**GTAATACGACTCACTATAGGG**GAAGTCTCATCGCAGCAAGG	
T7-14 R	**GTAATACGACTCACTATAGGG**CACTTGTTGGTTCTTCTTCTC	
T7-15 F	**GTAATACGACTCACTATAGGG**GACCACCCGGTTGCGGTAAAACC	
T7-15 R	**GTAATACGACTCACTATAGGG**CACGCAAGGTGAAGCCGAACG	
T7-16 F	**GTAATACGACTCACTATAGGG**CAGTGATCCATTCGATTGCTAC	
T7-16 R	**GTAATACGACTCACTATAGGG**GACGACAGGTGTGGTCTGTC	
T7-17 F	**GTAATACGACTCACTATAGGG**CATCTGGGACGATACGCTCATC	
T7-17 R	**GTAATACGACTCACTATAGGG**GATCTGTTGGGTAGATGTGGAC	
T7-18 F	**GTAATACGACTCACTATAGGG**GCTAGACCAGGGCTACTCAC	
T7-18 R	**GTAATACGACTCACTATAGGG**CTTCCTCGGTGTGGCCATTC	
T7-19 F	**GTAATACGACTCACTATAGGG**CGATCAGCACATGGGCGTTGTG	

Primer	Sequence 5'-3'	Use
T7-19 R	**GTAATACGACTCACTATAGGG**CCTCAGTTGGTGGATTGTAG	
T7-20 F	**GTAATACGACTCACTATAGGG**CATCGGTCAAGGACGCCAGAG	
T7-20 R	**GTAATACGACTCACTATAGGG**CAGATGGTCTGTTTGGCCTTC	
T7-21 F	**GTAATACGACTCACTATAGGG**GCACTCGAATCTTCACCAAC	
T7-21 R	**GTAATACGACTCACTATAGGG**GTTGGAGTGTGTCGCTAGGGAG	
qS7 F	CCAGGCTATCCTGGAGTTG	qPCR
qS7 R	GACGTGCTTGCCGGAGAAC	
qSFV F	GCAAGAGGCAAACGAACAGA	
qSFV R	GGGAAAAGATGAGCAAACCA	
q1 F	AATCGGTGGAAATCGTATCATC	
q1 R	CAGAGCCTTTTTGGTTTGGT	
q2 F	CGGTATGAAGGAAACGCAAC	
q2 R	GCGAACGGAACCTCAAAG	
q3 F	GATGAGATTCAGGACGAGTGTG	
q3 R	CACATCCGTATTGTCATCCTC	
q4 F	CATGGAGGTACGCGATTATG	
q4 R	CAGTTGCGATTTTGTCCACC	
q5 F	GAACAAACCCGATGAACTTAC	
q5 R	CGGGAATACGCCGATTTTAC	
q6 F	GAAATCCTGGTCCCGAGTG	
q6 R	TGGCGTGTTGGTAGTGTGTT	
q7 F	GATCGATTTGGTTCCCTCTC	
q7 R	CGTAAGCGTTCTTGTAGTGG	
q8 F	TCGGAGTGATTCTGGACGA	
q8 R	CTTCTCGGCTTCCTGTTGAG	
q9 F	CGTCACCGTATTCCTACCTCA	
q9 R	ATTGCGTTGTTCCTTTTTGG	
q10 F	AAGCAGCAACCACTTCAACA	
q10 R	TCATTGGGGGACCATCAC	
q11 F	AGTTCCCGAGTCACACCTCA	
q11 R	GCCTTTTCTGCGTCCAAGT	
q12 F	CTTGTATCGGTGGAACAAAC	
q12 R	CTCAGTACCCGACGTTTGATC	
q13 F	GAAGGTACAGGTGTCCACCAG	
q13 R	TACTTTCGGACCAGAGCAGAC	
q14 F	GAGTACAAGGCGCTGGAGATG	
q14 R	CGGATCGATGGTTTTCATTAC	
q15 F	GTGGTGCGCAATAATCTGCG	
q15 R	GACGCAGATACACATCGAAC	
q16 F	GATGAAATGCTTGCTGGTGA	
q16 R	TGACGAGGATGACGAGAGTG	
q17 F	CAAGCGGTCGTATAACGTGG	
q17 R	CATAGCGGATCAGAGCATCTC	
q18 F	AGCAATGTGTCCCAGAGGAG	
q18 R	AGCCGTTGTTTCCAGAGTTG	
q19 F	GCAAAGAAGCCGAAATCAAG	
q19 R	CCGAGTAGAAAGATGAACAGCA	
q20 F	CCGAAAACTGCCTACCAAAA	
q20 R	CAAGCGAAGAACCAAAGGTC	
q21 F	CGGCGACTGGATGCAGAAAAC	
q21 R	CCCTCCTGATCCGTAATCTC	

2.2 Methods

2.2.1 Ago2 mutant generation

A DNA fragment corresponding to nucleotides 2089–2919 of the *Ae. aegypti* Ago2 coding sequence (UniProt ID: C5J0H4) and containing the catalytic tetrad mutations D740A, E780A, D812A, and H950A was synthesised by GeneArt (Thermo Fisher Scientific). The Ago2mut fragment synthesis was performed by Dr. Melanie McFarlane, MRC-University of Glasgow Centre for Virus Research.

The destination plasmid pPUb-Zeo-2A2A-V5-Ago2wt was linearised by PCR to generate a vector backbone suitable for recombination cloning and the fragment of Ago2 mutant was amplified using gene-specific primers containing 15 nt overhangs homologous to the destination vector (Table 2-1). PCR reactions were performed using Phusion High-Fidelity DNA polymerase (Thermo Fisher Scientific). PCR products were purified using the QIAquick PCR purification kit (Qiagen) and DNA concentrations were measured using a NanoDrop spectrophotometer (Thermo Fisher Scientific).

To remove template plasmid DNA, the linearised vector PCR product was treated with *DpnI* (New England Biolabs) at 37°C for 1 hour, followed by purification using the QIAquick PCR purification kit (Qiagen). The synthesised mutant fragment was inserted into the linearised pPUb-Zeo-2A2A-V5-Ago2wt vector using In-Fusion Snap Assembly Master Mix (Takara) according to the manufacturer's instructions. Insert-to-vector ratios were calculated using the Takara In-Fusion molar ratio calculator.

The resulting ligation reactions (5 µL) were transformed into DH5α competent *E. coli* cells according to the manufacturer's protocol (Dummunee *et al.*, 2025). Subsequent cloning procedures are described in Section 2.2.19. The Ago2 mutant construct was then designated pPUb-Zeo-2A2A-V5-Ago2mut.

2.2.2 Production of stable cell lines

AF525 cells were transfected with 5 µg of *NotI*-linearised plasmid DNA (New England Biolabs) using DharmaFECT2 transfection reagent (Horizon Discovery)

according to the manufacturer's instructions to generate stable cell lines. Duplicate stable cell populations were generated for each construct.

At 24 hours post-transfection (h.p.t.), the culture medium was replaced with fresh growth medium containing zeocin (InvivoGen) at a final concentration of 100 µg/mL to select for transfected cells. Selection medium was replaced every 3–4 days for approximately four weeks until stable cell monolayers were established.

Following selection, cells were maintained in growth medium containing zeocin at 200 µg/mL during subsequent experiments (Dummunee *et al.*, 2025).

The constructs were re-sequenced after mutagenesis and subsequent generation of the cell lines to verify the presence of the intended mutations and to confirm that no unintended secondary mutations were introduced during the cloning process.

2.2.3 dsRNA production

Double-stranded RNA (dsRNA) targeting eGFP and firefly luciferase (FFLuc) was generated by *in vitro* transcription. DNA templates were amplified from pPUb-Zeo-2A2A-V5-eGFP and pGL3-PUb plasmids using gene-specific primers containing T7 RNA polymerase promoter sequences at the 5′ end (Table 2-1). PCR amplification was performed using KOD Hot Start DNA polymerase (Novagen).

The resulting PCR products were used as templates for dsRNA synthesis using the MEGAscript RNAi kit (Thermo Fisher Scientific) according to the manufacturer's instructions. Briefly, purified DNA templates were transcribed using T7 RNA polymerase, followed by RNase A and DNase I treatment to remove single-stranded RNA and residual DNA template. The dsRNA products were purified using column-based purification according to the manufacturer's protocol. dsRNA concentrations were measured using a NanoDrop spectrophotometer (Thermo Fisher Scientific).

For dsRNA knockdown experiments, AF5 cells were transfected with 100 ng dsRNA targeting individual transcripts, with dsRNA targeting eGFP used as a non-targeting control. At 24 hours post-transfection, cells were infected with SFV4(3H)-FFLuc at an MOI of 0.1 PFU/cell. At 24 h.p.i., cells were lysed in TRIzol reagent (Thermo

Fisher Scientific) for RNA extraction. Total RNA (1 µg) was used for cDNA synthesis as described in Section 2.2.11.

2.2.4 Transformation of *E. coli*

Plasmid constructs generated by In-Fusion cloning were transformed into chemically competent *E. coli* DH5α cells (Thermo Fisher Scientific). Competent cells were thawed on ice and gently mixed before adding 5 µL of the In-Fusion reaction mixture to 50 µL of competent cells. Transformation reactions were incubated on ice for 30 minutes, followed by heat shock at 42°C for 45 seconds and incubation on ice for 2 minutes. SOC medium (950 µL) was then added, and cells were incubated at 37°C with shaking at 225 rpm for 1 hour to allow recovery.

Following recovery, 200 µL of the transformation mixture was plated onto LB agar plates containing ampicillin (100 µg/mL) and incubated overnight at 37°C. Individual colonies were selected and cultured in LB broth supplemented with ampicillin (100 µg/mL) overnight at 37°C with shaking.

Individual colonies were screened by colony PCR. For each construct, at least eight colonies were picked using sterile pipette tips and streaked onto fresh LB agar plates containing ampicillin (100 µg/mL). The same pipette tip was then used to inoculate a GoTaq G2 PCR reaction containing construct-specific primers.

Colonies that yielded the correct PCR products were selected for small-scale plasmid preparation using the QIAprep Spin Miniprep Kit (Qiagen) according to the manufacturer's instructions. Plasmid constructs were verified by Sanger sequencing (Eurofins Genomics).

2.2.5 Transfection of BHK-21 cells SFV production

BHK-21 cells were used for the recovery and amplification of SFV from infectious cDNA clones. Cells were seeded at approximately 3×10^5 cells per well in 6-well plates and incubated overnight at 37°C with 5% CO_2.

The following day, cells were transfected with 1 µg of plasmid DNA (pCMV-SFV4(3H)-FFLuc or pCMV-SFV4) using DharmaFECT2 transfection reagent (Horizon Discovery) according to the manufacturer's instructions. At 72 hours post-transfection (h.p.t.), cell culture supernatants containing recombinant virus were harvested and clarified by centrifugation at 2,000 rpm for 10 minutes to remove cell debris.

Clarified supernatants were subsequently used to infect BHK-21 cells grown in T175 cm² flasks to amplify virus stocks. Infected cultures were incubated at 37°C for 48–72 hours until extensive cytopathic effect (CPE) was observed. Supernatants were then collected and clarified by centrifugation at 2,000 rpm for 10 minutes at 4°C. Virus stocks were aliquoted and stored at −70°C until further use.

2.2.6 Plaque assay

Virus titres were determined by plaque assay using BHK-21 cells. Cells were seeded in 6-well plates at a density of 1.8×10^5 cells per well and incubated overnight at 37°C with 5% CO_2. The following day, growth medium was removed and 200 µL of 10-fold serial dilutions of virus samples were added to the cells.

Plates were incubated for 1 hour at 37°C to allow virus adsorption, with gentle rocking every 15 minutes. After adsorption, the inoculum was removed and cells were overlaid with 2 mL of overlay medium consisting of a 1:1 mixture of 2× MEM supplemented with 4% FBS and 1.2% Avicel (FMC BioPolymer). Following incubation for 48 hours at 37°C, cells were fixed by adding 1 mL of 10% formalin (Merck) to each well and incubating for 1 hour.

The overlay was then removed, and cells were rinsed with water before staining with 0.1% toluidine blue (Merck) for 20 minutes with gentle shaking. Plates were washed with water, air-dried, and plaques were counted to calculate virus titres expressed as plaque-forming units per millilitre (PFU/mL).

2.2.7 Western blotting

Cells were harvested by scraping and pelleted by centrifugation at 200 × g for 5 minutes at room temperature. Cell pellets were lysed in 1× LDS sample buffer supplemented with 1× reducing agent (Thermo Fisher Scientific) and stored at −20°C.

For analysis, 10 µL of lysate was treated with 1 µL benzonase (Merck) to degrade nucleic acids and incubated at 95°C for 5 minutes. Samples were separated by SDS-PAGE on 4–12% Bis-Tris gels (Thermo Fisher Scientific). A LI-COR Chameleon molecular weight ladder (5 µL; LI-COR) was included as a protein size marker. Electrophoresis was performed at 110 V for 1.5 hours.

Proteins were transferred to nitrocellulose membranes (8.5 × 6.5 cm) using a semi-dry transfer system in 1× transfer buffer at 15 V for 30 minutes. Membranes were blocked for 1 hour at room temperature in blocking buffer consisting of 5% (w/v) skimmed milk in PBS-T.

Membranes were incubated overnight at 4°C with primary antibodies diluted in blocking buffer: mouse anti-V5 (1:2000; Abcam, ab27671) and mouse anti-α-tubulin (1:2000; Merck, T5168). Following incubation, membranes were washed three times with PBS-T and incubated with goat anti-mouse IgG secondary antibody (1:5000; LI-COR) for 1 hour at room temperature.

Membranes were washed twice with PBS-T followed by a final wash with distilled water. Protein bands were visualised using a LI-COR Odyssey DLx imaging system.

2.2.8 Growth curve of cells

Stable cell lines were seeded at a density of 8×10^4 cells per well in 24-well plates. Cell growth was monitored over time by counting cells at 0, 24, 48, 72, and 96 hours post-seeding.

At each time point, cells were detached by scraping and resuspended thoroughly. A 10 µL aliquot of the cell suspension was used for cell counting. Cell numbers were

determined using a Bio-Rad automated cell counter with Bio-Rad cell counting slides according to the manufacturer's instructions.

2.2.9 Viral replication assay

Cells were seeded at a density of 2.3 × 10^5 cells per well in 24-well plates. At 24 hours post-seeding, cells were infected with SFV4(3H)-FFLuc at multiplicities of infection (MOIs) of 0.1, 1, or 10.

At 24 hours post-infection (h.p.i.), cells were lysed in 1× Passive Lysis Buffer (PLB; Promega). Firefly luciferase activity was measured using the Firefly Luciferase Assay System (Promega) according to the manufacturer's instructions. Luminescence was quantified using a GloMax luminometer (Promega).

2.2.10 RNAi reporter assays

Cells were seeded at a density of 2.3 × 10^5 cells per well in 24-well plates. The following day, cells were co-transfected with plasmids expressing firefly luciferase (FFLuc; 50 ng) and Renilla luciferase (RLuc; 20 ng), the latter serving as an internal control. To induce RNAi-mediated silencing, cells were transfected with 20 ng of dsRNA targeting either FFLuc or eGFP (non-targeting control).

At 24 hours post-transfection (h.p.t.), cells were lysed in 1× Passive Lysis Buffer (PLB; Promega) and stored at −20°C. Firefly and Renilla luciferase activities were measured using the Dual-Luciferase Reporter Assay System (Promega) according to the manufacturer's instructions. Luminescence was quantified using a GloMax luminometer (Promega). Relative luciferase activity was calculated by normalising firefly luciferase activity to Renilla luciferase activity.

2.2.11 RT-qPCR

Cells were seeded at a density of 2.3 × 10^5 cells per well in 24-well plates. At 24 hours post-seeding, cells were infected with SFV4 at a multiplicity of infection (MOI) of 0.1. At 24 hours post-infection (h.p.i.), cells were lysed in 333 µL TRIzol reagent (Thermo Fisher Scientific) per well. Material from three wells was pooled for RNA extraction.

Total RNA was extracted according to the manufacturer's instructions. For cDNA synthesis, 1 µg of total RNA was reverse transcribed using SuperScript III reverse transcriptase (Thermo Fisher Scientific) and oligo$(dT)_{15}$ primers (Promega) as previously described (Schnettler *et al.*, 2013).

Quantitative PCR was performed using 2 µL of cDNA with gene-specific primers and SYBR Green master mix (Thermo Fisher Scientific). Amplification was carried out using a QuantStudio 3 Real-Time PCR System (Applied Biosystems). Expression of the SFV4 nsP3 gene was quantified and normalised to the ribosomal protein S7 transcript, which served as an internal control.

2.2.12 Cell preparation for small RNA sequencing and proteomics studies

For small RNA sequencing experiments, cells were seeded at a density of 7.6 × 10^6 cells per T25 cm² flask. After 24 hours, cells were infected with SFV4 at a multiplicity of infection (MOI) of 5. At 24 hours post-infection (h.p.i.), cells were harvested by centrifugation and lysed in 700 µL of IP lysis buffer (20 mM Tris-HCl pH 7.5, 150 mM NaCl, 5 mM $MgCl_2$, 0.5% NP-40) supplemented with protease inhibitors (cOmplete EDTA-free tablets, Roche) and phosphatase inhibitors (PhosSTOP, Roche).

For proteomics experiments, cells were seeded at the same density (7.6 × 10^6 cells per T25 cm² flask) in four biological replicates. After 24 hours, cells were either mock-infected or infected with SFV4 at an MOI of 5. At 24 h.p.i., cells were harvested and lysed in 1.4 mL of IP lysis buffer containing protease and phosphatase inhibitors as described above.

2.2.13 Immunoprecipitation (IP)

Cell lysates were clarified by centrifugation at 16,000 × g for 20 minutes at 4°C. The clarified supernatant was transferred to tubes containing 20 µL of protein G Dynabeads (Thermo Fisher Scientific) pre-bound to anti-V5 antibody and resuspended in IP lysis buffer.

To confirm protein expression prior to immunoprecipitation, 50 µL of clarified lysate was mixed with 10 µL of 1× LDS sample buffer (Thermo Fisher Scientific) and 4 µL of 1× reducing agent. Samples were heated at 95°C for 5 minutes and stored at −20°C for subsequent western blot analysis.

The remaining lysate was incubated with the Dynabeads–anti-V5 complex overnight at 4°C with rotation. The following day, beads were washed three times with wash buffer (50 mM Tris-HCl pH 7.5, 200 mM NaCl, 1 mM EDTA, 1% NP-40 supplemented with protease inhibitors).

Bound proteins were eluted in 60 µL of 100 mM triethylammonium bicarbonate (TEAB) containing 5% SDS. An aliquot (10 µL) of the eluted sample was reserved for western blot analysis.

2.2.14 Silver Staining

Immunoprecipitated protein samples were analysed by silver staining using the Pierce™ Silver Stain Kit (Thermo Fisher Scientific) according to the manufacturer's instructions. Silver staining was used to assess protein recovery following immunoprecipitation.

Protein expression and enrichment were further confirmed by western blotting of samples collected before and after immunoprecipitation. The remaining immunoprecipitated protein samples were submitted to the FingerPrints Proteomics Facility (University of Dundee) for downstream proteomic analysis.

2.2.15 Coomassie Protein Staining

The immunoprecipitated protein samples were electrophoresed and analysed by Coomassie blue staining (Abcam) according to the manufacturer's instructions. Gels were imaged on a Gel Imaging system (Thermo Fisher Scientific). BCA protein assays were used to quantify the concentration of protein present in each sample. Protein intensity was measured and assessed through comparison to a BSA protein standard curve.

2.2.16 Small RNA library construction and sequencing

Small RNA sequencing was performed by BGI (Beijing Genomics Institute) using their Small RNA Library Construction Protocol (DNBSEQ). 1µg of total RNA per sample was size separated via PAGE gel and products of 15-40nt were selected. The selected products first underwent 3' adaptor ligation by incubating at 70°C for 2 minutes, holding on ice for 1 minute then incubating at 25°C for 2 hours then holding at 4°C, the products then underwent 5' adaptor ligation by incubating at 70°C for 2 minutes, holding on ice for 1 minute, then incubating at 25°C for 1 hour before finally holding at 4°C. Reverse transcription was then carried out using the RT primer to the reaction and incubating at 65°C for 3 minutes and placing on ice for 1 minute. The RT mix containing FS reaction buffer, RNase inhibitor and the RT enzyme was prepared on ice and added to the reaction. The reaction was incubated at 42°C for 1 hour then 70°C for 15 minutes following by a hold at 4°C. Amplification was performed using a PCR primer mix. The reaction conditions consisted of an initial denaturation at 95°C for 3 minutes, followed by 16-17 cycles of 98°C for 20 seconds, 56°C for 15 seconds, 72°C for 15 seconds. A final extension of 10 minutes was carried out at 72°C followed by a 4°C hold. The PCR products were purified from PAGE gel and eluted in EB buffer. The products were circularised to form ssCir DNA libraries. The final libraries were quality assessed using an Agilent Technologies Fragment bioanalyzer. The library was sequenced on a DNBSEQ-G400 instrument, configured for 50 bases single-end reads.

2.2.17 Small RNA sequencing and analysis

Fastq files were cleaned up using fastp tool (v0.23.2) to trim adapters and remove poor quality reads under default conditions leaving reads lengths of 16-30 nt (Chen *et al.*, 2018). Using Bowtie2 (v2.4.5), the cleaned up reads were then mapped to the SFV genome (GenBank ID: KP699763) using the sensitive mapping flag (—sensitive) (Langmead and Salzberg, 2012). A histogram of read lengths and the first nucleotide bias graph was generated using viral_sRNA_tools/3_bam_sRNA_histogram.sh script, which utilises samtools (v1.16.1). The output files from Bowtie2 were then filtered to contain only 21nt read lengths. The coverage for each position in the SFV genome was calculated using the bedtools genome coverage tool and displayed in GraphPad Prism (v.10.0.2) (Quinlan and Hall, 2010). To determine the overlapping vsiRNAs, the overlap probability score (z-score) was calculated using the small RNA signatures Python script signature.py with settings of (--minquery 21 --maxquery 21 --mintarget 21 --maxtarget 21 --minscope 1 --maxscope 21) (Antoniewski, 2014). Paired reads were then normalised to “number of million reads per library” (Antoniewski, 2014).

Small RNA sequencing generated in this thesis have been deposited in the NCBI Sequence Read Archive (SRA), available under accession number PRJNA1057508. The Scripts used for the small RNA analysis are available from in the viral_sRNA_tools GitHub repository at https://github.com/rhparry/viral_sRNA_tools. Small RNA sequencing analysis was performed by Dr. Rhys Parry, University of Queensland.

2.2.18 Luciferase assay and catalytic tetrad activity

To assess the effect of catalytic tetrad mutations on viral replication, cells were seeded at a density of 2.3×10^5 cells per well in 24-well plates. At 24 hours post-seeding, cell monolayers were infected with SFV4(3H)-FFLuc at multiplicities of infection (MOIs) of 0.1, 1, or 10 PFU/cell. At 24 hours post-infection (h.p.i.), cells were lysed and viral replication was quantified by measuring firefly luciferase (FFLuc) activity as described above.

For dsRNA knockdown experiments, AF5 cells were seeded at a density of 2.3×10^5 cells per well in 24-well plates and incubated at 28°C for 24 hours. Cells were transfected with 100 ng dsRNA targeting transcripts of candidate proteins (21

different conditions in total), with dsRNA targeting eGFP used as a non-targeting control. At 24 hours post-transfection (h.p.t.), cells were infected with SFV4(3H)-FFLuc at an MOI of 0.1 PFU/cell. At 24 h.p.i., cells were lysed and firefly luciferase activity was measured to determine the effect of gene knockdown on viral replication.

2.2.19 Infection

For infection experiments, cells were seeded in 24-well plates or T25 cm² flasks and allowed to reach approximately 80% confluence prior to infection. The multiplicity of infection (MOI) was calculated using the standard formula shown below:

$$Volume\ virus\ stock\ (ml)\ = \frac{Number\ of\ cells\ \times\ Number\ of\ wells\ \times\ MOI}{Virus\ titre}$$

Virus inoculum was freshly prepared for each experiment. The required volume of virus stock was diluted in L-15 complete medium to a total volume of 200 µL for infection of cells in 24-well plates or 2 mL for T25 cm² flasks.

Growth medium was removed from the cells and replaced with the virus inoculum. Cells were incubated at 28°C for 1 hour to allow virus adsorption. Following adsorption, additional L-15 complete medium was added to a final volume of 1 mL per well in 24-well plates or 5 mL per T25 cm² flask.

Cells were then incubated at 28°C for 24 hours prior to downstream analyses.

2.2.20 In-Fusion cloning

Destination vectors were linearised by PCR. Inserts containing the gene or region of interest were amplified using PCR primers (Table 2-1) designed with 15–20 bp extensions homologous to the ends of the destination vector.

The linearised vector and PCR-amplified insert fragments were purified using a PCR purification kit (Qiagen) according to the manufacturer's instructions. The vector PCR product was treated with *DpnI* (New England Biolabs) to remove residual template plasmid DNA, followed by purification using the PCR purification kit (Qiagen) to remove enzyme and buffer components.

Cloning reactions were assembled using the In-Fusion® SNAP Assembly Master Mix (Takara) in a total reaction volume of 5 µL. Each reaction contained 1 µL of 5× In-Fusion enzyme premix, 0.5 µL of linearised vector (50–100 ng), 0.5 µL of insert DNA (50–100 ng), and 3 µL of nuclease-free water.

The reaction mixture was incubated at 50°C for 15 minutes in a thermal cycler before transformation into competent bacterial cells.

2.2.21 Plasmid amplification and isolation

For plasmid mini-preparation, PCR-positive colonies were inoculated into 5 mL LB broth supplemented with ampicillin (100 µg/mL) and incubated overnight at 37°C with shaking at 225 rpm. Plasmid DNA was isolated from the small-scale cultures using the QIAprep Spin Miniprep Kit (Qiagen) according to the manufacturer's instructions.

Purified plasmid DNA was quantified using a NanoDrop spectrophotometer (Thermo Fisher Scientific), and an aliquot was submitted for Sanger sequencing using the appropriate cloning primers.

Following sequence verification, 100 µL of the overnight culture was used to inoculate 100 mL LB broth supplemented with ampicillin (100 µg/mL). Cultures were incubated overnight at 37°C with shaking at 225 rpm.

Bacterial cultures were harvested by centrifugation at 4,000 × g for 15 minutes at room temperature. Plasmid DNA was then extracted using a plasmid MaxiPrep kit (Invitrogen) according to the manufacturer's instructions.

2.2.22 Polymerase Chain Reaction (PCR)

Polymerase Chain Reaction (PCR) was performed using KOD Hot Start DNA polymerase (Novagen) for high-fidelity amplification and GoTaq® G2 Flexi DNA polymerase (Promega) for standard amplification reactions.

PCR reactions were carried out in a total volume of 50 µL using the reaction mixes and cycling conditions described in Table 2-2 and 2-3, following the manufacturer's instructions.

Table 2-2 KOD Hot Start DNA Polymerase PCR reactions and conditions

KOD Hot Start DNA Polymerase Reaction	**1X**	**Conditions**		
KOD Hot start MasterMix DNA polymerase (0.04 U/µL)	25 µL	Initial denaturation (95°C)	2 minutes	1 cycle
KOD Hot start MasterMix DNA polymerase (0.04 U/µL)	25 µL	Initial denaturation (95°C)	2 minutes	30 cycles
10 µM Forward (5') primer	1.5 µL	Denaturation (95°C)	20 seconds	
10 µM Reverse (3') primer	1.5 µL	Annealing – (varying)	10 seconds (<500 bp)	
DNA (10 ng plasmid DNA/100 ng genomic DNA)	X µL	Extension – (70°C)	10 seconds/kb	
Nuclease-free H_2O	Y µL	Hold at 4°C	∞	1 cycle
Total	**50 µL**			

Table 2-3 GoTaq® G2 Flexi DNA polymerase PCR reactions and conditions

GoTaq® G2 Flexi DNA polymerase				
Reaction	**1X**	**Conditions**		
5X GoTaq Flexi buffer	10 µL	Initial denaturation – 95°C	2 minutes	1 cycle
25 mM $MgCl_2$	4 µL	Denaturation - 95°C	30 seconds	30 cycles
10 mM dNTPs	1 µL	Annealing – vary	30 seconds	
10 µM Forward (5') primer	1 µL	Extension – 72°C	1 minute/kb	
10 µM Reverse (3') primer	1 µL	Final extension – 72°C	7 minutes	1 cycle
DNA	(*)	Hold at 4°C	∞	
GoTaq® G2 Flexi DNA polymerase (5 U/µL)	0.5 µL			
Nuclease-free H_2O	32.5 µL			
Total	**50 µL**			

* DNA was used from bacterial colony submerged into the reaction mix using a pipette tip.

2.2.23 Agarose gel electrophoresis

Agarose gel electrophoresis was used to analyse plasmid and PCR products. Gels containing 0.7% agarose were used for plasmid DNA and 1% agarose gels were used for PCR products. Agarose (Invitrogen) was dissolved in 1× TAE buffer containing ethidium bromide (3 µL per 100 mL gel).

DNA samples were mixed with 6× DNA loading dye prior to electrophoresis. A 1 kb Plus DNA ladder (Thermo Fisher Scientific) was used as a molecular weight marker. Electrophoresis was performed at 100 V for 30 minutes. DNA bands were visualised using a UV transilluminator.

2.2.24 Gel Extraction

PCR products were separated by agarose gel electrophoresis, and the DNA bands of the expected size were excised using a sterile scalpel. Gel fragments were transferred to microcentrifuge tubes and DNA was purified using the QIAquick Gel

Extraction Kit (Qiagen) according to the manufacturer's instructions. Purified DNA samples were stored at −20°C.

2.2.25 Restriction enzyme digestion

DpnI digestion (New England Biolabs) was used to remove residual template plasmid DNA following PCR amplification. *DpnI* specifically cleaves methylated DNA, allowing selective digestion of the parental plasmid template.

Digestion reactions contained 17 µL DNA, 2 µL of 10× digestion buffer, and 1 µL *DpnI* enzyme. Reactions were incubated at 37°C for 20 minutes followed by heat inactivation at 80°C for 5 minutes. Digested products were subsequently analysed by agarose gel electrophoresis and purified where required.

2.2.26 Mass spectrometry

Immunoprecipitated protein samples derived from *Ae. aegypti* cell cultures were submitted to the FingerPrints Proteomics Facility (University of Dundee, UK) for mass spectrometry analysis. Samples were processed at the facility using S-Trap–based protein digestion followed by peptide clean-up prior to mass spectrometric analysis. Peptide concentrations were quantified prior to analysis.

Peptide mixtures were analysed by nano-liquid chromatography coupled to tandem mass spectrometry (nLC-MS/MS). Data-independent acquisition (DIA) was performed using an Ultimate 3000 RSLC nano-LC system (Thermo Fisher Scientific) coupled to an Orbitrap mass spectrometer (Thermo Fisher Scientific).

Raw mass spectrometry data were initially processed at the FingerPrints Proteomics Facility using Spectronaut Pulsar X software. For downstream analysis performed in this study, raw data files were analysed using MaxQuant for label-free quantification. Database searches were conducted against the *Ae. aegypti* proteome together with the SFV proteome and the enhanced green fluorescent protein (eGFP) sequence.

2.3 Software Packages

2.3.1 Bioinformatics and qPCR analysis

- Primer sequences were designed using Benchling and the NIH Primer-BLAST online tool.

- RT-qPCR data were acquired and analysed using QuantStudio software (Thermo Fisher Scientific).

- Mass spectrometry datasets were analysed using MaxQuant (Cox & Mann, 2008), Perseus (Tyanova et al., 2016), and R (version 4.3.1).

- Functional annotation and downstream analysis of identified proteins were performed using resources available through VectorBase.

2.3.2 Graphing, statistical analysis and figures

- Statistical analyses and graph generation were performed GraphPad Prism (version 10).

- Diagrams and schematic figures were generated using BioRender.

- Statistical analysis of mass spectrometry datasets was performed in R using an empirical Bayes moderated t-test, with p-values adjusted for multiple testing using the Benjamini–Hochberg correction.

Chapter 3: Characterisation of *Ae. aegypti*-derived Ago2 and its antiviral activity

Chapter 3 Characterisation of *Ae. aegypti*-derived Ago2 and its antiviral activity

3.1 Introduction

Arboviruses are transmitted by arthropod vectors and are predominantly RNA viruses, which can be grouped by genome type. These include linear positive-sense single-stranded RNA viruses (e.g., *Togaviridae* [genus *Alphavirus*], *Flaviviridae*), linear negative-sense single-stranded RNA viruses (*Rhabdoviridae*), segmented negative-sense RNA viruses (class *Bunyaviricetes*), or segmented linear double-stranded RNA viruses (Reoviridae) (Liu *et al.*, 2019, Kuhn *et al.*, 2024). Mosquitoes are key vectors for many arboviruses belonging to the families *Flaviviridae* and *Togaviridae* (genus Alphavirus), as well as viruses within the class *Bunyaviricetes*.

RNAi pathways act as a defence mechanism against viruses and other genomic parasites (Blair and Olson, 2015, Nandety *et al.*, 2015, Olson and Blair, 2015, Agboli *et al.*, 2019, Silver *et al.*, 2021). In mosquitoes, these innate immune pathways regulate arboviral infections by restricting viral replication to levels that do not significantly reduce mosquito lifespan while still permitting virus transmission. This balance is essential for maintaining vector competence (Blair and Olson, 2015, Samuel *et al.*, 2018, Gestuveo *et al.*, 2022b, Dong and Dimopoulos, 2023). Three major classes of small non-coding RNAs and their associated pathways participate in RNAi: short interfering RNAs (siRNAs), microRNAs (miRNAs), and PIWI-interacting RNAs (piRNAs). These classes differ primarily in their biogenesis pathways and biological functions (Olina *et al.*, 2018). Among them, the exo-siRNA pathway is considered the major antiviral RNAi response controlling virus replication in arthropod vectors (Blair and Olson, 2015).

The exo-siRNA pathway is triggered by double-stranded RNA (dsRNA) generated during viral replication. These dsRNA molecules are recognised and processed by the RNase III enzyme Dcr2. During arbovirus replication, viral RNA synthesis produces intracellular dsRNA intermediates that activate the exo-siRNA pathway and initiate antiviral responses (Olson and Blair, 2015). Dcr2 cleaves viral dsRNA into virus-derived small interfering RNAs (vsiRNAs), which in mosquitoes are typically 21 nucleotides in length. These vsiRNA duplexes are then incorporated into the RNA-induced silencing complex (RISC). Within this complex, Argonaute-2

(Ago2) retains one strand of the duplex as a guide strand while the passenger strand is degraded. The guide strand directs Ago2 to complementary viral RNA sequences, which are subsequently cleaved by Ago2 endonuclease activity (Agboli *et al.*, 2019, Bonning and Saleh, 2021, Scherer *et al.*, 2021).

Argonaute proteins are highly conserved across evolution and are widely expressed in almost all eukaryotic organisms. Based on their structure and mechanisms of action, eukaryotic Argonautes can be classified into three main clades: AGO, PIWI (P-element induced wimpy testis), and WAGO (worm-specific Argonautes). Ago proteins typically contain four major domains: the N-terminal domain, PAZ (PIWI-Argonaute-Zwille), MID (middle), and PIWI domains (Tolia and Joshua-Tor, 2007, Olina *et al.*, 2018, Rubio *et al.*, 2018) (Figure 3A-1). The catalytic active site of Ago proteins is located within the PIWI domain, which adopts a conserved RNase H-like fold (Song *et al.*, 2004, Jin *et al.*, 2021). This RNase H fold is essential for endonuclease activity and target RNA cleavage. In many RNase H enzymes, the catalytic site consists of a conserved Asp-Glu-Asp-Asp (DEDD) tetrad. However, not all Ago proteins retain this canonical motif (Jin *et al.*, 2021). In several Argonaute proteins the catalytic residues form a DEDX motif (where X can be N, D or H). This catalytic tetrad is common in many prokaryotic Ago proteins. In contrast, some Argonaute proteins are catalytically inactive. For example, human Ago1 (hAgo1) and hAgo4 lack slicer activity due to alterations in this catalytic motif (Hauptmann *et al.*, 2013, Jin *et al.*, 2021). Experimental insertion of the DEDH motif into the PIWI domain of hAgo1 has been shown to restore endonuclease activity. Among the four human Argonaute proteins (hAgo1–4), only hAgo2 exhibits slicer activity (Song *et al.*, 2004, Olina *et al.*, 2018, Jin *et al.*, 2021).

SFV belongs to the genus Alphavirus within the family *Togaviridae*. In humans, SFV infection typically causes mild febrile illness, whereas it is highly pathogenic in rodents. SFV is widely used as a model virus for studying viral replication, host–virus interactions, and innate immune responses (Atkins *et al.*, 1985, Kim *et al.*, 2004, Mazzon *et al.*, 2018). Alphavirus replication produces dsRNA intermediates that are recognised by the siRNA pathway (Myles *et al.*, 2008, Siu *et al.*, 2011). Previous studies have shown that absence of Ago2 results in increased SFV replication and viral RNA levels, indicating that SFV is particularly sensitive to Ago2-mediated antiviral responses, whereas replication of other arboviruses such as ZIKV

is not significantly affected under similar conditions (Scherer *et al.*, 2021). Therefore, SFV provides a useful experimental model to investigate Ago2-dependent antiviral mechanisms.

In this chapter, the catalytic tetrad within the PIWI domain of *Ae. aegypti* Ago2 was examined to determine its role in antiviral RNAi activity. Using the established SFV infection model, this study aimed to investigate whether the catalytic residues required for Ago2 slicing activity contribute to antiviral responses in mosquito cells.

3.2 Objectives

Given the limited understanding of Argonaute-2 function in mosquito antiviral RNA interference, this chapter aimed to investigate whether the catalytic residues within the PIWI domain of *Ae. aegypti* Ago2 contribute to antiviral RNAi activity. Using SFV as a model arbovirus system, the functional relevance of the Ago2 catalytic tetrad was examined through a combination of sequence analysis, mutagenesis, infection assays, and small RNA profiling.

Specifically, this chapter aimed:

1. To determine whether a conserved catalytic tetrad is present within the PIWI domain of *Ae. aegypti* Ago2.

2. To determine whether the catalytic tetrad is required for Ago2-mediated antiviral activity against SFV.

3. To investigate the effect of catalytic tetrad mutation on RNAi silencing activity and virus-derived small RNA processing.

3.3 Results

3.3.1 Identification of the Ago2 catalytic tetrad in mosquitoes

Previous studies have reported the presence of a catalytic tetrad containing DEDX (X = N, D, or H) in Argonaute proteins from humans, bacteria, and yeast; however, functional characterisation of these catalytic residues in mosquito Ago2 remains limited (Jin *et al.*, 2021). Because the catalytic tetrad is located within the PIWI domain and is responsible for the endonuclease “slicer” activity of Argonaute proteins, identifying whether these residues are conserved in mosquito Ago2 is important for understanding its potential role in antiviral RNAi responses.

In this study, a potential Ago2 catalytic tetrad was investigated across four insect species: *Ae. aegypti*, *Ae. albopictus*, *Anopheles gambiae*, and *D. melanogaster*. These species were selected because they represent important mosquito vectors as well as the model insect *D. melanogaster*, in which RNAi pathways have been extensively characterised. Multiple sequence alignment of Ago2 protein sequences from these species was performed to identify conserved residues within the PIWI domain.

The alignment revealed conserved amino acids corresponding to a potential Ago2 catalytic tetrad at positions D740, E780, D812, and H950 (relative to the *Ae. aegypti* Ago2 sequence) in all four species analysed (Figure 3-1B). The conservation of these residues across dipteran species suggests that the catalytic tetrad is likely maintained as part of the functional architecture of Ago2. These conserved residues within the PIWI domain are predicted to form the catalytic centre responsible for Ago2-mediated target RNA cleavage and therefore represent key determinants of Ago2 slicing activity.

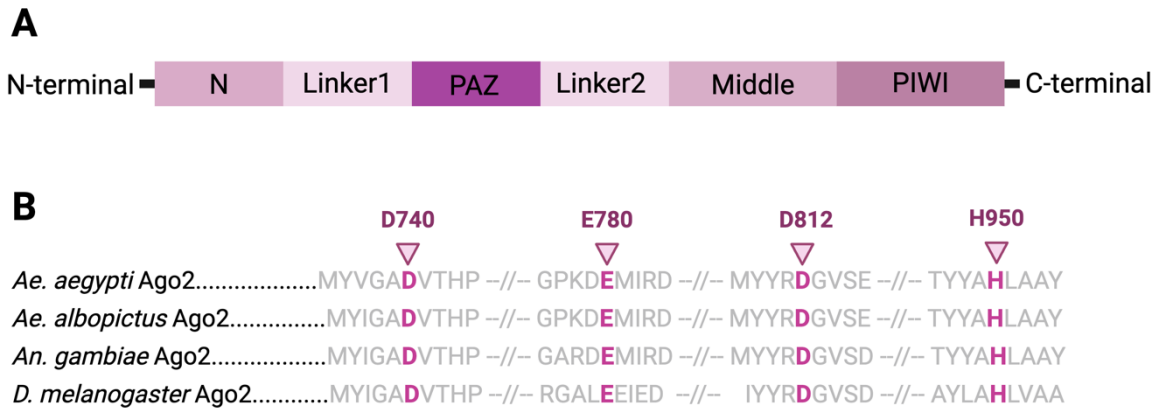

Figure 3-1 Multiple sequence alignment of the conserved DEDH motif in mosquito Ago2 proteins.

(A) Schematic diagram of the Ago2 domain structure. (B) Multiple amino acid sequence alignment of the catalytic DEDH motif among *Ae.* aegypti Ago2 (UniProt ID: C5J0H4), *Ae.* albopictus Ago2 (UniProt ID: I3VLA6), *An. gambiae* Ago2 (UniProt ID: A0A453Z118), and *D. melanogaster* Ago2 (UniProt ID: Q9VUQ5). Ago2 protein sequences were aligned using Benchling (https://www.benchling.com/). Conserved residues corresponding to the catalytic tetrad (D740, E780, D812, and H950) are numbered relative to the Ae. aegypti Ago2 sequence.

3.3.2 Expression of Ago2 in stable cell lines

To determine whether the identified catalytic tetrad was essential for Ago2 function in *Ae. aegypti*, the DEDH motif was mutated to assess its role in slicing activity. The DEDH residues in the pPUb-Zeo-2A2A-V5-Ago2wt plasmid previously described by Varjak *et al*. (2017b) were mutated to alanine to generate the pPUb-Zeo-2A2A-V5-Ago2mut construct. This construct, together with the previously generated pPUb-Zeo-2A2A-V5-Ago2wt plasmid, was used to generate cell lines constitutively expressing these proteins. The AF525 cell line was used for these experiments because it is an Ago2 knockout cell line lacking endogenous Ago2 activity (Fredericks *et al.*, 2019, Scherer *et al.*, 2021).

AF525 cells were transfected with pPUb-Zeo-2A2A-V5-Ago2wt, pPUb-Zeo-2A2A-V5-Ago2mut, and pPUb-Zeo-2A2A-V5-eGFP, which served as the control construct previously generated (Varjak *et al.*, 2017b). Zeocin was used as the selection agent during passaging to isolate AF525 cells stably expressing V5-tagged Ago2wt, Ago2mut, or eGFP. Two independent clones were generated for each construct. Protein expression in the stable cell lines was assessed by Western blotting before and after freezing of the stocks. AF525-V5-Ago2wt, AF525-V5-Ago2mut, and AF525-V5-eGFP all expressed the proteins of interest between passages 0 and 20 (Figure 3-2A). These cell lines were subsequently stored in liquid nitrogen between passages 5 and 25. Protein expression following thawing and extended passaging was further evaluated by Western blot analysis at passages 5, 10, 20, and 25 (Figure 3-2B).

The growth properties of the two clones generated for each stable cell line were also assessed to determine whether insertion of the constructs affected cell proliferation. Cells were seeded at a density of 8×10^4 cells per well in a 24-well plate and counted at 0, 24, 48, 72, and 96 hours post-seeding. The resulting growth curves demonstrated that all clones exhibited comparable growth characteristics (Figure 3-2C and 3-2D).

Both stable cell line clones showed similar protein expression profiles and comparable growth properties under the conditions tested, suggesting that they behaved similarly. As no substantial differences were observed between the clones, clone 1 was selected for all subsequent experiments described in this study.

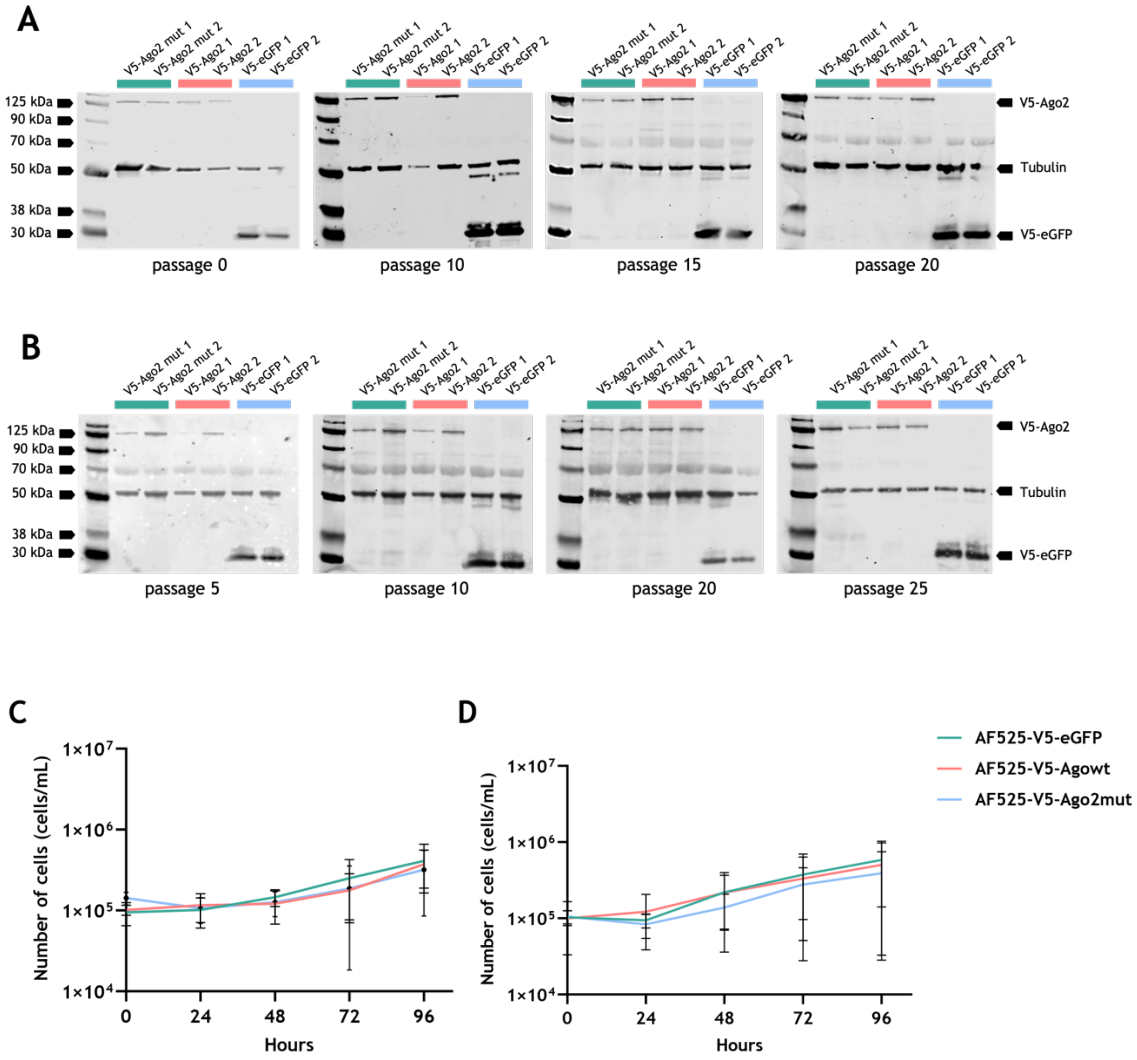

Figure 3-2 Protein expression and growth properties of AF525-V5-Ago2wt, AF525-V5-Ago2mut, and AF525-V5-eGFP stable cell lines.

(A) Expression of the proteins of interest in cell lysates from the stable cell lines following initial generation (passages 0, 10, 15, and 20) and (B) after thawing from frozen stocks (passages 5, 10, 20, and 25). V5-tagged proteins were detected in both Ago2 and eGFP expressing cell lines using an anti-V5 antibody, with tubulin used as a loading control. Growth curves of both clones of the stable cell lines were measured at 0, 24, 48, 72, and 96 hours post-seeding. Panels (C) and (D) show the growth curves for clone 1 and clone 2 of each cell line, respectively. Each time point represents the mean ± SD of experiments performed in triplicate.

3.3.3 The DEDH catalytic tetrad is critical for antiviral Ago2 function

To investigate the antiviral activity of Ago2, SFV replication levels were assessed in AF525 clone 1 cell lines (AF525-V5-Ago2wt, AF525-V5-Ago2mut, and AF525-V5-eGFP). Cells were infected with luciferase-expressing SFV4(3H)-FFLuc. Luciferase activity was used as a proxy for viral replication because reporter expression

depends on viral replicative processes. Luciferase activity was significantly increased in AF525-V5-Ago2mut cells infected with SFV4(3H)-FFLuc compared with AF525-V5-Ago2wt cells, indicating impaired antiviral activity when the catalytic tetrad was mutated (Figure 3-3A). In addition, no substantial difference in viral replication levels was observed between the Ago2 mutant cell line and the eGFP control cells (Figure 3-3A). These results indicate that the slicer activity associated with the catalytic tetrad is required for the antiviral function of Ago2 against this alphavirus.

To further confirm the antiviral activity of Ago2, viral replication was also quantified by RT-qPCR and plaque assay following SFV4 infection. Significantly higher viral genome copy numbers were detected in Ago2mut cells compared with Ago2wt cells (Figure 3-3B). Consistent with this result, plaque assays showed an approximately 1000-fold increase in virus titre in the mutant cells compared with the wildtype cells (Figure 3-3C). Together, these results demonstrate that the catalytic tetrad is required for effective antiviral Ago2 activity.

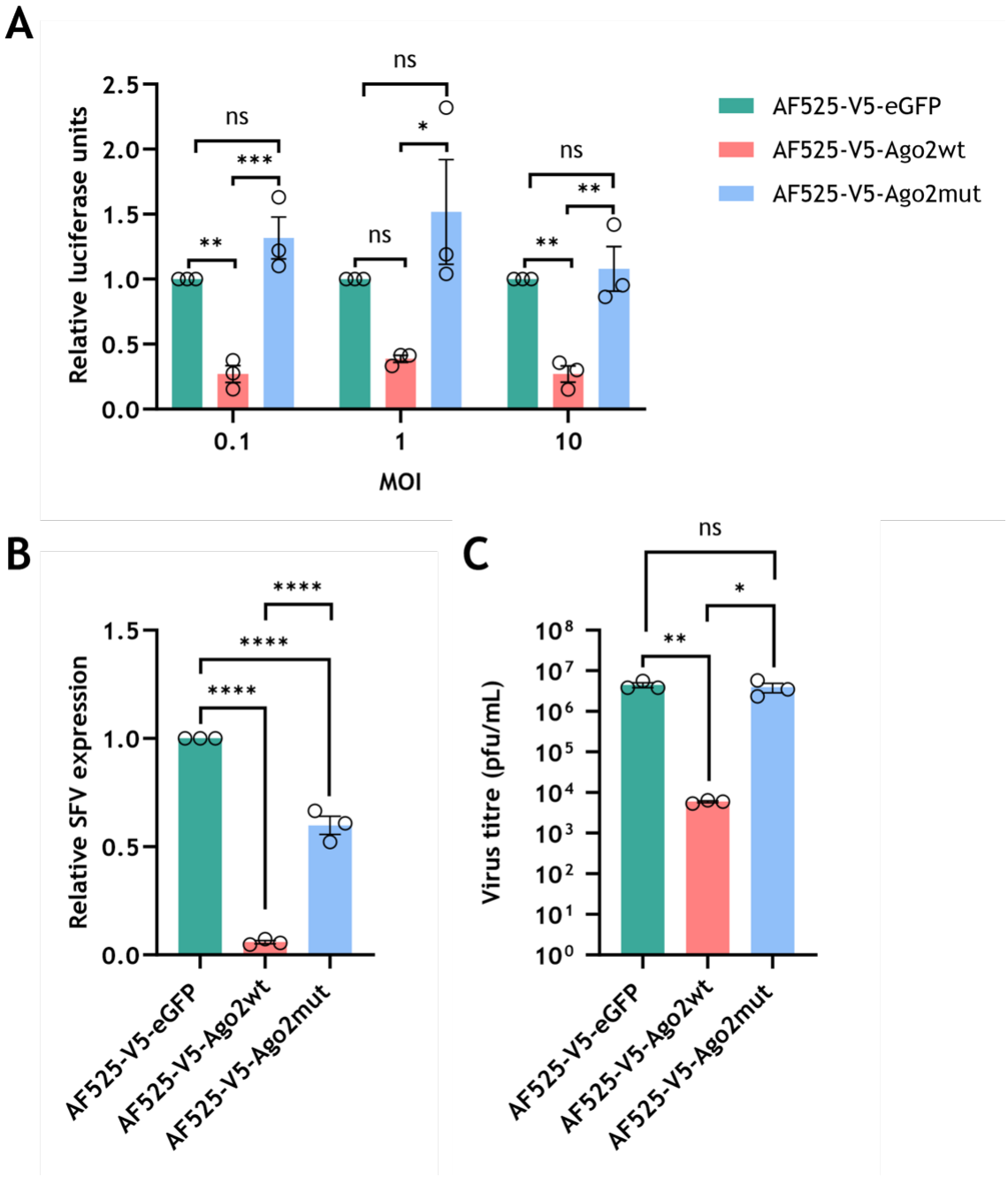

Figure 3-3 Catalytic tetrad mutation and its effect on viral replication.

(A) AF525-V5-Ago2wt, AF525-V5-Ago2mut, and AF525-V5-eGFP cells were infected with SFV4(3H)-FFLuc at MOIs of 0.1, 1, and 10 PFU/cell. At 24 h.p.i, cells were lysed and relative luciferase activity was measured and normalised to the AF525-V5-eGFP control cells. (B) Viral genome copy numbers were determined by RT-qPCR following SFV4 infection at an MOI of 1 PFU/cell. (C) Supernatants from the experiment in (B) were subjected to plaque assay to determine virus titres. Statistical significance was determined using one-way ANOVA; ns = not significant, *p ≤ 0.05, **p ≤ 0.01, ***p ≤ 0.001, ****p ≤ 0.0001.

3.3.4 RNAi reporter assays to assess the importance of the catalytic tetrad in Ago2

RNAi activity in *Ae. aegypti* Ago2 knockout cells (AF525) stably expressing eGFP (control), Ago2wt, or Ago2mut was assessed using a dual luciferase reporter assay. Two reporter plasmids, pPUb-RLuc and pPUb-FFLuc, were used in this experiment. The pPUb-RLuc plasmid expresses Renilla luciferase and served as an internal control, while pPUb-FFLuc expresses firefly luciferase and was used as the RNAi target. This assay allowed the relative silencing efficiency of Ago2 to be quantified by measuring changes in firefly luciferase activity relative to Renilla luciferase.

Cells were co-transfected with the reporter plasmids and either dseGFP, which does not target the firefly luciferase transcript and therefore serves as a negative control, or dsFFLuc, which specifically targets the firefly luciferase mRNA for RNAi-mediated silencing. In cells expressing wildtype Ago2 (AF525-V5-Ago2wt), the firefly luciferase signal was strongly reduced when dsFFLuc was present compared with the dseGFP control, indicating efficient RNAi-mediated gene silencing. In contrast, this reduction in firefly luciferase activity was not observed in the Ago2mut or eGFP control cell lines.

The residual reduction in FFLuc activity observed in the Ago2mut and eGFP cells may reflect the contribution of other endogenous small RNA pathways independent of Ago2-mediated exo-siRNA activity, such as miRNA or piRNA pathways. Therefore, although Ago2 catalytic activity is essential for efficient exo-siRNA pathway, some partial silencing may still occur through alternative RNA regulatory mechanisms.

The absence of effective silencing in the Ago2 mutant cells indicates that mutation of the catalytic tetrad disrupts Ago2 slicing activity and prevents efficient RNAi-mediated target degradation (Figure 3-4). These results demonstrate that the catalytic tetrad is required for Ago2-mediated RNAi activity and confirm that functional slicer activity is necessary for efficient operation of the exo-siRNA pathway in mosquito cells.

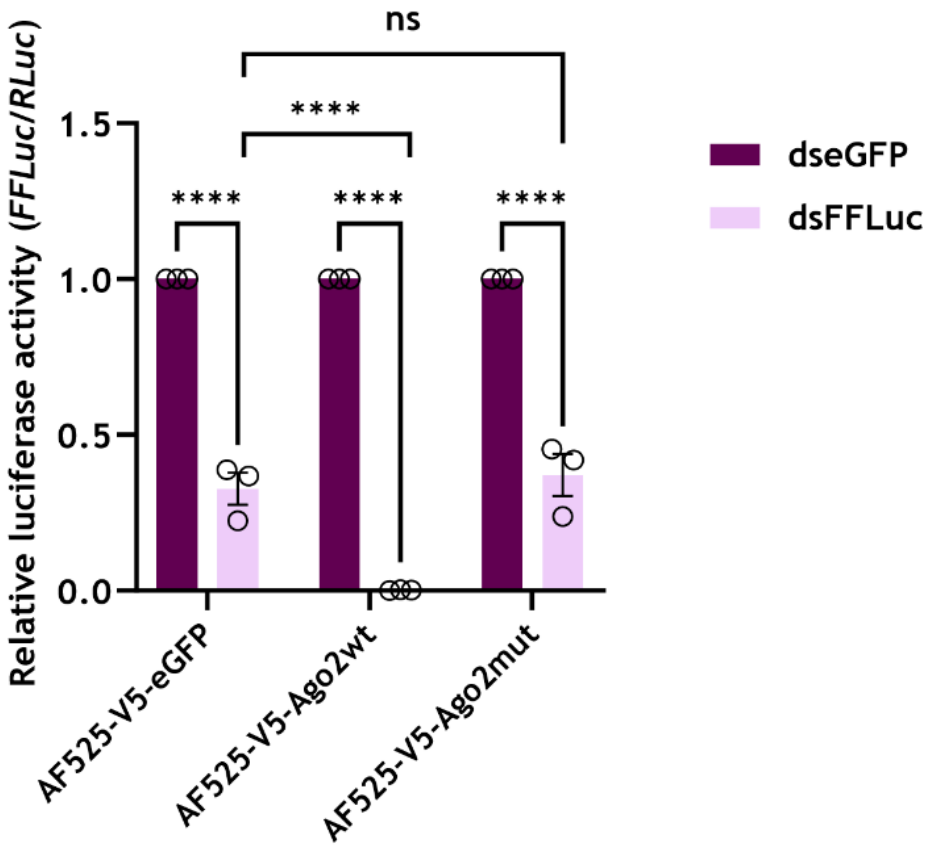

Figure 3-4 Effect of catalytic tetrad mutation on exo-siRNA pathway activity.

AF525-V5-Ago2wt, AF525-V5-Ago2mut, and AF525-V5-eGFP cells were transfected with firefly luciferase (FFLuc) and Renilla luciferase (RLuc) reporter plasmids together with either dsRNA targeting FFLuc (dsFFLuc; purple) or eGFP (dseGFP; pink). Cells were lysed at 24 h post-transfection. Relative luciferase activity (FFLuc/RLuc) was measured and normalised to control cells. Bars represent the mean of experiments performed in technical triplicate from three independent experiments ± SEM. Statistical significance was determined using two-way ANOVA; ns = not significant, ****$p \leq 0.0001$.

3.3.5 The mutated DEDH catalytic tetrad affects small RNA processing by Ago2

To determine the effect of the Ago2 catalytic tetrad on small RNA processing, virus-derived small RNA (vsiRNA) profiles were analysed in the stable cell lines expressing Ago2wt, Ago2mut, or eGFP control. Cells were infected with SFV4 at a multiplicity of infection (MOI) of 5 PFU/cell for 24 hours before being lysed and subjected to immunoprecipitation using an anti-V5 antibody. Following immunoprecipitation, RNAs associated with Ago2wt, Ago2mut, or eGFP were extracted and analysed by small RNA sequencing.

The sequencing libraries contained approximately 12 million reads per sample (Table 3-1). Analysis of read length distribution showed that the Ago2wt and Ago2mut libraries consisted predominantly of 21 nt reads, representing approximately 80–90% of the total reads (Figure 3-5A). This size distribution is consistent with cleavage of viral double-stranded RNA by Dicer-2, which typically generates 21 nt siRNAs. Mapping of 21 nt vsiRNAs across the SFV genome showed reads originating from both the positive (pink) and negative (blue) strands (Figure 3-5B), indicating that vsiRNAs were produced from replicative intermediates of the viral RNA genome.

A slightly higher number of SFV-derived small RNA reads was observed in the Ago2mut samples compared with Ago2wt (Figure 3-5C). Analysis of vsiRNA duplex formation revealed that both Ago2wt and Ago2mut samples displayed the highest z-score probabilities for 19 nt overlapping vsiRNA duplexes. However, the absolute number of vsiRNA duplexes overlapping between 18–21 nt was higher in Ago2mut samples (Figure 3-6A). Notably, a significantly greater number of duplex pairs were detected in Ago2mut compared with Ago2wt (Figure 3-6B). This accumulation of vsiRNA duplexes in Ago2mut cells is consistent with a defect in passenger strand cleavage, as mutation of the catalytic tetrad prevents Ago2-mediated slicing activity. As a result, the passenger strand cannot be efficiently cleaved and removed, leading to accumulation of intact vsiRNA duplexes.

Table 3-1 Initial quality control summary of small RNA sequencing libraries.

The table shows the total number of reads per FASTQ library, the number of reads mapping to the SFV genome, and the corresponding percentage of mapped reads for samples derived from AF525-V5-eGFP, AF525-V5-Ago2wt, and AF525-V5-Ago2mut cell lines.

Sample	Read in library	Mapping to SFV	%
eGFP1_1.fq	12682605	545352.015	4.30 %
eGFP2_1.fq	12621900	749741	5.94 %
eGFP3_1.fq	12758264	1279653.879	10.03 %
Ago2wt1_1.fq	12728091	3700056.054	29.07 %
Ago2wt2_1.fq	12622513	2173596.739	17.22 %
Ago2wt3_1.fq	12813315	2329460.667	18.18 %
Ago2mut1_1.fq	12667799	4916372.792	38.81 %
Ago2mut2_1.fq	12769114	2722375.105	21.32 %
Ago2mut3_1.fq	12762643	2541042.221	19.91 %

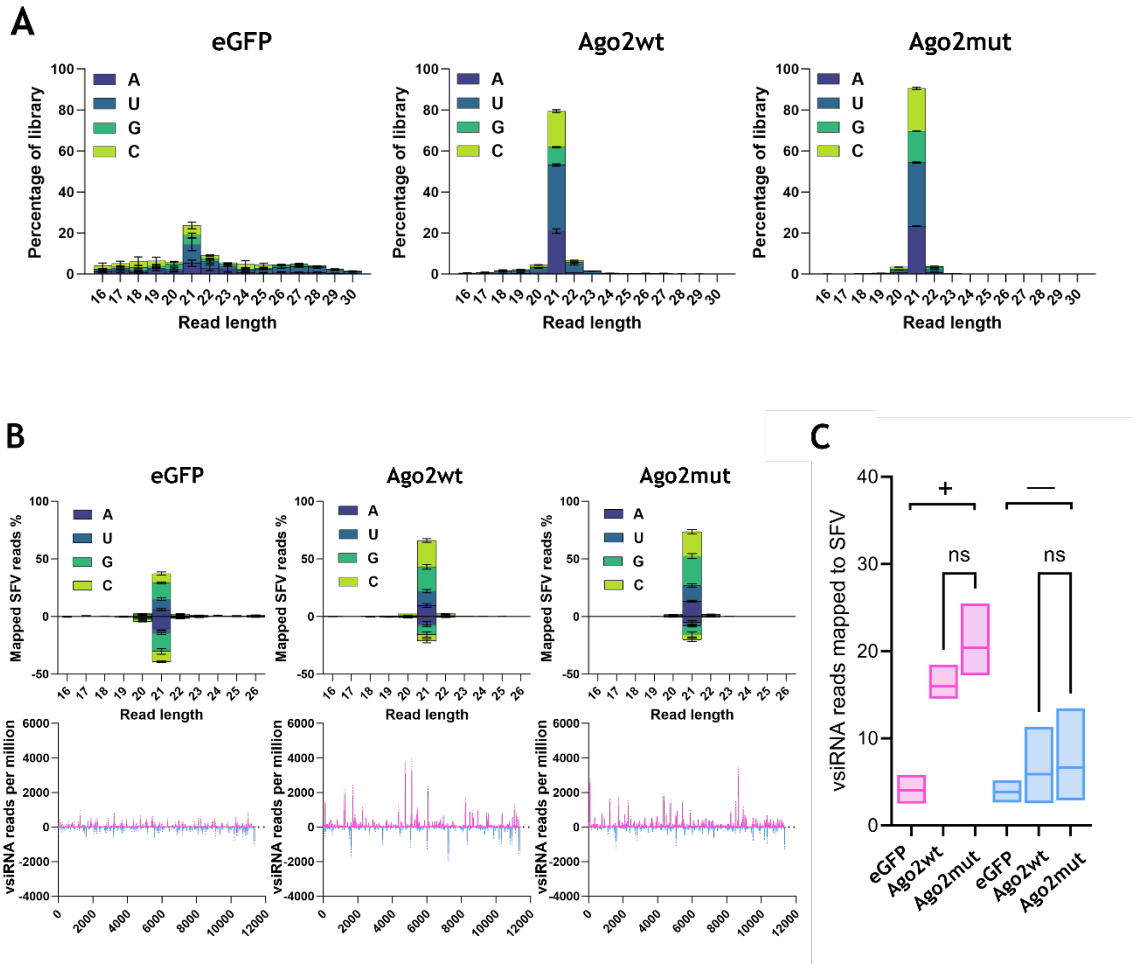

Figure 3-5 Effect of catalytic tetrad mutation on vsiRNA profiles in AF525 cells.

Small RNA sequencing was performed on AF525-V5-Ago2wt, AF525-V5-Ago2mut, and AF525-V5-eGFP cells following infection with SFV4 at an MOI of 5 PFU/cell for 24 hours. (A) Read length distribution of small RNAs. (B) Histogram of small RNA reads 16–26 nt in length mapped to the SFV genome (GenBank ID: KP699763), showing reads derived from the genome (positive strand) and antigenome (negative strand). Colours indicate first nucleotide bias for each read length. Values are shown as mean percentage of mapped reads (Y axis) from three independent experiments ± SEM. Coverage of SFV-derived 21 nt vsiRNAs across the genome (pink) and antigenome (blue) is shown as reads per million mapped reads from three independent experiments ± SEM. (C) Percentage of total 16–26 nt small RNA reads that mapped to the SFV genome (pink) or antigenome (blue) across all treatments. Statistical significance was determined using one-way ANOVA with Tukey's multiple comparisons test; ns = not significant.

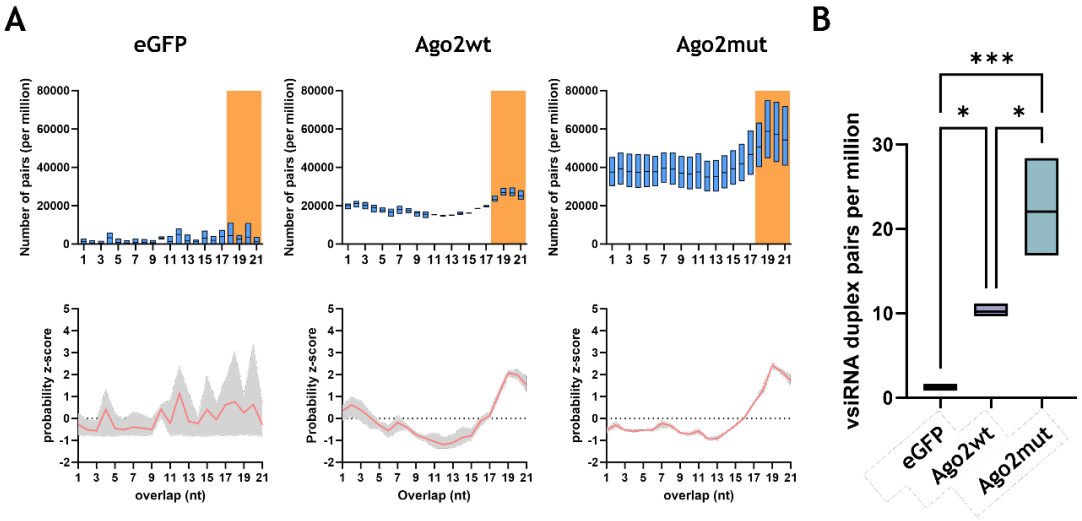

Figure 3-6 Mutation of the Ago2 catalytic tetrad results in accumulation of vsiRNA duplexes.

(A) Number of overlapping vsiRNA duplex pairs normalised per million SFV-mapped reads. Orange highlights indicate the predominant 18–21 nt overlap typical of Dcr2

(B) processing. The lower panel shows the probability (z-score) of overlapping 21 nt vsiRNA duplexes. (B) Number of the most abundant vsiRNA duplexes overlapping by 18–21 nt across AF525 cell line derivatives, normalised to the number of mapped reads per million. Data represent the mean of three independent experiments with the range indicated. Statistical significance was determined using one-way ANOVA with Tukey's multiple comparisons test; *$p < 0.05$, ***$p \leq 0.001$.

3.4 Discussion

RNAi has been studied widely in *D. melanogaster*, which is a model insect also for the exo-siRNA pathway, while this work remains limited in mosquitoes with regards to regulation, control, and function (Blair, 2011, Bonning and Saleh, 2021, Silver *et al.*, 2021). Dcr2 is a key protein in the exo-siRNA pathway. Previous work at CVR has identified conserved and functional amino acids of Dcr2 that are critical for silencing activity and the antiviral response against SFV (Gestuveo *et al.*, 2022a) and indicated that Dcr2 is essential for siRNA size regulation (Reuter *et al.*, 2025). However, Ago2 in *Ae. aegypti* remains relatively understudied. The function of Ago2 and the presence and role of the DEDH catalytic tetrad were therefore investigated in this project. hAgo1 is considered catalytically inactive due to the absence of the DEDX motif in the PIWI domain. However, slicing activity can be restored by inserting a DEDH motif into the PIWI domain (Hauptmann *et al.*, 2013, Jin *et al.*, 2021). Therefore, the role and relevance of the catalytic tetrad across Ago proteins remains an important question.

To address this, multiple sequence alignments were performed to investigate whether a DEDH catalytic tetrad was present in mosquito Ago2, particularly in *Ae. aegypti*. The conserved amino acids aligned to the *Ae. aegypti* Ago2 sequence identified residues D740, E780, D812 and H950 located within the PIWI domain. These residues correspond to the predicted catalytic tetrad responsible for endonuclease activity in most Argonaute proteins. The conservation of these residues across mosquito species and *D. melanogaster* suggests that the catalytic mechanism of Ago2 is likely preserved among dipteran insects.

To investigate the functional role of these residues, all four positions of the DEDH tetrad were mutated to alanine and stable cell lines expressing either wildtype or mutant Ago2 were generated. Infection experiments using SFV4 demonstrated that mutation of the catalytic tetrad resulted in a loss of antiviral activity. Cells expressing Ago2mut showed significantly increased viral replication compared with cells expressing Ago2wt, as demonstrated by luciferase reporter assays, RT-qPCR, and plaque assays. These findings indicate that the catalytic tetrad is required for Ago2-mediated antiviral defence against SFV.

The reporter assay experiments further supported this conclusion. In the dual luciferase reporter system, efficient silencing of the firefly luciferase reporter was observed in cells expressing Ago2wt, whereas no effective silencing was detected in cells expressing Ago2mut. The Ago2 mutant behaved similarly to the eGFP control cells, indicating that mutation of the catalytic tetrad disrupts the slicing activity required for RNAi-mediated target degradation. These results confirm that the catalytic tetrad is essential for functional RNAi activity and demonstrate that Ago2-mediated cleavage of target RNA is a key step in the exo-siRNA pathway.

Small RNA sequencing provided additional insight into the mechanism underlying this loss of antiviral activity. The size distribution and genomic mapping of vsiRNAs were largely similar between Ago2wt and Ago2mut samples, with most reads corresponding to the expected 21 nt products generated by Dcr2. This indicates that upstream steps of the RNAi pathway, including dsRNA recognition and Dicer2-mediated processing, remain intact in the absence of Ago2 slicing activity. However, a significant accumulation of vsiRNA duplexes was observed in Ago2mut samples compared with Ago2wt. This accumulation is consistent with a defect in passenger strand cleavage during RISC maturation. In normal RNAi processing, Ago2 cleaves the passenger strand of the siRNA duplex, allowing the guide strand to remain associated with the RISC complex. In the absence of a functional catalytic tetrad, this cleavage cannot occur, resulting in the accumulation of intact vsiRNA duplexes. This accumulation pattern is consistent with previous findings in Ago2 mutant *Drosophila* infected with vesicular stomatitis virus (VSV), in which impaired Ago2 catalytic activity led to accumulation of vsiRNA duplexes (Mueller *et al*., 2010).

These observations demonstrate that while Dicer2-mediated production of vsiRNAs is unaffected by mutation of the catalytic tetrad, efficient antiviral RNAi requires the downstream slicing activity of Ago2. Therefore, dicing alone is insufficient for antiviral defence, and complete functionality of the RNAi pathway is necessary for effective viral restriction. The results presented here highlight the importance of Ago2-mediated cleavage in the antiviral response of mosquito cells.

Although this study provides clear evidence that the catalytic tetrad is essential for Ago2 antiviral activity against SFV, several limitations remain. The experiments were performed using a single mosquito species and a single model alphavirus

infection system. It therefore remains to be determined whether the requirement for Ago2 catalytic activity extends to other arboviruses, such as flaviviruses or bunyaviruses, which replicate differently within mosquito cells. Future studies examining additional viruses and vector species will help to determine whether this mechanism represents a broadly conserved feature of mosquito antiviral immunity.

Overall, this study provides functional evidence that the DEDH catalytic tetrad is required for the antiviral activity of *Ae. aegypti* Ago2. The results demonstrate that efficient antiviral defence via the exo-siRNA pathway depends not only on Dicer2-mediated generation of vsiRNAs but also on Ago2-mediated slicing activity. These findings contribute to a better understanding of RNAi-mediated antiviral defence in mosquito vectors and provide a foundation for future studies investigating how this pathway regulates infection by diverse arboviruses.

Chapter 4:
Proteomic analysis of the Ago2 interactome

Chapter 4 Proteomic analysis of the Ago2 interactome

4.1 Introduction

Argonaute-2 (Ago2) and its function in the RNAi pathway have been extensively characterised in the model organism *D. melanogaster*. However, knowledge of the RNAi pathway in mosquitoes remains limited. To exploit Ago2, or the broader RNAi pathway, as part of virus control strategies in mosquitoes, it is essential to better understand Ago2 and its antiviral activities. Arbovirus infection in mosquitoes provides a useful context in which to explore these interactions. In this chapter, novel proteins interacting with Ago2, as well as new roles for known proteins, were investigated for their potential application in future biological vector control strategies.

4.1.1 Ago2 interactors in mosquitoes

4.1.1.1 Dcr2

Dcr2 is an RNase III enzyme that cleaves long dsRNA into 21 nt siRNAs that feed into the exo-siRNA antiviral pathway. In this pathway, virus-derived siRNAs are incorporated into Argonaute-2 (Ago2), the catalytic component of the RNA-induced silencing complex (RISC), to guide sequence-specific cleavage of viral RNA. Subsequently, the 21 nt siRNAs are loaded into Ago2 via cofactors such as R2D2 and Loqs2 to form the RNA-induced silencing complex (RISC) (Blair and Olson, 2015, Samuel *et al.*, 2018, Dong and Dimopoulos, 2023). Various studies have revealed that loss of Dcr2 function results in reduced siRNA production and substantially higher replication of arboviruses (Gestuveo *et al.*, 2022a, Merkling *et al.*, 2023, Reuter *et al.*, 2025). Dcr2 function also varies by species and tissue in the *Aedes* midgut, where antiviral RNAi can be inherently limited. Efficient activity of Dicer-2 requires additional cofactors, such as Loqs2, in the midgut (Olmo *et al.*, 2018). Recent structural and evolutionary studies have highlighted that the Dcr2–R2D2 complex (Section 4.1.1.2) is rapidly evolving under viral pressure. This complex is important for both siRNA production and the loading of siRNAs onto Ago2 for target silencing (Yamaguchi *et al.*, 2022).

4.1.1.2 R2D2

R2D2 acts as a Dcr2 cofactor in the mosquito siRNA pathway and facilitates loading of siRNA duplexes into Ago2. In mosquitoes, Dcr2 forms a complex with R2D2 to mediate the loading of virus-derived siRNAs into the RNA-induced silencing complex (RISC). Previous studies showed that R2D2 is critical for siRNA strand selection. R2D2 recognises the central region of the siRNA duplex (nucleotides g5–15 and p5–15) as well as the thermodynamically stable end containing nucleotides g16–20 of the guide strand and p1–4 of the passenger strand (Yamaguchi *et al.*, 2022). The Dcr2–R2D2 complex can bind an siRNA duplex without mismatches (Tomari *et al.*, 2007). Importantly, impairment of R2D2 in *Ae. aegypti* increased DENV replication and enhanced virus transmission, highlighting its antiviral role (Sánchez-Vargas *et al.*, 2009). Comparative evolutionary studies also suggest that R2D2 and related RNAi cofactors vary across several insect orders (Coleoptera, Diptera, Hemiptera, Hymenoptera and Lepidoptera), potentially influencing RNAi efficiency in different species (Arraes *et al.*, 2021).

4.1.1.3 Loqs2

Loqs2 acts as a specialised cofactor that enhances the efficiency of the Ago2-dependent antiviral siRNA pathway in *Ae. aegypti*. Although Loqs2 has not been demonstrated to associate directly with Ago2, genetic and proteomic evidence indicates that it interacts with upstream components of the Ago2-dependent pathway, such as Dcr2 and other dsRNA-binding proteins, to promote the production and loading of 21 nt virus-derived siRNAs (vsiRNAs) (Blair, 2011, Olmo *et al.*, 2018). In the absence of Loqs2, siRNA biogenesis is impaired, resulting in reduced activation of Ago2. Loqs2 expression is stage- and tissue-specific and is not detected in the *Ae. aegypti* midgut (Olmo *et al.*, 2018, Estevez-Castro *et al.*, 2024).

4.1.1.4 Ago2 interactors in *D. melanogaster*

In *D. melanogaster*, the best-characterised Ago2 partners are Dcr2 and R2D2, which together form the RISC-loading complex (RLC) responsible for transferring siRNA duplexes into Ago2 (Liu *et al.*, 2003, Tomari *et al.*, 2004). The Tudor domain protein Tudor-SN (SND1) also co-purifies with Ago2-containing complexes and is involved in the degradation of RNA fragments generated after Ago2-mediated

slicing (Caudy *et al.*, 2003). Additional Ago2 interaction partners identified in D. melanogaster are summarised in Table 4-1.

Table 4-1 Reported Ago2 interacting proteins in *D. melanogaster*, including protein descriptions and BioGRID database references.

Interactor	Description	Reference
FMR1	CG6203 gene product from transcript CG6203-RC	https://thebiogrid.org/63147/summary/drosophila-melanogaster/fmr1.html
VIG	vasa intronic gene	https://thebiogrid.org/60903/summary/drosophila-melanogaster/vig.html
BAN	bantam	https://thebiogrid.org/2592925/summary/drosophila-melanogaster/ban.html
DCR-2	Dicer-2	https://thebiogrid.org/62681/summary/drosophila-melanogaster/dcr-2.html
RM62	CG10279 gene product from transcript CG10279-RK	https://thebiogrid.org/65943/summary/drosophila-melanogaster/rm62.html
DCR-1	Dicer-1	https://thebiogrid.org/67642/summary/drosophila-melanogaster/dcr-1.html
HSC70-4	Heat shock protein cognate 4	https://thebiogrid.org/66904/summary/drosophila-melanogaster/hsc70-4.html
NELF-E	Negative elongation factor E	https://thebiogrid.org/64390/summary/drosophila-melanogaster/nelf-e.html
R2D2	CG7138 gene product from transcript CG7138-RA	https://thebiogrid.org/60205/summary/drosophila-melanogaster/r2d2.html
TDRD3	tudor domain containing 3 ortholog (*H. sapiens*)	https://thebiogrid.org/64938/summary/drosophila-melanogaster/tdrd3.html
TH	thread	https://thebiogrid.org/65064/summary/drosophila-melanogaster/th.html
TUDOR-SN	CG7008 gene product from transcript CG7008-RB	https://thebiogrid.org/63603/summary/drosophila-melanogaster/tudor-sn.html
W	white	https://thebiogrid.org/57802/summary/drosophila-melanogaster/w.html
BARR	barren	https://thebiogrid.org/61258/summary/drosophila-melanogaster/barr.html
BFT	bereft	https://thebiogrid.org/2592552/summary/drosophila-melanogaster/bft.html
CG6686	CG6686 gene product from transcript CG6686-RB	https://thebiogrid.org/60661/summary/drosophila-melanogaster/cg6686.html
CG9302	CG9302 gene product from transcript CG9302-RA	https://thebiogrid.org/60785/summary/drosophila-melanogaster/cg9302.html
CP190	Centrosomal protein 190kD	https://thebiogrid.org/66912/summary/drosophila-melanogaster/cp190.html
CR18854	pseudo	https://thebiogrid.org/1455262/summary/drosophila-melanogaster/cr18854.html
CRY	cryptochrome	https://thebiogrid.org/67302/summary/drosophila-melanogaster/cry.html
CTCF	CG8591 gene product from transcript CG8591-RA	https://thebiogrid.org/64257/summary/drosophila-melanogaster/ctcf.html
DCO	discs overgrown	https://thebiogrid.org/68523/summary/drosophila-melanogaster/dco.html
DREP-2	DNA fragmentation factor-related protein 2	https://thebiogrid.org/61791/summary/drosophila-melanogaster/drep-2.html
EIF-4E	Eukaryotic initiation factor 4E	https://thebiogrid.org/69740/summary/drosophila-melanogaster/eif-4e.html

Interactor	Description	Reference
ELP1	Elongator complex protein 1	https://thebiogrid.org/66527/summary/drosophila-melanogaster/elp1.html
FOXO	forkhead box, sub-group O	https://thebiogrid.org/66786/summary/drosophila-melanogaster/foxo.html
GIG	gigas	https://thebiogrid.org/65467/summary/drosophila-melanogaster/gig.html
HSP83	Heat shock protein 83	https://thebiogrid.org/63886/summary/drosophila-melanogaster/hsp83.html
IR76A	Ionotropic receptor 76a	https://thebiogrid.org/65426/summary/drosophila-melanogaster/ir76a.html
IRD5	immune response deficient 5	https://thebiogrid.org/69058/summary/drosophila-melanogaster/ird5.html
LAM	Lamin	https://thebiogrid.org/59950/summary/drosophila-melanogaster/lam.html
ME31B	maternal expression at 31B	https://thebiogrid.org/60455/summary/drosophila-melanogaster/me31b.html
MUS308	mutagen-sensitive 308	https://thebiogrid.org/66664/summary/drosophila-melanogaster/mus308.html
P53	CG33336 gene product from transcript CG33336-RB	https://thebiogrid.org/77545/summary/drosophila-melanogaster/p53.html
PDK1	Phosphoinositide-dependent kinase 1	https://thebiogrid.org/63582/summary/drosophila-melanogaster/pdk1.html
PIG-S	Phosphatidylinositol glycan anchor biosynthesis, class S ortholog (*H. sapiens*)	https://thebiogrid.org/67901/summary/drosophila-melanogaster/pig-s.html
PPK28	pickpocket 28	https://thebiogrid.org/59002/summary/drosophila-melanogaster/ppk28.html
PROSALPHA7	Proteasome alpha7 subunit	https://thebiogrid.org/61847/summary/drosophila-melanogaster/prosalpha7.html
PTEN	CG5671 gene product from transcript CG5671-RB	https://thebiogrid.org/68762/summary/drosophila-melanogaster/pten.html
PUM	pumilio	https://thebiogrid.org/66261/summary/drosophila-melanogaster/pum.html
PUR-ALPHA	Purine-rich binding protein-alpha	https://thebiogrid.org/68630/summary/drosophila-melanogaster/pur-alpha.html
RHEB	Ras homolog enriched in brain ortholog (H. sapiens)	https://thebiogrid.org/72870/summary/drosophila-melanogaster/rheb.html
RICTOR	rapamycin-insensitive companion of Tor	https://thebiogrid.org/59224/summary/drosophila-melanogaster/rictor.html
RTI	rotini	https://thebiogrid.org/59630/summary/drosophila-melanogaster/rti.html
S6KII	Ribosomal protein S6 kinase II	https://thebiogrid.org/59412/summary/drosophila-melanogaster/s6kii.html
SMD1	Small ribonucleoprotein particle protein SmD1	https://thebiogrid.org/69191/summary/drosophila-melanogaster/smd1.html
SMG	smaug	https://thebiogrid.org/64438/summary/drosophila-melanogaster/smg.html
TAF11	TBP-associated factor 11	https://thebiogrid.org/60390/summary/drosophila-melanogaster/taf11.html
TSC1	CG6147 gene product from transcript CG6147-RA	https://thebiogrid.org/67795/summary/drosophila-melanogaster/tsc1.html
UEV1A	CG10640 gene product from transcript CG10640-RB	https://thebiogrid.org/64079/summary/drosophila-melanogaster/uev1a.html

Interactor	Description	Reference
MSL-2	male-specific lethal 2	https://thebiogrid.org/59776/summary/drosophila-melanogaster/msl-2.html

4.2 Objectives

Chapter 3 indicated DEDH catalytic tetrad is required for antiviral activity in mosquito cell lines. To characterise the protein interaction network associated with mosquito Ago2 and determine how this network changes during arbovirus infection, a proteomics-based strategy combined with functional screening was employed. The specific objectives of this chapter were:

1. To define the Ago2 interactome in *Ae. aegypti* cells under mock and SFV4 infection conditions using immunoprecipitation coupled with quantitative mass spectrometry.

2. To compare Ago2-associated proteins between mock and infected conditions and classify enriched interactors into functional protein groups.

3. To identify candidate Ago2-associated proteins for functional investigation and evaluate their effects on viral replication using a dsRNA knockdown screen.

4. To characterise the role of selected Ago2-interacting proteins in RNAi activity by assessing their effects on virus-derived siRNA production.

4.3 Results

To define the mosquito Ago2 interactome, V5-tagged Ago2 was immunoprecipitated from AF525 cells under mock conditions and following SFV4 infection. V5-eGFP-expressing cells were used as a negative control for non-specific binding. Immunoprecipitated samples from four biological replicates were subjected to mass spectrometry analysis to identify proteins enriched in Ago2 complexes. Subsequent analyses compared the Ago2 interactome between mock and infected conditions to identify infection-dependent interactions.

Chapter 3 confirmed the presence of the DEDH catalytic tetrad of Ago2 in mosquitoes and demonstrated that this tetrad is required for antiviral activity. To investigate Ago2 interactions during viral infection, a proteomics approach was used to analyse the Ago2 interactome in the presence and absence of SFV4.

To confirm expression of the target proteins in the stable cell lines, Western blotting was performed on four biological replicates of AF525 cells stably expressing V5-Ago2wt or V5-eGFP, infected with or without SFV4. Samples were analysed before immunoprecipitation (INPUTs) and after immunoprecipitation (IP). The INPUT Western blots for the four replicates show the lysates that were used for the IP experiments (Figure 4-1).

V5-Ago2wt was detected in the Ago2 lysate samples at approximately 115 kDa in all four replicates. Similarly, V5-eGFP was detected in the control lysate samples at approximately 27 kDa in both infected and uninfected conditions. The SFV4 infection-specific protein nsP3, an SFV non-structural protein involved in viral replication complex formation, was detected only in the SFV4-infected samples in the INPUT lanes at approximately 70 kDa. As expected, SFV nsP3 was not detected after IP because the anti-V5 antibody used for immunoprecipitation specifically recognises the V5-tagged Ago2wt or eGFP proteins (Figure 4-1).

Together, these results confirmed that the samples were of sufficient quality for subsequent mass spectrometry analysis.

4.3.1 Validation of V5-Ago2 immunoprecipitation samples prior to proteomic analysis

Total protein in the V5-eGFP and V5-Ago2wt samples was assessed using silver staining and Coomassie blue staining following immunoprecipitation (IP). Total protein was confirmed across all four replicates, and clear protein bands were observed before the samples were sent for mass spectrometry analysis (Figure 4-2A and B).

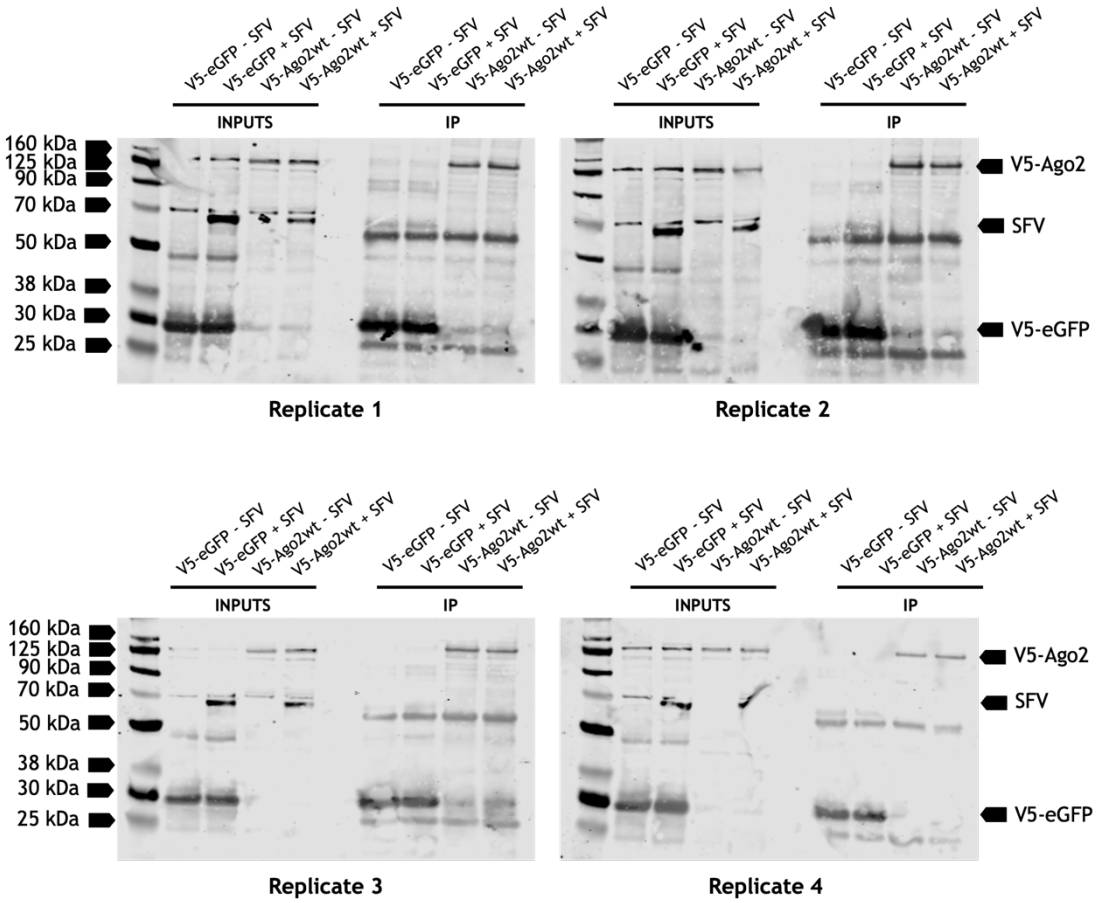

Figure 4-1 Expression of V5-Ago2wt or V5-eGFP control proteins in AF525 cells stably expressing these constructs in the presence or absence of SFV4.

Target protein expression was analysed by Western blotting before immunoprecipitation (INPUTs) and after immunoprecipitation (IP). Mouse anti-V5 (1:2000) and rabbit anti-SFV (1:5000) were used as primary antibodies. After overnight incubation, secondary antibodies goat anti-mouse IgG (1:5000) and goat anti-rabbit IgG (1:5000) were applied prior to detection.

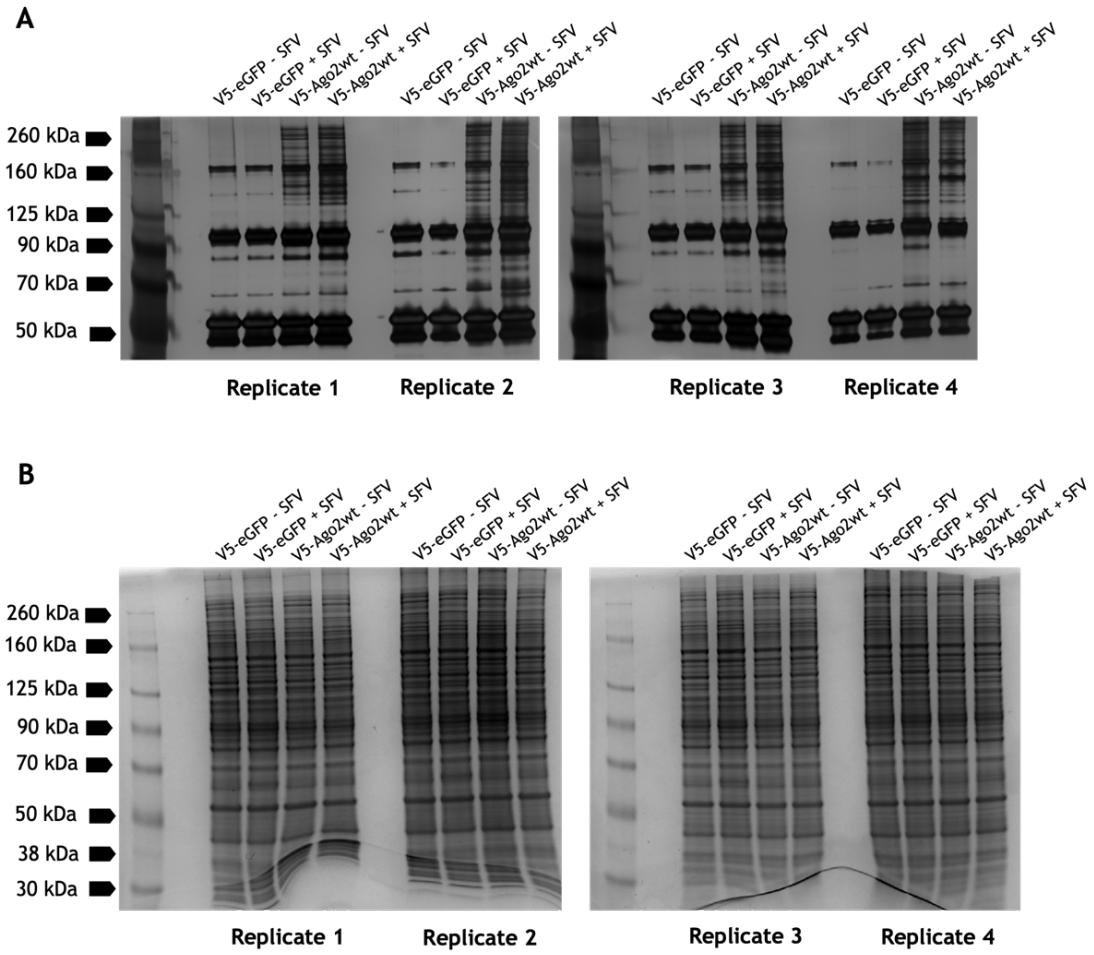

Figure 4-2 The total protein detection in AF525 cells stably expressing these V5 tagged proteins in the presence and absence of SFV4.

(A) Silver staining confirmed total proteins after IP. (B) Coomassie blue staining confirmed total proteins after IP.

4.3.2 The interactome of *Ae. aegypti* Ago2 in presence and absence of SFV

Ago2 functions as a key effector of the antiviral RNAi pathway in mosquitoes, but the protein interaction networks associated with Ago2 during viral infection are not fully understood. Therefore, this experiment aimed to determine how Ago2 interactions change in the presence or absence of SFV4 infection, to assess whether regulatory proteins influencing Ago2 and RNAi activity are altered during viral infection.

AF525 knock-in cell lines (clone 1 of each Ago2 construct) were used to examine interactions between Ago2 and host proteins when SFV4 was present or absent. Raw mass spectrometry data were analysed using MaxQuant, and Perseus software was used for data annotation and statistical analysis of the proteomics experiment. Histograms illustrate the distribution of LFQ protein abundance values obtained from the mass spectrometry dataset following processing in MaxQuant and Perseus, rather than the total protein concentration of each sample. The purpose was to assess data normalisation and overall consistency between samples before downstream analysis. In some replicates, the distribution of LFQ protein abundance values was less apparent, which may reflect a lower number of quantified proteins or reduced signal intensity in those samples. This could result from sample-to-sample variation during sample preparation, differences in protein recovery, peptide detection efficiency, or subsequent filtering during data processing in Perseus. Therefore, these plots were used as an initial quality control step to assess the overall consistency of protein intensity distributions across replicates prior to downstream analysis. (Figure 4-3).

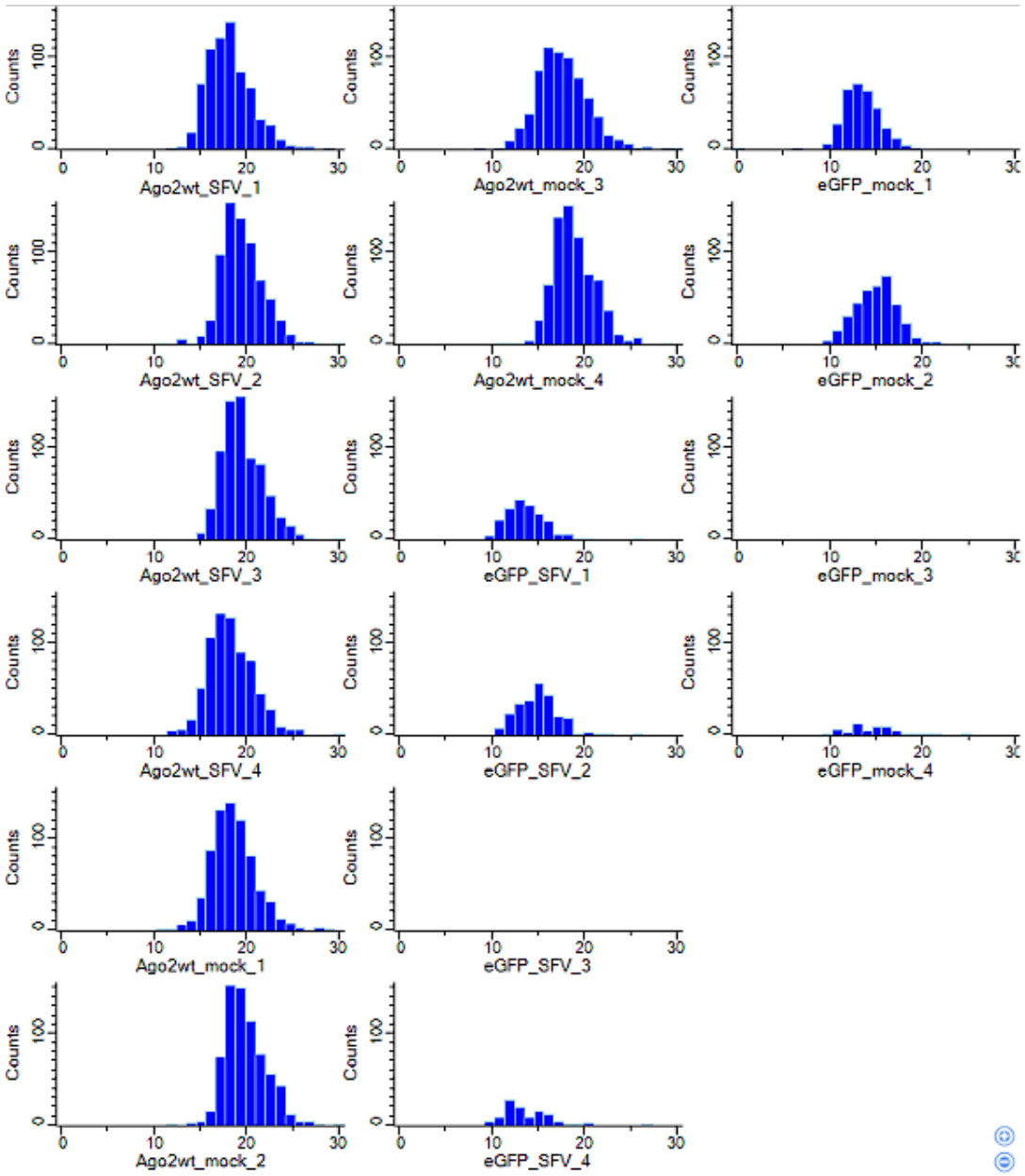

Figure 4-3 Distribution of normalised protein abundance values across proteomic samples under four experimental conditions in the presence or absence of SFV4 infection.

Histograms show the distribution of log2-transformed normalised protein intensity values detected by mass spectrometry for each biological replicate. The four experimental conditions analysed were Ago2wt + SFV4, Ago2wt mock, eGFP + SFV4, and eGFP mock. Similar distribution patterns across samples indicate consistent protein quantification and successful data normalisation prior to downstream comparative analyses.

Immunoprecipitations (IPs) from AF525-V5-Ago2wt mock and AF525-V5-eGFP mock control cells revealed clear differences in the volcano plots, where each dot represents a different protein. The first volcano plot (Figure 4-4) shows the cut-off curve used to determine significant enrichment. In this comparison, 207 proteins were identified as Ago2-specific interactors under mock (uninfected) condition, indicating that these proteins were enriched in Ago2 immunoprecipitates compared with the eGFP control.

The second volcano plot (Figure 4-5) compares AF525-V5-Ago2wt with SFV4 infection and AF525-V5-eGFP with SFV4 infection. In this case, 130 proteins above the cut-off curve were identified as significant Ago2 interactors under infection conditions.

The third volcano plot compares the Ago2 interactome in the presence and absence of SFV4 infection. In this analysis, only one protein was significantly upregulated in the infected condition: the SFV4 polyprotein P1234 (Figure 4-6). This protein represents the full viral replicase polyprotein, which undergoes proteolytic cleavage to produce the individual non-structural proteins responsible for regulating replication stages and assembly of the viral replication complex (Vasiljeva *et al.*, 2003, Pietilä *et al.*, 2017, Lello *et al.*, 2021).

Lists of Ago2 interactors and the grouping of Ago2 interactors identified in the mock condition, the SFV4-infected condition, and the overlapping group are presented in Tables 4-2, 4-3, 4-4, 4-5, 4-6, and 4-7 respectively.

Comparison of the SFV4-infected and mock groups showed that 28 of the 130 proteins were upregulated in the presence of SFV4, whereas approximately 50% of the proteins (105 out of 207) were detected only in the absence of virus infection. In addition, 102 proteins were identified in both the SFV4-infected and uninfected conditions (Figure 4-7).

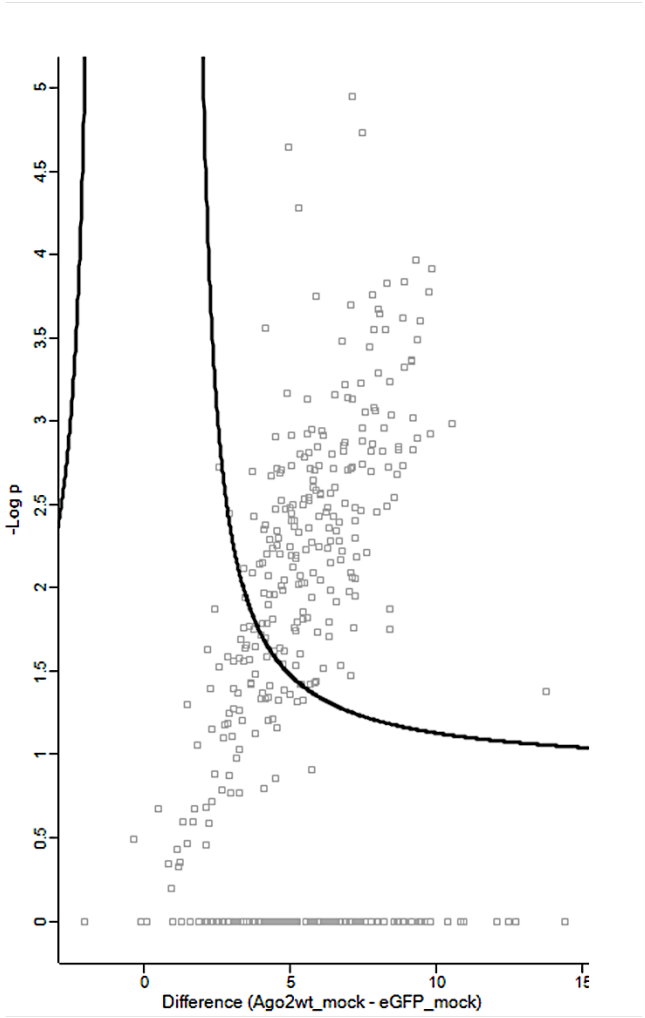

Figure 4-4 Proteomics analysis of *Ae. aegypti* Ago2 under mock condition.

Volcano plots generated after immunoprecipitation (IP) show the results of a two-sample t-test used to compare protein enrichment between Ago2wt mock and eGFP mock conditions. The data were analysed using an S0 value of 1 and a false discovery rate (FDR) of 0.01 to identify and visualise Ago2 interactors.

Table 4-2 Proteins significantly enriched in Ago2 immunoprecipitates under mock conditions.

No.	UniProt ID	VectorBase ID	Protein name
1	A0A0N8ES32	AAEL017164-PB	Putative mRNA cleavage factor i subunit/cpsf subunit
2	A0A1S4F0P9	AAEL002107	Sulphide quinone reductase
3	A0A1S4F0V4	AAEL002083-PA	DEAD box ATP-dependent RNA helicase
4	A0A1S4F1P1	AAEL002407	DNA repair protein xp-e
5	A0A1S4F242	AAEL002488-PA	ATP-dependent RNA helicase DDX1
6	A0A1S4F250	AAEL002563	Nuclear matrix protein
7	A0A1S4F8F0	AAEL004716-PA	Chromodomain-helicase-DNA-binding protein 1
8	A0A1S4F8M7; A0A6I8T9Z4; A0A6I8TA35; A0A6I8TAX9	AAEL004694	Munc13-4
9	A0A1S4F969	AAEL004977	Sec24B protein, putative
10	A0A1S4FDZ4	AAEL006552	WD-repeat protein
11	A0A1S4FEC3; A0A6I8TDE9; Q175F8	AAEL006684	Glyoxylate reductase 1 homolog; Glyoxylate reductase 1 homolog; Cytokine-like nuclear factor N-PAC
12	A0A1S4FGV6	AAEL007546	Actin-related protein 2/3 complex subunit
13	A0A1S4FIN9; A0A6I8TFU5	AAEL008171	Double-stranded RNA-binding protein zn72d
14	A0A1S4FKA5	AAEL008687	Loquacious
15	A0A1S4FP45	AAEL022213-PA	26S proteasome non-ATPase regulatory subunit 6
16	A0A1S4FP86	AAEL009946	DnaJ homolog subfamily B member 11 precursor
17	A0A1S4FQG3	AAEL010402-PD	DEAD box ATP-dependent RNA helicase
18	A0A1S4FSQ2	AAEL011105	Adducin
19	A0A1S4FW12	AAEL012243-PA	RRM domain-containing protein
20	A0A1S4G0U3	AAEL014057-PA	U1-type domain-containing protein
21	A0A1S4G3C4	AAEL014961-PA	GDP-mannose 4,6-dehydratase
22	A0A1S4G731	AAEL017524-PA	Procollagen-proline 4-dioxygenase
23	A0A6I8T2V8	AAEL000081	Peroxisome assembly factor-2 (peroxisomal-type ATPase 1)
24	A0A6I8T510	AAEL002178-PD	5-formyltetrahydrofolate cyclo-ligase
25	A0A6I8T5A7	AAEL002437	Symplekin
26	A0A6I8T705	AAEL002764-PE	Dihydrolipoyllysine-residue succinyltransferase component of 2-oxoglutarate dehydrogenase complex, mitochondrial
27	A0A6I8T8P4	AAEL003953-PD	MAP/microtubule affinity-regulating kinase 2,4
28	A0A6I8T9Y5; A0A6I8TE70; A0A6I8TE76; A0A6I8TEM6	AAEL007404	DUF4211 domain-containing protein
29	A0A6I8TA52	AAEL004227	Myosin VI
30	A0A6I8TAB4	AAEL004859-PB	ATP-dependent RNA helicase
31	A0A6I8TB87; Q179S6	AAEL005528-PA	Rasputin
32	A0A6I8TBK1; A0A6I8TH48	AAEL009070-PD	HTH La-type RNA-binding domain-containing protein
33	A0A6I8TBW1	AAEL009326	Fragile X mental retardation syndrome-related protein 1, putative

No.	UniProt ID	VectorBase ID	Protein name
34	A0A6I8TC00; Q16VW0	AAEL009422-PF	C2H2-type domain-containing protein
35	A0A6I8TDL3	AAEL011187	U520
36	A0A6I8TGC9; Q16YF3	AAEL008562-PA	Unspecified product
37	A0A6I8TGI7	AAEL008921	Myosin regulatory light chain 2 smooth muscle
38	A0A6I8TGL5; A0A6I8TQK0; A0A6I8TS46; Q16EQ1	AAEL015065-PA	Spectrin
39	A0A6I8TGT3	AAEL008714-PB	Uncharacterized protein
40	A0A6I8TIN4	AAEL019529-PA	Splicing factor 3B subunit 3
41	A0A6I8TLC6; Q16NS4	AAEL011870-PA	Rap55
42	A0A6I8TMN3; Q16PT4	AAEL011527-PA	Eukaryotic translation initiation factor
43	A0A6I8TMQ2; A0A6I8TYX4; A0A6I8TZ06; A0A6I8U1W8	AAEL020992-PF	E3 ubiquitin-protein ligase hyd
44	A0A6I8TMS0; A0A6I8TP85	AAEL000769	Arginine/serine-rich splicing factor
45	A0A6I8TPB5	AAEL013888-PB	Pre-mRNA-processing factor 39
46	A0A6I8TQ65; A0A6I8U0V9	AAEL023037-PC	Ribose-phosphate diphosphokinase
47	A0A6I8TQF4	AAEL014931-PI	Sarm1
48	A0A6I8TS81	AAEL024720-PA	5'-3' exoribonuclease
49	A0A6I8TXM0	AAEL020820-PA	Uncharacterized protein
50	A0A6I8TY80; A0A6I8TYH5; A0A6I8TZ18; A0A6I8U162	AAEL020525-PB	Eukaryotic translation initiation factor 4 gamma
51	A0A6I8U2E5	AAEL023265-PA	SAP domain-containing protein
52	A0A6I8U3U1	AAEL022113-PA	RRM domain-containing protein
53	A0A6I8U472; A0A6I8U974	AAEL026260-PA	Ras-associating domain-containing protein
54	A0A6I8U526; A0A6I8U723	AAEL024235-PH	Talin
55	A0A6I8U6I1; A0A6I8UA62	AAEL028188-PD	Cysteine proteinase
56	A0A6I8UA36	AAEL027978-PW	Uncharacterized protein
57	A0A6R5HP02	AAEL008749	UDP-glucuronosyltransferase
58	A0A6R5I1F9	AAEL024802-PB	Endoplasmic reticulum chaperone BIP
59	A0A6R8H194; Q16UF8	AAEL023347-PA	Eukaryotic translation initiation factor 3 subunit D
60	J9E9C4	AAEL017213-PA	DNA-directed RNA polymerase subunit beta
61	J9HGY8	AAEL017030-PA	Unspecified product
62	O16109	AAEL008787	V-type proton ATPase catalytic subunit A
63	Q16EF6	AAEL015216-PA	Serine/threonine-protein kinase vrk
64	Q16FD1	AAEL014816-PA	Unspecified product
65	Q16FL6	AAEL014715	Eukaryotic translation initiation factor 3 subunit L (eIF3l)
66	Q16HY2	AAEL013869-PA	RNA-binding protein
67	Q16IV9	AAEL013530-PA	Cullin
68	Q16JA1	AAEL013390-PA	Polo kinase

No.	UniProt ID	VectorBase ID	Protein name
69	Q16N14	AAEL012122-PA	26S proteasome regulatory subunit S3
70	Q16N28	AAEL012094-PB	Casein kinase ii, alpha chain (cmgc group iv)
71	Q16TC4	AAEL010296-PA	Carboxylase:pyruvate/acetyl-coa/propionyl-coa
72	Q16US7	AAEL024434	60S ribosomal protein L13a
73	Q16UX4	AAEL009769-PA	Unspecified product
74	Q16UX6	AAEL004294	Dihydrolipoamide acetyltransferase component of pyruvate dehydrogenase complex
75	Q16VD3	AAEL009607	Protein lingerer
76	Q16VZ4	AAEL009414-PA	NADH-ubiquinone oxidoreductase 39 kda subunit
77	Q16Y81	AAEL008621-PA	Cdk1
78	Q170C2	AAEL007945	Eukaryotic translation initiation factor 3 subunit H (eIF3h)
79	Q171B3	AAEL007698-PA	PIWI
80	Q171P3	AAEL003522	Protein arginine N-methyltransferase
81	Q172D2	AAEL007439-PB	Myosin light chain 1
82	Q173Y9	AAEL006977-PA	Serine/threonine protein phosphatase 2a regulatory subunit a
83	Q174Q1	AAEL000092	Glutathione transferase
84	Q174Z3	AAEL006741-PA	Unspecified product
85	Q175A5	AAEL006748-PA	RNA-binding protein 8A
86	Q176A9	AAEL010340	Splicing factor, arginine/serine-rich 1 Serine/arginine rich splicing factor
87	Q177E2	AAEL006748-PA	Histone H3
88	Q177Q3	AAEL006050-PA	Nuclear RNA export factor 2 (NXF2), putative
89	Q178R6	AAEL005817	60S ribosomal protein L26
90	Q17A05	AAEL005455	CTP synthase
91	Q17A32	AAEL005413-PB	Mitochondrial ribosomal protein, S11, putative
92	Q17AG6	AAEL005288-PA	E3 ubiquitin-protein ligase KCMF1
93	Q17BB3	AAEL005025-PA	U1 small nuclear ribonucleoprotein, putative
94	Q17D30	AAEL004347	Eukaryotic translation initiation factor 3 subunit M (eIF3m)
95	Q17D61	AAEL004320-PA	WOC protein, putative
96	Q17EV4	AAEL003670-PA	Myelinprotein expression factor
97	Q17HZ7	AAEL002508	26S protease regulatory subunit 6a
98	Q17LJ1	AAEL001352-PA	Scaffold attachment factor b
99	Q17N60	AAEL000823	60S ribosomal protein L35a
100	Q17Q06	AAEL000175-PB	Eukaryotic translation initiation factor 3 subunit C (eIF3-S8)
101	Q1HQD9	AAEL005355	Small nuclear ribonucleoprotein-associated protein Small nuclear ribonucleoprotein sm
102	Q1HQX3	AAEL005222	Calmodulin
103	Q1HQY6	AAEL002334	Eukaryotic translation initiation factor 3 subunit E (eIF3e)
104	Q1HR05	AAEL009275-PB	Serine/threonine-protein phosphatase protein phosphatase-1
105	Q1HRP3	AAEL001759-PA	40S ribosomal protein S9

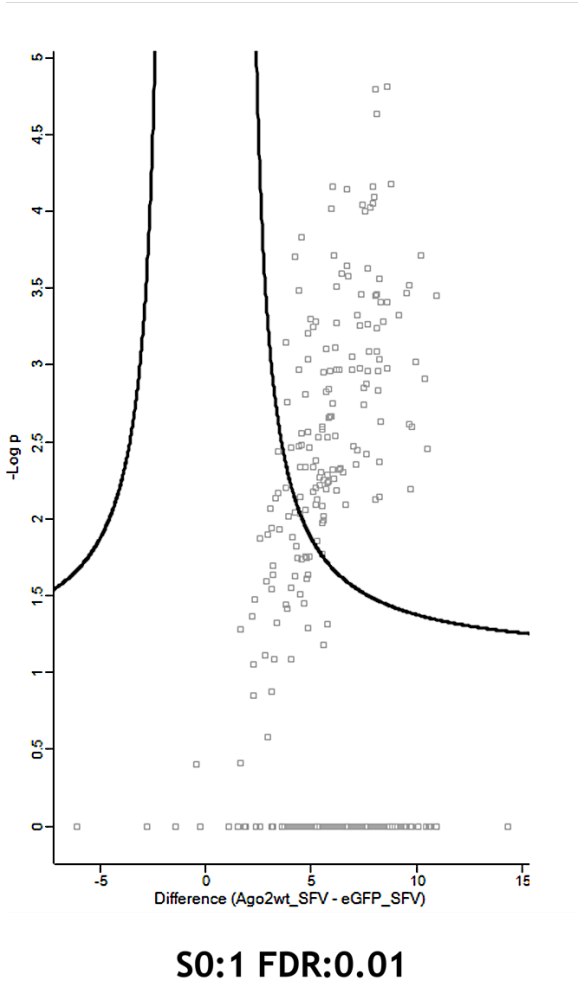

Figure 4-5 Proteomics analysis of *Ae. aegypti* Ago2 in the presence of SFV4 infection.

Volcano plots generated after immunoprecipitation (IP) show the results of a two-sample t-test comparing protein enrichment between Ago2wt and eGFP samples under SFV4 infection. The data were analysed using an S0 value of 1 and a false discovery rate (FDR) of 0.01 to identify and visualise Ago2 interactors.

Table 4-3 Proteins significantly enriched in Ago2 immunoprecipitates during SFV4 infection.

No.	UniProt ID	Vectorbase ID	Protein name
1	A0A0E3T4T7	-	Polyprotein P1234
2	A0A1S4EZR6	AAEL001715-PB	T-complex protein 1 subunit epsilon chaperonin
3	A0A1S4F7M2	AAEL004338-PA	Pyruvate dehydrogenase E1 component subunit beta
4	A0A1S4FCM2; A0A1S4FCS4	AAEL006095	Gelsolin precursor
5	A0A6I8T4Y3; Q17LH0	AAEL001356-PA	RNA-binding protein
6	A0A6I8T705	AAEL002764-PE	Dihydrolipoyllysine-residue succinyltransferase component of 2-oxoglutarate dehydrogenase complex, mitochondrial
7	A0A6I8TC94	AAEL009061	RRM domain-containing protein
8	A0A6I8TNG8	AAEL012171	RNA recognition motif protein split ends
9	A0A6I8TQ71; A0A6I8TSV1	AAEL017315-PC	Uncharacterized protein
10	A0A6I8TRB9	AAEL017437-PC	Nop domain-containing protein
11	A0A6I8TV54; A0A6I8U1S1; A0A6I8U5Y2	AAEL027250-PA	H15 domain-containing protein
12	A0A6I8U062	AAEL021140-PA	CCHC-type domain-containing protein
13	A0A6I8U6N0	AAEL023850-PA	Bifunctional glutamate/proline--tRNA ligase
14	J9HFM9	AAEL017516-PB	Unspecified protein
15	J9HTV7	AAEL017419-PA	Unspecified protein
16	Q16GV5	AAEL014250-PA	insect replication protein a
17	Q16T24	AAEL010403-PA	Past-1
18	Q170W6	AAEL007778-PA	Leucine-rich transmembrane protein
19	Q173N8	AAEL007042-PC	Far upstream (fuse) binding protein
20	Q176M6	AAEL006315-PA	26S proteasome non-ATPase regulatory subunit 2
21	Q17EQ5	AAEL003664-PB	Lupus la ribonucleoprotein
22	Q17H72	AAEL002761-PB	Tropomyosin invertebrate
23	Q17HJ3	AAEL002658-PB	AMP dependent ligase
24	Q1HR40	AAEL008257	Heterogeneous nuclear ribonucleoprotein 27c
25	Q1HRI6	AAEL014562	60S ribosomal protein L12
26	Q1HRT6	AAEL025362-PA	60S ribosomal protein L10
27	Q52UT2	AAEL004175-PA	40S ribosomal protein S17
28	Q9XYC8	AAEL005798-PA	Vacuolar proton pump subunit B

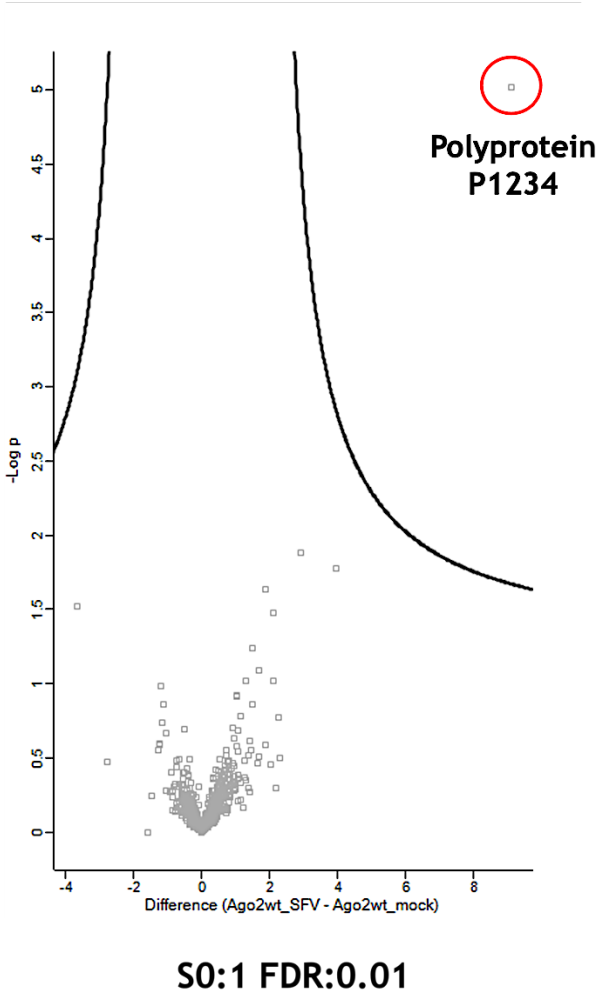

Figure 4-6 Proteomics analysis of *Ae. aegypti* Ago2 in the presence and absence of SFV4 infection.

Volcano plots generated after immunoprecipitation (IP) show the results of a two-sample t-test comparing protein enrichment between Ago2wt cells infected with SFV4 and Ago2wt mock samples. The data were analysed using an S0 value of 1 and a false discovery rate (FDR) of 0.01 to identify and visualise Ago2 interactors.

Together, these analyses identified many proteins associated with Ago2 under both mock and infected conditions. Most interactors were detected in the mock condition, whereas a smaller subset was enriched during SFV4 infection. In addition, a substantial number of proteins were detected in both conditions, suggesting the presence of a stable Ago2-associated complex that is maintained independently of infection.

Table 4-4 Proteins enriched in V5-Ago2 immunoprecipitates under both mock and SFV4-infected conditions.

No.	UniProt ID	VectorBase ID	Protein name
1	A0A1S4EV42	AAEL000159	Nipsnap
2	A0A1S4EZB3	AAEL001623	Proteasome activator subunit REG
3	A0A1S4EZS3	AAEL001769-PA	DEAD box ATP-dependent RNA helicase
4	A0A1S4F345	AAEL002906	26S proteasome non-ATPase regulatory subunit 1
5	A0A1S4F3P7	AAEL003106	Clathrin coat associated protein ap-50
6	A0A1S4F7I3; A0A6I8T9H8	AAEL004415	Fuse-binding protein-interacting repressor siahbp1
7	A0A1S4F9X3	AAEL004110	Cdk10/11
8	A0A1S4FE42	AAEL006634	Acetyl-coa acetyltransferase, mitochondrial (acetoacetyl-coa thiolase)
9	A0A1S4FE53; A0A6I8TD93	AAEL003518	Calcium-transporting ATPase
10	A0A1S4FLY4	AAEL009320-PA	T-complex protein 1 subunit alpha chaperonin
11	A0A1S4FXA4	AAEL012826-PA	Replication protein A subunit
12	A0A1S4FYC2	AAEL006287	PIWI
13	A0A1S4FYI5	AAEL013098-PA	Coatomer subunit alpha
14	A0A1S4G5R5	AALF028653-PA	H/ACA ribonucleoprotein complex subunit
15	A0A1S4G5W3; J9HFH4	AAEL017116-PB	Unspecified product
16	A0A6I8T3U9	AAEL001009	Dab2-interacting protein
17	A0A6I8T424	AAEL000832	Cleavage and polyadenylation specificity factor cpsf
18	A0A6I8T7A4	AAEL002879	Heterogeneous nuclear ribonucleoprotein r
19	A0A6I8T8D6	AAEL005861-PB	Sortilin-related receptor
20	A0A6I8T9E9; A0A6I8TD96; A0A6I8TEL1; Q174K3	AAEL006876-PA	Igf2 mRNA binding protein, putative;Igf2 mRNA binding protein, putative;Igf2 mRNA binding protein, putative
21	A0A6I8T9P7; A0A6I8T9Q2; A0A6I8TDM5; A0A6I8TDN4; A0A6I8TE27; A0A6I8TE32; A0A6I8TE48; A0A6I8TE53; A0A6I8TF22; A0A6R5HFP6	AAEL007132	Dynein heavy chain
22	A0A6I8TAV1	AAEL005165	Chaperone protein DNAj
23	A0A6I8TDY2; Q16PF3	AAEL011650-PB	AP complex subunit beta
24	A0A6I8TEN4; Q0IEY3	AAEL007718-PA	Eukaryotic translation initiation factor 3 subunit B
25	A0A6I8TMM2	AAEL002792	Dynein light chain
26	A0A6I8TNI7; A0A6I8TPE2	AAEL009345	Prohibitin
27	A0A6I8TQE6; A0A6I8TZ11; A0A6I8U596; Q17ES2	AAEL023180-PA	Histone H2B

No.	UniProt ID	VectorBase ID	Protein name
28	A0A6I8TTD0; A0A6R5I3N1	AAEL019466-PG	Mothers against decapentaplegic homolog
29	A0A6I8TTM8; A0A6I8U6N7; A0A6I8U908	AAEL026069-PE	Acetyl-CoA carboxylase
30	A0A6I8TVN6	AAEL019669-PA	CSD domain-containing protein
31	A0A6I8TWN0	AAEL019777-PA	B30.2/SPRY domain-containing protein
32	A0A6I8U220	AAEL023022-PA	RNA-binding protein 25
33	A0A6I8U2L9	AAEL024500-PA	Coatomer subunit epsilon
34	A0A6I8U337	AAEL025078-PA	Protein SEC13 homolog
35	A0A6I8U7S6	AAEL004546	Coatomer subunit beta
36	A0A6I8U913	AAEL000746	Isocitrate dehydrogenase [NADP]
37	J9EAN1	AAEL017421-PA	Unspecified product
38	Q0IEM1	AAEL009496-PA	40S ribosomal protein S7
39	Q16GE2	AAEL014414-PA	DEAD box ATP-dependent RNA helicase
40	Q16HL9	AAEL013982-PA	RNA binding motif protein 4,lark
41	Q16JS6	AAEL013230	Coatomer subunit delta
42	Q16K15	AAEL013144-PA	Eukaryotic translation initiation factor 3 subunit I
43	Q16KL0	AAEL012943-PA	26S proteasome regulatory subunit 7
44	Q16KL2	AAEL012944-PB	60S ribosomal protein L11
45	Q16M56	AAEL012419	26S proteasome subunit S9
46	Q16PF7	AAEL011656-PA	40S ribosomal protein S15
47	Q16PP1	AAEL011568-PA	Unspecified product
48	Q16QU2	AAEL011180-PA	Unspecified product
49	Q16RY3	AAEL010787-PA	DEAD box ATP-dependent RNA helicase
50	Q16SH1	AALF006251-PA	Vesicle-fusing ATPase
51	Q16TA2	AAEL010341-PA	RuvB-like helicase 2 RuvB-like helicase 2 (EC 3.6.4.12)(Reptin)
52	Q16UB0	AAEL009959-PA	Pre-mRNA splicing factor prp8
53	Q16UH6	AAEL009914-PA	Small nuclear ribonucleoprotein Sm D2
54	Q16X83	AAEL008938-PA	Unspecified product
55	Q16XK3	AAEL008848	ATP synthase subunit gamma
56	Q16Y09	AAEL008700-PA	Unspecified product
57	Q16YK5	AAEL008517-PA	Elongation factor Tu
58	Q16ZH3	AAEL008188-PA	60S ribosomal protein L6
59	Q171Y9; Q171Z0	AAEL007484	Protein transport protein SEC23
60	Q173M7	AAEL007078-PA	Eukaryotic translation initiation factor 3 subunit A
61	Q174C6	AAEL006946-PA	Chaperonin
62	Q174U3	AAEL021422-PA	60S ribosomal protein L18a
63	Q174Z2	AAEL006751-PA	Unspecified product
64	Q178C4	AAEL005947-PB	G-rich sequence factor-1, putative
65	Q17B45	AAEL002848	Tubulin beta chain
66	Q17CI5	AAEL004546	Coatomer subunit beta
67	Q17CP2	AAEL004469-PE	AP-2 complex subunit alpha adaptin, alpha/gamma/epsilon
68	Q17D57	AAEL004317-PA	Unspecified product
69	Q17FP1	AAEL003336-PA	RNA-splicing ligase RtcB homolog

No.	UniProt ID	VectorBase ID	Protein name
70	Q17GX9	AAEL002848	Tubulin beta chain
71	Q17KF0	AAEL001706-PA	NTF2-related export protein
72	Q17Q33	AAEL000147-PA	Single-stranded DNA binding protein, putative
73	Q1HQJ0	AAEL000701	60S ribosomal protein L4
74	Q1HQM1	AAEL004563	26S protease regulatory subunit S10b
75	Q1HQU2	AAEL004325-PA	60S ribosomal protein L5
76	Q1HQY1	AAEL012095	26S protease regulatory subunit
77	Q1HR13	AAEL009345	Prohibitin
78	Q1HR24	AAEL005266-PC	40S ribosomal protein S14
79	Q1HR32	AAEL000987	60S ribosomal protein L8
80	Q1HR36	AAEL006885-PA	14-3-3 protein zeta
81	Q1HR53	AAEL004172	Tubulin alpha chain
82	Q1HR62	AAEL008481-PB	60S ribosomal protein L18
83	Q1HR65	AAEL011471-PG	60S ribosomal protein L17
84	Q1HR76	AAEL013272-PA	60S ribosomal protein L37
85	Q1HR99	AAEL010821-PA	60S acidic ribosomal protein P0
86	Q1HRL8	AAEL009747-PA	40S ribosomal protein S18
87	Q1HRM5	AAEL012686-PA	40S ribosomal protein S23
88	Q1HRP1	AAEL011447-PB	60S ribosomal protein L14
89	Q1HRP2	AALB004974	60S ribosomal protein L22
90	Q1HRQ2	AAEL007656	Activated protein kinase C receptor
91	Q1HRQ6	AAEL009151-PA	40S ribosomal protein S15/S22
92	Q1HRQ7	AAEL012175	ATP synthase subunit alpha
93	Q1HRQ9	AAEL008103-PB	40S ribosomal protein S8
94	Q1HRR3	AAEL005901-PC	40S ribosomal protein S3a
95	Q1HRS9	AAEL020447-PA	40S ribosomal protein S20
96	Q1HRT9	AAEL013625-PA	40S ribosomal protein S5
97	Q1HRU0	AAEL004855-PA	ADP/ATP translocase
98	Q1HRV1	AAEL008582	40S ribosomal protein S2
99	Q535V4	AAEL018120-PG	Ribosomal protein S6 kinase
100	Q9GN74	AAEL006698-PA	60S ribosomal protein L31
101	Q9GNE2	AAEL015006-PB	60S ribosomal protein L23
102	Q9GSB1	AAEL002372-PB	40S ribosomal protein S11

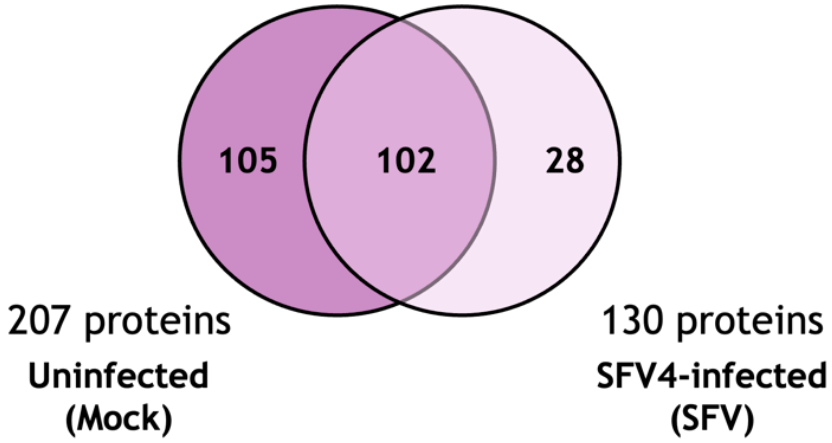

Figure 4-7 Venn diagram showing upregulated Ago2 interactors in the presence and absence of SFV4 infection.

Table 4-5 Proteins enriched in V5-Ago2 immunoprecipitates under mock condition.

Mock group		
No.	**Protein group**	**Members**
1	RNAi & RNA Metabolism (Core Ago2-related machinery)	DEAD-box RNA helicases (DDX1 and others) Double-stranded RNA-binding protein Zn72D Loquacious (dsRNA processing cofactor) Rasputin Fragile X mental retardation-related protein 5'–3' exoribonuclease PIWI RNA-binding protein 8A NXF2 (RNA export factor) RRM-domain containing proteins U1-type domain-containing protein Splicing factors
2	Translation Machinery	Multiple eIF3 subunits 40S and 60S ribosomal proteins (L13a, L26, L35a, S9, S11, etc.) Ribose-phosphate diphosphokinase CTP synthase
3	Protein Degradation (Ubiquitin–Proteasome System)	26S proteasome subunits (S3, S6) Cullin E3 ubiquitin ligases (HYD, KCMF1)
4	Cytoskeleton & Intracellular Transport	Myosin VI Myosin light chain Talin Spectrin Adducin Actin-related protein 2/3 Sec24B MAP kinase (microtubule affinity regulating kinase)
5	Stress Response & Chaperones	DnaJ homolog ER chaperone BiP Calmodulin
6	Metabolism & Mitochondrial Proteins	Pyruvate dehydrogenase complex components NADH dehydrogenase Isocitrate-related enzymes Glutathione transferase Peroxisome assembly factor
7	Signalling & Kinases	Cdk1 Polo kinase VRK kinase Casein kinase II Protein phosphatases Sarm1
8	Chromatin & Nuclear Structure	Histone H3 Chromodomain-helicase DNA binding protein Scaffold attachment factor
9	Unknown/uncharacterised proteins	Unspecified product/ Uncharacterised protein

Table 4-6 Functional classification of proteins enriched in V5-Ago2 immunoprecipitates during SFV4 infection.

SFV-infected group		
No.	**Protein group**	**Members**
1	Viral Protein	Polyprotein P1234 (SFV4 viral non-structural polyprotein)
2	RNA Binding & Processing	RNA-binding proteins RRM domain proteins Lupus La ribonucleoprotein hnRNP 27c Nop domain-containing protein
3	Translation & Ribosome	60S L10, L12 40S S17
4	Proteasome	26S proteasome regulatory subunit 2
5	Cytoskeleton	Gelsolin Tropomyosin
6	Metabolism & Mitochondria	Pyruvate dehydrogenase E1 beta 2-oxoglutarate dehydrogenase complex component AMP-dependent ligase
7	Chaperones	T-complex protein 1 (CCT epsilon)
8	DNA Replication / Genome Maintenance	Replication protein A
9	Transport & Membrane	Vacuolar proton pump subunit B Leucine-rich transmembrane protein
10	Unknown/uncharacterised proteins	Unspecified product/ Uncharacterised protein

Table 4-7 Functional classification of proteins enriched in V5-Ago2 immunoprecipitates under both mock and SFV4 infection conditions.

Overlapping group No.	Protein group	Members
1	Translation & Ribosomal Proteins (Highly enriched)	40S ribosomal proteins (S2, S3a, S5, S6, S7, S8, S11, S14, S15, S17, S18, S20, S23) 60S ribosomal proteins (L4, L5, L6, L8, L11, L14, L17, L18, L18a, L22, L23, L31, L37) Ribosomal protein S6 kinase
2	RNA Processing & Helicases	DEAD-box helicases RuvB-like helicase 2 Pre-mRNA splicing factor PRP8 H/ACA ribonucleoprotein subunit Igf2 mRNA binding protein RNA-binding protein 25 G-rich sequence factor
3	Proteasome & Protein Turnover	26S proteasome subunits (multiple) Proteasome activator REG
4	Cytoskeleton & Motor Proteins	Dynein heavy chain Dynein light chain Tubulin alpha & beta AP-2 complex Coatomer subunits (alpha, beta, delta, epsilon) SEC13 / SEC23 Vesicle-fusing ATPase
5	Metabolism & Mitochondria	Isocitrate dehydrogenase Acetyl-CoA carboxylase ATP synthase (alpha, gamma) ADP/ATP translocase
6	Signalling & Regulatory Proteins	Cdk10/11 14-3-3 protein zeta Mothers against decapentaplegic (Smad homolog) PKC receptor
7	Chromatin & Nuclear	Histone H2B NTF2 export protein Single-stranded DNA binding protein
8	Unknown/uncharacterised proteins	Unspecified product/ Uncharacterised protein

In the mock condition, the Ago2 interactome was enriched for proteins associated with RNA processing and RNAi-related pathways. A total of 207 Ago2 interactors were identified, of which 105 were uniquely enriched in the mock group (Table 4-2). These interactors were classified into nine functional protein categories (Table 4-5). Several enriched proteins are known components or regulators of RNAi pathways, including Loqs, a dsRNA-binding protein required for efficient siRNA production, and PIWI, a component of the piRNA pathway involved in transposon silencing. DEAD-box RNA helicases such as DDX1 were also detected and are associated with RNA duplex unwinding and RNA granule formation. In addition, the dsRNA-binding protein Zn72D, which contributes to dsRNA processing and stability of RNAi components, was identified. Other enriched interactors included Rasputin, which is linked to stress granule formation and viral replication control, Rap55, which functions in translational repression and mRNA decay, and Fragile X-related protein, which modulates RISC function and regulates translation of RNAi-targeted mRNAs. A 5′–3′ exoribonuclease involved in mRNA degradation downstream of RISC cleavage was also detected.

During SFV4 infection, the Ago2 interactome shifted towards proteins associated with viral replication and host cellular processes exploited by the virus. In this condition, 28 Ago2 interactors were uniquely enriched (Table 4-3) and classified into ten functional categories (Table 4-6). The viral polyprotein P1234 was the only SFV non-structural protein detected in the interactome. Several host proteins identified in group 2 were RNA-binding proteins that may be utilised by SFV to regulate viral RNA translation and replication, including a CCHC-type domain-containing RNA-binding protein and heterogeneous nuclear ribonucleoprotein (hnRNP 27c). In addition, gelsolin precursor, classified in group 5, regulates actin assembly and disassembly, which is important for intracellular virus trafficking in mosquito cells. Vacuolar proton pump subunit B (V-ATPase), classified in group 9, is involved in endosomal acidification, a process required for alphavirus entry into mosquito cells. Overall, the enriched proteins in the infection condition were associated with viral entry, intracellular trafficking, cytoskeletal remodelling, metabolic processes, and host proteostasis pathways that are commonly targeted during viral infection.

The overlapping interactors identified in Table 4-4 (102 proteins) likely represent a core Ago2-associated complex that is maintained regardless of infection status.

These proteins were classified into eight functional categories (Table 4-7) and were detected in both mock and SFV4-infected conditions. Proteins in group 1 were primarily associated with translational machinery and ribosome-associated Ago2 complexes, whereas proteins in group 4 were involved in vesicle trafficking and intracellular transport.

Together, these results indicate that Ago2 interacts predominantly with RNA processing factors and RNAi cofactors under mock conditions, whereas during SFV4 infection the Ago2 interactome shifts towards proteins associated with viral replication, cellular stress responses, and metabolic adaptation. The overlapping interactors likely represent a stable core complex of proteins associated with translation, ribosomes, cytoskeletal regulation, and proteostasis.

4.3.3 Candidate proteins

The overlapping set of 102 proteins identified in both mock- and SFV4-infected V5-Ago2 immunoprecipitates was considered a consistently Ago2-associated interactome, as these proteins were reproducibly detected irrespective of infection status. Accordingly, proteins detected in both experimental conditions were classified as consistent Ago2 interactors.

From this overlapping group, 21 candidate proteins were prioritised for downstream functional screening by dsRNA-mediated silencing (Figure 4-8). Candidate selection was performed using a biologically guided filtering strategy aimed at identifying potential Ago2-specific antiviral regulators while minimising indirect effects arising from disruption of essential cellular machinery. The list of these 21 candidate proteins is shown in Table 4-8.

Proteins associated with core translational processes, ribosomal subunits, or general viral replication-related cellular functions were excluded from prioritisation. These proteins were not selected because their depletion would be expected to broadly impair cellular viability or reduce viral replication independently of antiviral RNAi activity, thereby confounding interpretation of functional assays.

Priority was instead given to proteins with predicted regulatory, RNA-associated, trafficking, or signalling-related functions, as well as several uncharacterised proteins that could represent previously unknown antiviral cofactors in *Ae. aegypti*. Thus, the final panel of 21 candidates represented a targeted subset of reproducibly Ago2-associated proteins selected for their potential to specifically modulate antiviral RNAi responses.

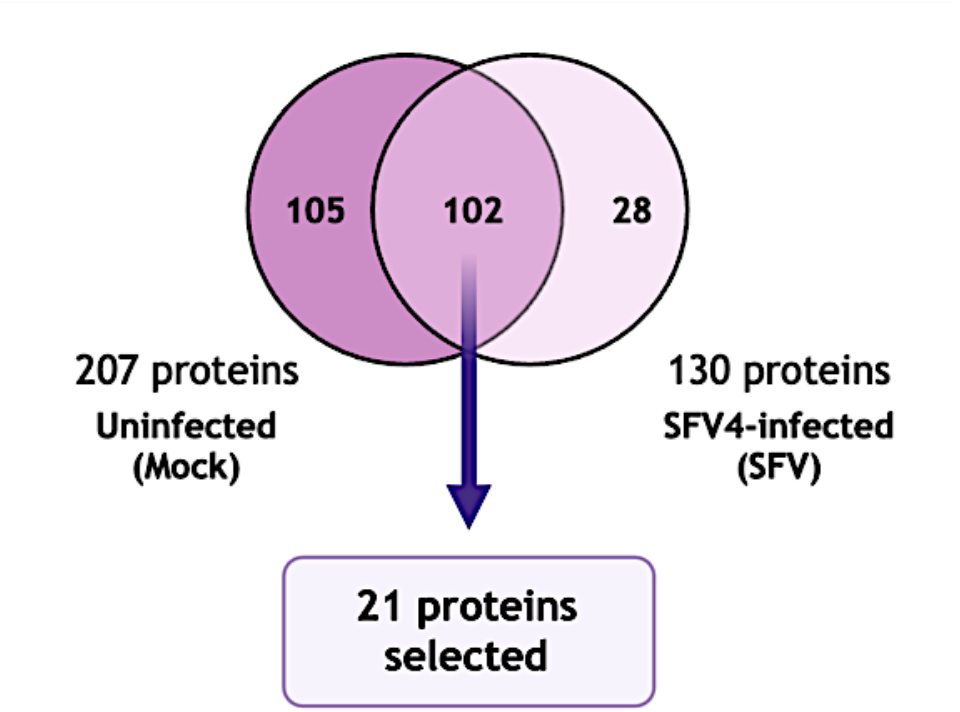

Figure 4-8 Selection of twenty-one candidate proteins.

The 21 interaction partners were selected from the overlapping group identified in the proteomics analysis of AF525-V5-Ago2wt and AF525-V5-eGFP cells in the presence and absence of SFV4. These candidate proteins were subsequently used for a dsRNA knockdown screen.

Table 4-8 Candidate Ago2-interacting proteins selected for functional validation following proteomic analysis.

No.	UniProt ID	VectorBase ID	Protein name
1	A0A1S4EV42	AAEL000159	Nipsnap
2	A0A1S4F3P7	AAEL003106	Clathrin coat associated protein ap-50
3	A0A1S4F7I3; A0A6I8T9H8	AAEL004415	Fuse-binding protein-interacting repressor siahbp1
4	A0A1S4G5W3; J9HFH4	AAEL017116-PB	Unspecified product
5	A0A6I8T3U9	AAEL001009	Dab2-interacting protein
6	A0A6I8T9E9; A0A6I8TD96; A0A6I8TEL1; Q174K3	AAEL006876-PA	Igf2 mRNA binding protein, putative
7	A0A6I8TAV1	AAEL005165	Chaperone protein DNAj
8	A0A6I8TNI7; A0A6I8TPE2	AAEL009345	Prohibitin
9	A0A6I8TUE6	AAEL018313	Unspecified product
10	A0A6I8TVN6	AAEL019669-PA	Unspecified product
11	A0A6I8TWN0	AAEL019777-PA	Unspecified product
12	Q16GE2	AAEL014414-PA	DEAD box ATP-dependent RNA helicase
13	Q16HL9	AAEL013982-PA	RNA binding motif protein 4, lark
14	Q16PP1	AAEL011568-PA	Unspecified product
15	Q16SH1	AALF006251-PA	Spermatogenesis associated factor
16	Q16X83	AAEL008938-PA	Unspecified product
17	Q16Y09	AAEL008700-PA	Unspecified product
18	Q174Z2	AAEL006751-PA	Unspecified product
19	Q17CP2	AAEL004469-PE	Adaptin, alpha/gamma/epsilon
20	Q17D57	AAEL004317-PA	Unspecified product
21	Q17Q33	AAEL000147-PA	Single-stranded DNA binding protein, putative

4.3.4 The knockdown and antiviral activity of selected mosquito interactors

The results of the knockdown and antiviral activity assays were presented for each of the four replicates individually to facilitate interpretation of proteins that produced consistent effects across experiments. Knockdown experiments were performed by transfecting dsRNA targeting each candidate protein together with SFV4(3H)-FFLuc into AF5 cells. dsRNA targeting eGFP was used as a control.

At 24 hours post-infection (h.p.i), RT-qPCR analysis revealed significantly reduced levels of viral RNA for most candidate proteins in replicates 2 and 4, indicating successful knockdown (Figure 4-9B and 4-9D). In replicates 1 and 3, knockdown of candidate protein 9 appeared less effective, whereas efficient knockdown was observed in replicates 2 and 4.

Luciferase assays performed in parallel showed that virus replication increased significantly following knockdown of candidate protein 12 (AAEL014414-PA) in all four replicates, suggesting that this protein may have antiviral activity. In addition, knockdown of several other proteins, including candidate proteins 10, 15, 16, and 18, showed increased viral replication in three out of the four replicates (Figure 4-9E–H).

Notably, candidate protein 12 showed consistent results for both knockdown efficiency and antiviral activity across all four replicates (Figure 4-9). Based on these observations, candidate protein 12 was selected for further investigation.

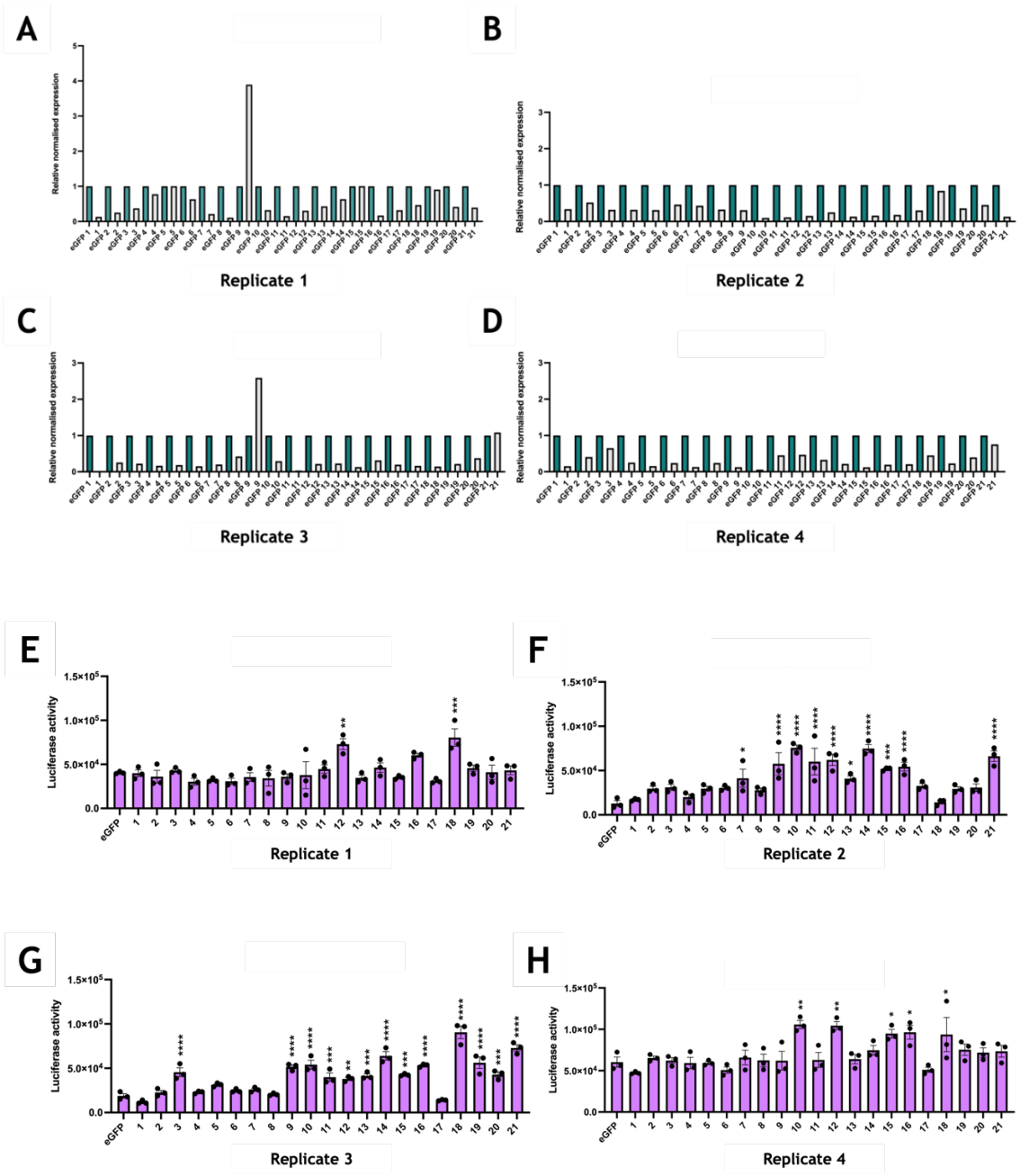

Figure 4-9 Knockdown efficiency and antiviral activity of the 21 selected candidate proteins.

AF5 cells were transfected with 100 ng dsRNA targeting transcripts of each candidate protein, with dsRNA targeting eGFP (dseGFP) used as a non-targeting control. At 24 hours post-transfection (h.p.t.), cells were infected with SFV4(3H)-FFLuc at a multiplicity of infection (MOI) of 0.1 PFU/cell. At 24 hours post-infection (h.p.i), cells were lysed for RNA extraction and, in parallel, lysed for measurement of luciferase activity. (A–D) RT-qPCR results are shown individually for four biological replicates. The mRNA levels of the target were shown in relative normalised expression. (E–H) Luciferase activity results are also shown separately for each biological replicate, with error bars representing ± SD from experiments performed in technical triplicate. Each protein is referred to by its VectorBase ID as follows: 1 (AAEL000159), 2 (AAEL003106), 3 (AAEL004415), 4 (AAEL017116-PB), 5 (AAEL001009), 6 (AAEL006876-PA), 7 (AAEL005165), 8 (AAEL009345), 9 (AAEL018313), 10 (AAEL019669-PA), 11 (AAEL019777-PA), 12 (AAEL014414-PA), 13 (AAEL013982-PA), 14 (AAEL011568-PA), 15 (AALF006251-PA), 16 (AAEL008938-PA), 17 (AAEL008700-PA), 18 (AAEL006751-PA), 19 (AAEL004469-PE), 20 (AAEL004317-PA), and 21 (AAEL000147-PA). Statistical significance was determined using ordinary one-way ANOVA with Dunnett's multiple comparisons test (*p < 0.05).

4.3.5 The effect of Ago2 interactors on RNAi

Western blotting was performed on V5-Ago2wt samples across four biological replicates to confirm the expression and immunoprecipitation of V5-tagged Ago2 proteins prior to downstream small RNA sequencing. During immunoprecipitation, protein G beads coupled with anti-V5 antibodies were used to capture V5-Ago2wt protein complexes. V5-Ago2wt was successfully detected in both the input and immunoprecipitated fractions, confirming efficient enrichment of the tagged protein by anti-V5-mediated pull-down. In contrast, SFV proteins, which do not contain a V5 tag, were detected only in the input fractions prior to immunoprecipitation, with a major band observed at approximately 70 kDa. These results confirmed the expression of both V5-Ago2wt and SFV proteins in the stable cell lines. Following confirmation of protein expression and successful immunoprecipitation, RNA was extracted from the samples for subsequent small RNA sequencing (Figure 4-10).

This experiment was performed in AF525 cells expressing V5-tagged Ago2 constructs to enable efficient immunoprecipitation of Ago2-containing complexes. The sequencing data therefore represent Ago2-associated small RNAs rather than the total cellular small RNA population.

Among the proteins identified in the Ago2 interactome, candidate protein 12 (AAEL014414-PA), a DEAD-box ATP-dependent RNA helicase, was selected for further investigation and designated AAIP12 (*Aedine* Ago2 Interacting Protein 12). To investigate the overall population of virus-derived siRNAs (vsiRNAs), AF525 cells were transfected with dsRNA targeting AAIP12 and subsequently infected with SFV4. Analysis of vsiRNA duplexes showed a slight decrease in overlapping pairs and z-score values compared with the control. The highest number of overlapping vsiRNA duplexes occurred between 18 and 21 nt (Figure 4-11). AAIP12 showed the highest z-score probability for 19 nt overlapping vsiRNA duplexes (Figure 4-11A).

The read length distribution of vsiRNAs indicated that approximately 65% of reads in the AAIP12 library were 21 nt in length (Figure 4-12A). In addition, no clear difference was observed in the distribution of small RNAs mapped to the SFV genome (Figure 4-12B). Together, these results suggest that knockdown of AAIP12 does not substantially affect Ago2-associated vsiRNA production under the conditions tested.

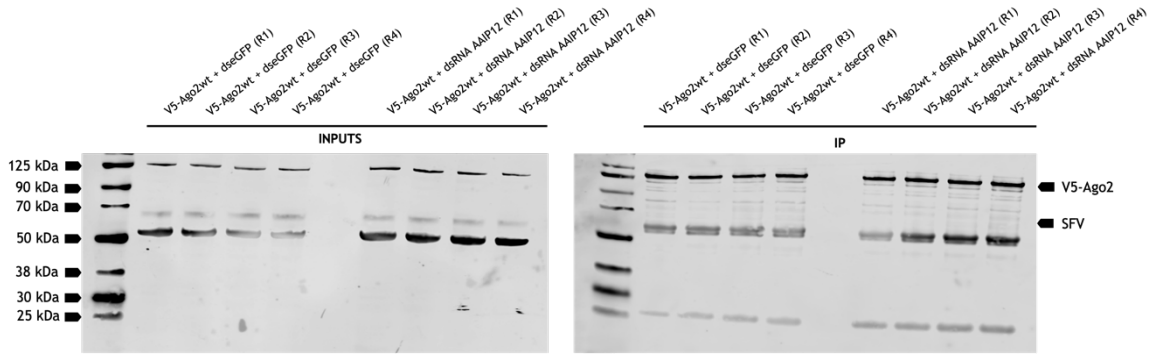

Figure 4-10 Expression of Ago2wt in AF525 cells stably expressing V5-tagged Ago2 following transfection of dsRNA targeting candidate protein 12 and subsequent SFV4 infection.

AF525-V5-Ago2wt cells were transfected with 100 ng dsRNA targeting candidate protein 12, with 10 ng dsRNA targeting eGFP (dseGFP) used as a control. At 24 hours post-transfection (h.p.t.), cells were infected with SFV4 at a multiplicity of infection (MOI) of 5 PFU/cell. At 24 hours post-infection (h.p.i), cell pellets were collected for immunoprecipitation (IP). The IP pull-down samples were used for RNA extraction, and target protein expression was analysed by Western blotting before (INPUTs) and after IP.

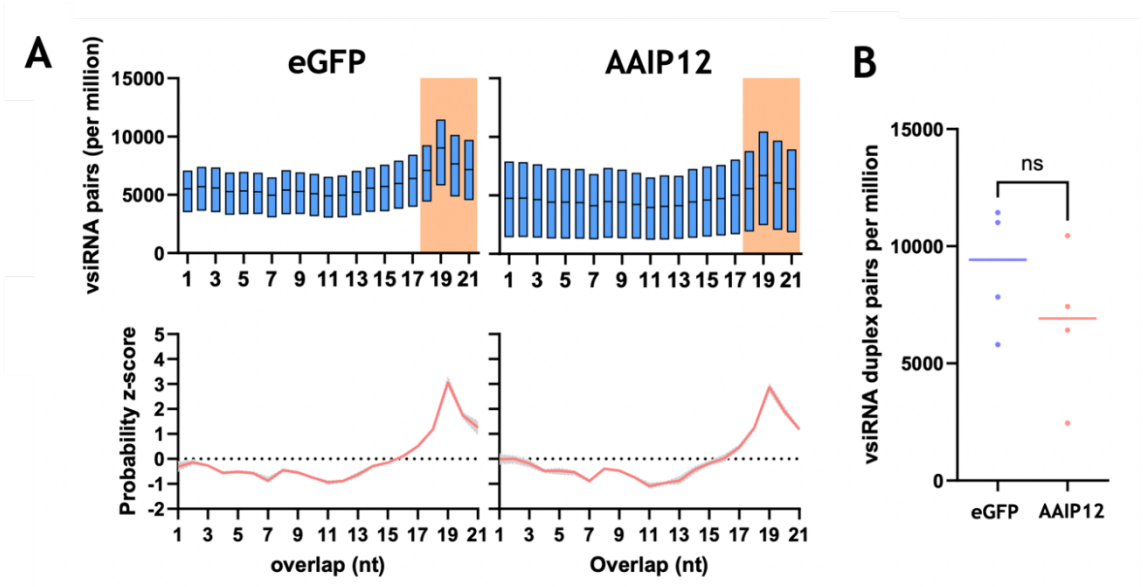

Figure 4-11 Analysis of vsiRNA duplex pairs and z-scores.

(A) Number of overlapping vsiRNA duplex pairs (21 nt), normalised per million mapped SFV reads. The predominance of vsiRNA duplex overlaps between 18 and 21 nt is highlighted in orange, with the corresponding probability z-score of overlapping 21 nt vsiRNA reads shown below. (B) Number of the most abundant 21 nt vsiRNA duplexes overlapping by 18–21 nt across AF525 cell line derivatives, normalised per million mapped reads. Each graph represents the mean of independent experiments (n = 4), with the range indicated. Statistical significance was determined using ordinary one-way ANOVA with Tukey's multiple comparisons test (ns = not significant).

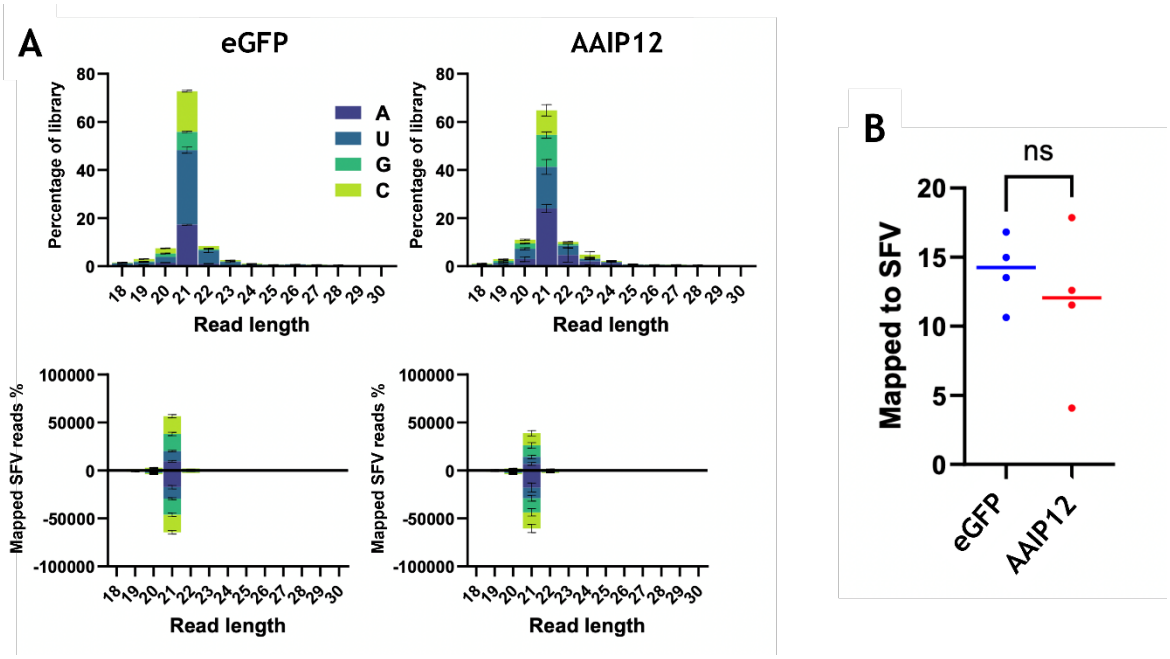

Figure 4-12 Read length distribution and small RNAs mapped to the SFV genome.

(A) Distribution of small RNA read lengths. (B) Small RNAs mapped across the SFV genome. Statistical analysis was performed using ordinary one-way ANOVA with Tukey's multiple comparisons test (ns = not significant).

4.4 Discussion

This chapter examined the Ago2 interactome in mosquito cells under mock conditions and during SFV4 infection to identify proteins associated with Ago2 and determine whether these interactions changed during viral infection. The proteomics analysis revealed three main features of the dataset. First, under mock conditions the Ago2 interactome was enriched for proteins associated with RNA processing and RNAi-related pathways. Second, during SFV4 infection the interactome shifted towards proteins linked to viral replication and host cellular processes commonly exploited by the virus. Third, a substantial overlapping group of proteins was identified in both mock and infected conditions, suggesting the presence of a stable Ago2-associated core complex that was maintained regardless of infection status.

Under mock conditions, Ago2 associated with multiple proteins involved in RNA metabolism, RNA binding and post-transcriptional regulation. These included Loqs, PIWI, DEAD-box RNA helicases, Zn72D, Rasputin, Rap55 and Fragile X-related protein. This pattern was consistent with the established role of Ago2 as a central component of the mosquito exo-siRNA pathway and suggested that Ago2 existed within a broader network of RNA regulatory factors rather than functioning in isolation. Loqs was of particular interest in this group. In mosquitoes, Loqs has been shown to support efficient small RNA production and has also been identified as a proviral host factor in the context of arbovirus infection (Besson *et al.*, 2022). Its enrichment in the mock Ago2 interactome suggested that Ago2 may be positioned within RNA regulatory complexes that have both antiviral and proviral potential, depending on cellular context and viral infection status. The absence of Loqs from the infected-specific dataset did not necessarily indicate that it was irrelevant during infection. It was possible that Loqs remained associated with Ago2 below the chosen significance threshold or that its function during SFV4 infection was regulated post-transcriptionally rather than through major changes in protein enrichment.

In contrast, the SFV4-infected Ago2 interactome was smaller and more focused, with only 28 proteins uniquely enriched in infected samples. These proteins were primarily associated with RNA binding, intracellular trafficking, cytoskeletal regulation, metabolism and proteostasis. This suggested that during infection Ago2

became associated with proteins linked more directly to the altered cellular environment created by virus replication. The most notable infection-specific interactor was the SFV4 polyprotein P1234. This was the only viral protein detected in the infected interactome and represented a particularly interesting result. The alphavirus non-structural polyprotein P1234 is processed into nsP1, nsP2, nsP3 and nsP4, which together control viral RNA synthesis and replication complex assembly (Vasiljeva *et al.*, 2003, Pietilä *et al.*, 2017, Lello *et al.*, 2021). Detection of P1234 in the Ago2 interactome suggested that Ago2 may associate either directly with one or more viral non-structural proteins, or indirectly through shared association with viral RNA or replication complexes. This finding raised the possibility that Ago2 was recruited to sites of viral replication, or that SFV replication machinery and Ago2 occupied overlapping intracellular environments during infection.

Although only one protein was significantly enriched in the direct comparison between infected and mock Ago2 samples, this did not necessarily indicate that infection had little effect on the Ago2 interactome. The stringent statistical cut-off used for the proteomics analysis may have limited the number of differentially enriched proteins detected. In addition, many infection-dependent interactions may have been weak, transient, or mediated indirectly through RNA, making them difficult to detect robustly in this experimental setting. It was therefore likely that infection caused remodelling of the Ago2 interactome in a more subtle manner than a simple gain-or-loss model would suggest. This interpretation was consistent with the presence of a large overlapping group of proteins shared between mock and infected conditions.

The overlapping group, consisting of 102 interactors, was one of the most informative parts of the dataset. These proteins were enriched for translation-related proteins, ribosomal proteins, vesicle trafficking components, cytoskeletal and motor proteins, and proteostasis-related factors. This suggested that a substantial proportion of the Ago2 interactome represented a constitutive Ago2-associated platform that persisted independently of infection status. Rather than being assembled only in response to infection, Ago2 appeared to exist within a stable cellular environment linked to RNA handling, translation and intracellular transport. This was biologically plausible, as effective RNA silencing requires coordination between small RNA loading, target recognition, mRNA turnover and spatial

organisation within the cytoplasm. The presence of ribosome-associated and trafficking-associated proteins may therefore reflect the broader cellular context in which Ago2 functions in mosquito cells.

Several interactors identified in this chapter had not previously been reported as Ago2-associated proteins, particularly in mosquitoes. This was important because current understanding of Ago2-interacting proteins has been shaped largely by studies in *D. melanogaster*. The mosquito Ago2 interactome identified here differed considerably from previously described *Drosophila* datasets, suggesting that Ago2 may engage with a more vector-specific set of proteins in mosquito cells. This was particularly relevant in the context of arbovirus infection, where mosquito cells must tolerate persistent or non-lytic infection while still restricting virus replication sufficiently to maintain vector competence. For example, vacuolar proton pump subunit B (V-ATPase), identified in the infected interactome, had not previously been highlighted as an Ago2 interactor in *D. melanogaster*. V-ATPase is required for endosomal acidification and is therefore important for alphavirus entry through pH-dependent membrane fusion (Kielian *et al.*, 2010). Its association with Ago2 during infection may indicate that Ago2 becomes linked to cellular compartments involved in virus entry, trafficking, or downstream processing of viral RNA. While this does not imply a direct mechanistic role for V-ATPase in RNAi, it does support the idea that the mosquito Ago2 interactome is shaped by the demands of arbovirus infection in a way that is not fully captured by *Drosophila*-based models.

To move beyond descriptive proteomics, 21 proteins from the overlapping group were selected for functional follow-up using a dsRNA knockdown screen. These proteins were chosen because they were not obviously direct components of viral replication or translation and therefore had the potential to represent previously unrecognised regulators of Ago2 or RNAi-related activity. The screening results showed that several candidates affected SFV4 replication in some replicates, but only candidate protein 12 (AAEL014414-PA) produced a consistent antiviral phenotype across all four experiments. This highlighted the importance of reproducibility as a selection criterion in functional follow-up of proteomics datasets. Many interactors identified by proteomics may be context-dependent or have subtle effects, whereas AAIP12 emerged as the strongest and most robust candidate for further study.

AAIP12, annotated as a DEAD-box ATP-dependent RNA helicase, was therefore prioritised for downstream analysis. Knockdown of AAIP12 reproducibly increased SFV4 replication, suggesting that it had antiviral activity. However, the subsequent small RNA sequencing analysis did not reveal major changes in Ago2-associated vsiRNA profiles following AAIP12 knockdown. Read length distribution remained dominated by 21 nt vsiRNAs, overlap signatures were broadly maintained, and no obvious change was detected in the distribution of small RNAs mapped to the SFV genome. These findings suggested that AAIP12 did not substantially alter canonical Ago2-associated vsiRNA production under the conditions tested. This result did not exclude a role for AAIP12 in Ago2 biology. Instead, it suggested that the antiviral phenotype associated with AAIP12 knockdown may occur downstream of vsiRNA biogenesis, or through a mechanism that does not cause a major detectable change in the vsiRNA parameters measured here. For example, AAIP12 may influence Ago2 localisation, RISC efficiency, target engagement, turnover of cleaved RNAs, or another antiviral process that indirectly affected SFV4 replication. It was also possible that the effects of AAIP12 on Ago2 function were subtle and not captured by the current sequencing analysis.

Several limitations should be considered when interpreting this dataset. The interactome was defined in a mosquito-derived cell line rather than in whole mosquitoes and therefore may not fully reflect tissue-specific interactions that occur *in vivo*. In addition, SFV4 was used as a model alphavirus, and Ago2-associated proteins may differ during infection with other arboviruses, such as flaviviruses. The immunoprecipitation-based approach also could not distinguish direct protein-protein interactions from indirect associations mediated through RNA or larger protein complexes. Finally, the analysis was performed at a single infection time point, meaning that temporal changes in the Ago2 interactome were not captured.

Overall, this chapter provided the first systematic analysis of the mosquito Ago2 interactome under mock and arbovirus-infected conditions. The results showed that Ago2 associated with RNAi- and RNA-processing factors under mock conditions, shifted towards infection-associated host and viral factors during SFV4 infection, and retained a core set of overlapping interactors likely to represent a stable Ago2-associated complex. Functional screening identified AAIP12 as a reproducible antiviral candidate, although its effect did not appear to involve major changes in

Ago2-associated vsiRNA production. Together, these findings expanded current understanding of mosquito Ago2 biology and identified candidate pathways and proteins that may contribute to antiviral defence and, potentially, future strategies aimed at reducing vector competence.

Chapter 5:
General Discussion

Chapter 5 General Discussion

RNAi represents the primary antiviral defence mechanism in insects and plays a central role in shaping the interaction between arboviruses and their mosquito vectors. Within this system, the exo-siRNA pathway recognises viral double-stranded RNA (dsRNA) produced during replication and directs sequence-specific degradation of viral RNA (Aliyari and Ding, 2009, Kemp and Imler, 2009). At the core of this pathway lies Argonaute-2 (Ago2), the catalytic component of the RNA-induced silencing complex (RISC), which uses virus-derived siRNAs (vsiRNAs) as guides to target complementary viral RNA molecules (Hammond *et al.*, 2001, Meister *et al.*, 2004). Although the antiviral role of Ago2 has been well established in model systems such as *D. melanogaster*, comparatively less is known about the molecular mechanisms governing Ago2 activity in mosquito cells, particularly in the context of arbovirus infection (Obbard *et al.*, 2006, Varjak *et al.*, 2017a). Understanding how Ago2 functions in vector cells is therefore important for both fundamental virology and for understanding the biological factors that influence arbovirus transmission.

The work presented in this thesis aimed to address two major questions regarding Ago2-mediated antiviral immunity in mosquito cells. First, the contribution of Ago2 catalytic activity to antiviral defence against SFV was investigated. Second, the Ago2 interactome was explored to identify host proteins that may regulate Ago2 activity or participate in antiviral RNAi responses. Together, these approaches provide new insight into how Ago2 contributes to antiviral defence in mosquito cells and identify potential new host factors that may influence arbovirus replication.

5.1 Ago2 catalytic activity and antiviral RNAi

A central objective of this thesis was to determine whether the catalytic activity of Ago2 is required for effective antiviral defence in mosquito cells. Using mosquito cell lines deficient in Ago2 activity, recombinant cell lines expressing either wild-type Ago2 or catalytic mutants of the Ago2 tetrad were generated. This system provided a powerful approach to directly test the contribution of Ago2 catalytic residues to antiviral RNAi activity.

Ago2 contains a conserved catalytic tetrad located within the PIWI domain that is responsible for endonucleolytic cleavage of target RNA (Ma *et al.*, 2004, Miyoshi *et al.*, 2005). This catalytic activity allows Ago2 to slice complementary RNA molecules guided by bound siRNAs and represents the key effector step of the RNA-induced silencing complex. In the context of antiviral RNAi, cleavage of viral RNA by Ago2 is expected to play a critical role in limiting viral replication (Li *et al.*, 2002, Sabin *et al.*, 2009). The results presented in this thesis demonstrate that mutation of the Ago2 catalytic tetrad disrupts this antiviral activity, confirming that catalytic slicing activity is essential for effective suppression of SFV replication in mosquito cells.

These findings reinforce the importance of Ago2 catalytic function within the exo-siRNA pathway. While the generation of vsiRNAs through Dcr2-mediated processing of viral double-stranded RNA is an important step in antiviral RNAi (Deddouche *et al.*, 2008, Morazzani *et al.*, 2012), the data presented here suggest that dicing alone is insufficient to suppress viral replication. Instead, the subsequent Ago2-mediated cleavage of viral RNA appears to represent a critical step in the antiviral response (Mueller *et al*., 2010). This observation highlights the importance of fully functional RISC complexes in mediating antiviral activity and suggests that impairment of Ago2 slicing activity may substantially reduce the effectiveness of the RNAi pathway.

Importantly, these findings also raise broader questions regarding the precise mechanisms through which Ago2 mediates antiviral effects in mosquito cells. While catalytic slicing clearly plays a central role, it remains possible that Ago2 also contributes to antiviral immunity through additional mechanisms. In other systems, Argonaute proteins have been shown to participate in translational repression, RNA stability regulation, and interactions with other RNA-binding proteins (Ender and Meister, 2010, Iwakawa and Tomari, 2022). It is therefore conceivable that Ago2 may function not only as a catalytic effector but also as a scaffold that recruits additional host factors involved in antiviral responses. The identification of Ago2-associated proteins in this thesis supports the possibility that Ago2 operates within a larger network of RNA-binding proteins and regulatory factors.

The observation that catalytic activity is required for efficient antiviral defence also provides insight into the broader biology of arbovirus infection in mosquito vectors.

Arboviruses typically establish persistent infections in mosquitoes without causing significant pathology. One possible explanation for this phenomenon is that antiviral RNAi limits viral replication but does not eliminate infection (Blair and Olson, 2015, Varjak *et al.*, 2017b). The catalytic activity of Ago2 may therefore represent an important component of the balance between viral replication and host defence that allows long-term virus persistence in vector populations.

Future studies could further investigate the role of Ago2 catalytic activity *in vivo*. For example, generating mosquitoes carrying mutations in Ago2 catalytic residues would provide valuable insight into whether the slicing function of Ago2 is equally important across different tissues and infection contexts.

5.2 RNAi pathway dynamics and arbovirus persistence

The results obtained in this thesis also contribute to a broader understanding of how the RNAi pathway shapes virus–vector interactions. The exo-siRNA pathway in mosquitoes produces predominantly 21-nucleotide vsiRNAs derived from viral double-stranded RNA intermediates (Bronkhorst *et al.*, 2012, Marques *et al.*, 2013). These vsiRNAs guide Ago2-mediated cleavage of viral RNA, thereby restricting viral replication.

However, despite the effectiveness of this pathway, arboviruses are rarely eliminated from mosquito cells. Instead, they persist at reduced replication levels. This observation suggests that antiviral RNAi functions primarily to control viral replication rather than to eradicate infection (Blair and Olson, 2015). The results presented here are consistent with this model, demonstrating that disruption of Ago2 catalytic activity leads to increased viral replication, while functional Ago2 contributes to the suppression of viral RNA.

An intriguing question arising from these findings is whether modifications to the RNAi machinery could alter the efficiency of antiviral responses. For example, the length of siRNAs produced during Dcr2-mediated cleavage is determined by structural features of the enzyme, including the spacing between the PAZ and RNase III domains (Macrae *et al.*, 2006). In principle, mutations that alter these

structural features could generate siRNAs of different lengths. Whether such alterations might enhance or impair antiviral activity remains unknown. Longer or shorter siRNAs could potentially influence target recognition or RISC stability, thereby affecting antiviral efficacy.

Similarly, modifications to the PAZ domain of Ago2 could influence how small RNAs are bound and presented to target RNA molecules (Lingel *et al.*, 2003, Lingel *et al.*, 2004). Such alterations might change the efficiency of RISC assembly or the stability of guide RNA binding. Investigating these structural aspects of the RNAi machinery could provide new insights into the determinants of antiviral RNAi efficiency and may reveal strategies for enhancing antiviral responses in mosquito vectors.

5.3 The Ago2 interactome and regulation of antiviral RNAi

To further understand how Ago2 activity may be regulated, the second major objective of this thesis was to identify proteins that interact with Ago2 during viral infection. Using proteomics approaches, the Ago2 interactome was characterised in both infected and uninfected mosquito cells.

The results revealed a diverse set of Ago2-associated proteins, including RNA-binding proteins, RNA processing factors, and proteins of currently unknown function. These findings support the idea that Ago2 does not function in isolation but rather operates as part of a broader network of host proteins involved in RNA metabolism and antiviral responses.

Interestingly, comparison of infected and uninfected samples revealed both shared and infection-specific interactions. The presence of certain proteins in both conditions suggests that some Ago2 interactions represent core components of RNAi machinery. In contrast, infection-specific interactions may reflect host responses to viral replication or viral attempts to manipulate host antiviral pathways.

One particularly notable observation was the presence of a PIWI family protein within the overlap group of interactors detected in both infected and control samples. PIWI proteins are typically associated with the piRNA pathway, which plays an

important role in transposon silencing and has also been implicated in antiviral responses in mosquitoes (Brennecke *et al.*, 2007, Miesen *et al.*, 2016). The interaction between Ago2 and PIWI proteins may therefore represent an example of crosstalk between small RNA pathways, highlighting the complexity of antiviral RNA regulation in mosquito cells (Varjak *et al.*, 2017b).

Among the identified interactors, the DEAD-box RNA helicase AAEL014414-PA (AAIP12) emerged as a particularly interesting candidate. RNA helicases are known to participate in a wide range of RNA-related processes, including RNA processing, translation, and antiviral sensing (Fullam and Schroder, 2013). Functional screening of candidate interactors revealed that knockdown of AAIP12 resulted in increased viral replication, suggesting that this protein may contribute to antiviral defence.

Although the precise mechanism through which AAIP12 influences viral replication remains unclear, several possibilities can be considered. DEAD-box helicases are often involved in remodelling RNA structures and facilitating RNA-protein interactions. AAIP12 may therefore contribute to the formation or stability of RNAi complexes or participate in the processing of viral RNA substrates. Alternatively, it may act independently of the RNAi pathway but influence viral replication through other RNA-related mechanisms.

5.4 Limitations of the study

While the findings presented in this thesis provide valuable insights into Ago2 function and antiviral RNAi, several limitations should be considered. First, much of the work was conducted in mosquito cell lines rather than in whole mosquitoes. Although cell culture systems provide powerful tools for mechanistic studies, they may not fully capture the complexity of antiviral responses in living organisms.

Second, proteomic approaches are inherently limited by detection sensitivity and experimental conditions. It is therefore possible that additional Ago2-interacting proteins were not detected in the present analysis.

Finally, functional validation was performed for only a subset of candidate interactors identified in the proteomics analysis. Additional candidates identified in

the interactome analysis may also contribute to antiviral defence and warrant further investigation.

5.5 Future directions

The work presented in this thesis opens several avenues for future research. One important direction will be the functional characterisation of additional Ago2-interacting proteins identified in the proteomic analysis. Systematic screening using RNAi knockdown or CRISPR-based gene editing could reveal additional host factors that contribute to antiviral RNAi or regulate viral replication.

Another important area for future study is the investigation of Ago2 catalytic mutants *in vivo*. Generating mosquitoes carrying mutations in Ago2 catalytic residues would allow direct assessment of the role of slicing activity in vector competence and arbovirus transmission.

Further work could also explore whether the mechanisms identified in this thesis are conserved across different arboviruses. While the present study focused on SFV as a model alphavirus, many arboviruses transmitted by mosquitoes belong to different viral families.

5.6 Conclusion

In summary, this thesis provides new insight into the molecular mechanisms underlying Ago2-mediated antiviral immunity in mosquito cells. The results demonstrate that catalytic activity of Ago2 is essential for efficient suppression of SFV replication, highlighting the importance of RISC-mediated RNA cleavage in antiviral RNAi. In addition, the identification of Ago2-associated proteins reveals a broader network of host factors that may regulate RNAi activity and influence virus replication.

Together, these findings contribute to a deeper understanding of antiviral RNAi mechanisms and provide a foundation for future studies exploring how host factors regulate arbovirus infection in mosquito vectors.

Chapter 6: References

Chapter 6 References

Achee, N. L., Gould, F., Perkins, T. A., Reiner, R. C., Jr., Morrison, A. C.*, et al.* 2015. A critical assessment of vector control for dengue prevention. *PLoS Negl Trop Dis,* 9**,** e0003655.

Adhami, J. & Reiter, P. 1998. Introduction and establishment of Aedes (Stegomyia) albopictus skuse (Diptera: Culicidae) in Albania. *Journal of the American Mosquito Control Association,* 14**,** 340-343.

Agboli, E., Leggewie, M., Altinli, M. & Schnettler, E. 2019. Mosquito-specific viruses—transmission and interaction. *Viruses,* 11**,** 873.

Alexander, A. J., Salvemini, M., Sreenu, V. B., Hughes, J., Telleria, E. L.*, et al.* 2023. Characterisation of the antiviral RNA interference response to Toscana virus in sand fly cells. *PLoS Pathogens,* 19**,** e1011283.

Aliyari, R. & Ding, S.-W. 2009. Antiviral immunity in arthropods. *Nature,* 461**,** 802-809.

Aliyari, R., Wu, Q., Li, H. W., Wang, X. H., Li, F.*, et al.* 2008. Mechanism of induction and suppression of antiviral immunity directed by virus-derived small RNAs in Drosophila. *Cell Host Microbe,* 4**,** 387-97.

Altinli, M., Leggewie, M., Badusche, M., Gyanwali, R., Scherer, C.*, et al.* 2022. Antiviral RNAi response against the insect-specific Agua Salud alphavirus. *Msphere,* 7**,** e01003-21.

Anderson, M. A., Gross, T. L., Myles, K. M. & Adelman, Z. N. 2010. Validation of novel promoter sequences derived from two endogenous ubiquitin genes in transgenic Aedes aegypti. *Insect molecular biology,* 19**,** 441-449.

Angelini, P., Macini, P., Finarelli, A., Po, C., Venturelli, C.*, et al.* 2008. Chikungunya epidemic outbreak in Emilia-Romagna (Italy) during summer 2007. *Parassitologia,* 50**,** 97.

Antoniewski, C. 2014. Computing siRNA and piRNA overlap signatures. *Methods Mol Biol,* 1173**,** 135-46.

Arias-Goeta, C., Moutailler, S., Mousson, L., Zouache, K., Thiberge, J.-M.*, et al.* 2014. Chikungunya virus adaptation to a mosquito vector correlates with only few point mutations in the viral envelope glycoprotein. *Infection, Genetics and Evolution,* 24**,** 116-126.

Arraes, F. B. M., Martins-De-Sa, D., Noriega Vasquez, D. D., Melo, B. P., Faheem, M.*, et al.* 2021. Dissecting protein domain variability in the core RNA interference machinery of five insect orders. *RNA biology,* 18**,** 1653-1681.

Atkins, G., Sheahan, B. & Mooney, D. 1990. Pathogenicity of Semliki Forest virus for the rat central nervous system and primary rat neural cell cultures: possible implications for the pathogenesis of multiple sclerosis. *Neuropathology and Applied Neurobiology,* 16**,** 57-68.

Atkins, G. J., Sheahan, B. J. & Dimmock, N. J. 1985. Semliki Forest virus infection of mice: a model for genetic and molecular analysis of viral pathogenicity. *Journal of General Virology,* 66**,** 395-408.

Bagny, L., Delatte, H., Elissa, N., Quilici, S. & Fontenille, D. 2009. Aedes (Diptera: Culicidae) vectors of arboviruses in Mayotte (Indian Ocean): distribution area and larval habitats. *Journal of medical entomology,* 46**,** 198-207.

Bang, Y. & Pant, C. 1972. A field trial of Abate larvicide for the control of Aedes aegypti in Bangkok, Thailand. *Bulletin of the World Health Organization,* 46**,** 416.

Barletta, A. B. F., Silva, M. C. L. N. & Sorgine, M. H. F. 2012. Validation of Aedes aegypti Aag-2 cells as a model for insect immune studies. *Parasites & vectors,* 5**,** 148.

Benedict, M. Q., Levine, R. S., Hawley, W. A. & Lounibos, L. P. 2007. Spread of the tiger: global risk of invasion by the mosquito Aedes albopictus. *Vector-borne and zoonotic Diseases,* 7**,** 76-85.

Benelli, G. & Mehlhorn, H. 2016. Declining malaria, rising of dengue and Zika virus: insights for mosquito vector control. *Parasitol Res,* 115**,** 1747-54.

Bernhardt, S. A., Simmons, M. P., Olson, K. E., Beaty, B. J., Blair, C. D.*, et al.* 2012. Rapid intraspecific evolution of miRNA and siRNA genes in the mosquito Aedes aegypti. *PLoS One,* 7**,** e44198.

Bernstein, E., Caudy, A. A., Hammond, S. M. & Hannon, G. J. 2001. Role for a bidentate ribonuclease in the initiation step of RNA interference. *Nature,* 409**,** 363-6.

Besson, B., Lezcano, O. M., Overheul, G. J., Janssen, K., Spruijt, C. G.*, et al.* 2022. Arbovirus-vector protein interactomics identifies Loquacious as a co-factor for dengue virus replication in Aedes mosquitoes. *PLoS Pathogens,* 18**,** e1010329.

Blair, C. D. 2011. Mosquito RNAi is the major innate immune pathway controlling arbovirus infection and transmission. *Future microbiology,* 6**,** 265-277.

Blair, C. D. & Olson, K. E. 2015. The role of RNA interference (RNAi) in arbovirus-vector interactions. *Viruses,* 7**,** 820-43.

Blaszczyk, J., Tropea, J. E., Bubunenko, M., Routzahn, K. M., Waugh, D. S.*, et al.* 2001. Crystallographic and modeling studies of RNase III suggest a mechanism for double-stranded RNA cleavage. *Structure,* 9**,** 1225-36.

Bonning, B. C. & Saleh, M.-C. 2021. The interplay between viruses and RNAi pathways in insects. *Annual Review of Entomology,* 66**,** 61-79.

Braack, L., Almeida, A. P. G. D., Cornel, A. J., Sweaepoel, R. & Jager, C. D. 2018. Mosquito-borne arboviruses of African origin: review of key viruses and vectors. *Parasites & Vectors*, 11, 1-26.

Brackney, D. E., Scott, J. C., Sagawa, F., Woodward, J. E., Miller, N. A.*, et al.* 2010. C6/36 Aedes albopictus cells have a dysfunctional antiviral RNA interference response. *PLoS neglected tropical diseases,* 4**,** e856.

Braks, M. A., Honório, N. A., Lourenço-De-Oliveira, R., Juliano, S. A. & Lounibos, L. P. 2003. Convergent habitat segregation of Aedes aegypti and Aedes albopictus (Diptera: Culicidae) in southeastern Brazil and Florida. *Journal of medical entomology,* 40**,** 785-794.

Brennecke, J., Aravin, A. A., Stark, A., Dus, M., Kellis, M.*, et al.* 2007. Discrete small RNA-generating loci as master regulators of transposon activity in Drosophila. *Cell,* 128**,** 1089-103.

Bronkhorst, A. W., Van Cleef, K. W., Vodovar, N., Ince, I. A., Blanc, H.*, et al.* 2012. The DNA virus Invertebrate iridescent virus 6 is a target of the Drosophila RNAi machinery. *Proc Natl Acad Sci U S A,* 109**,** E3604-13.

Brown, D. T. Alphavirus growth in cultured vertebrate and invertebrate cells. Vectors in virus biology, 1984. 113-133.

Brown, K. A., Shi, M., Firth, A. E., Ergünay, K., Wolf, Y.*, et al.* 2024. Promote order Bunyavirales to class and split the class into two orders; add one family, three genera, and seven species; and move and rename one species. *Current ICTV Taxonomy Release.* Jena, Germany: International Committee on the Taxonomy of Viruses

Caudy, A. A., Ketting, R. F., Hammond, S. M., Denli, A. M., Bathoorn, A. M.*, et al.* 2003. A micrococcal nuclease homologue in RNAi effector complexes. *Nature,* 425**,** 411-414.

Caudy, A. A., Myers, M., Hannon, G. J. & Hammond, S. M. 2002. Fragile X-related protein and VIG associate with the RNA interference machinery. *Genes Dev,* 16**,** 2491-6.

Campbell, C. L., Black, W. C., Hess, A. M. & Foy, B. D. 2008 Comparative genomics of small RNA regulatoty pathway components in vector mosquitoes. *BMC Genomics*, 9, 1-16.

Charlier, N., Leyssen, P., Pleij, C. W., Lemey, P., Billoir, F.*, et al.* 2002. Complete genome sequence of Montana Myotis leukoencephalitis virus, phylogenetic analysis and comparative study of the 3′ untranslated region of flaviviruses with no known vector. *Journal of General Virology,* 83**,** 1875-1885.

Chase, C. C. 2022. Togaviridae and flaviviridae. *Veterinary microbiology***,** 552-572.

Chen, S., Zhou, Y., Chen, Y. & Gu, J. 2018. fastp: an ultra-fast all-in-one FASTQ preprocessor. *Bioinformatics,* 34**,** i884-i890.

Chevillon, C., Briant, L., Renaud, F. & Devaux, C. 2008. The Chikungunya threat: an ecological and evolutionary perspective. *Trends in microbiology,* 16**,** 80-88.

Chung, W.-J., Okamura, K., Martin, R. & Lai, E. C. 2008. Endogenous RNA interference provides a somatic defense against Drosophila transposons. *Current Biology,* 18**,** 795-802.

Coffinet, T., Mourou, J., Pradines, B., Toto, J., Jarjaval, F.*, et al.* 2007. First record of Aedes albopictus in Gabon. *Journal of the American Mosquito Control Association,* 23**,** 471-472.

Contigiani, M. S. & Diaz, L. A. 2016. Togaviridae. *Arthropod borne diseases.* Springer.

Coombs, K. & Brown, D. T. 1987. Topological organization of Sindbis virus capsid protein in isolated nucleocapsids. *Virus research,* 7**,** 131-149.

Coulanges, P., Clerc, Y., Jousset, F., Rodhain, F. & Hannoun, C. 1979. Dengue on Réunion. Isolation of a strain at the Pasteur Institute of Madagascar.

Czech, B., Malone, C. D., Zhou, R., Stark, A., Schlingeheyde, C.*, et al.* 2008. An endogenous small interfering RNA pathway in Drosophila. *Nature,* 453**,** 798-802.

Dalla Pozza, G. & Majori, G. 1992. First record of Aedes albopictus establishment in Italy. *Journal of the American Mosquito Control Association,* 8**,** 318-320.

Deddouche, S., Matt, N., Budd, A., Mueller, S., Kemp, C.*, et al.* 2008. The DExD/H-box helicase Dicer-2 mediates the induction of antiviral activity in drosophila. *Nat Immunol,* 9**,** 1425-32.

Dietrich, I., Shi, X., Mcfarlane, M., Watson, M., Blomström, A.-L.*, et al.* 2017. The antiviral RNAi response in vector and non-vector cells against orthobunyaviruses. *PLoS neglected tropical diseases,* 11**,** e0005272.

Dong, S. & Dimopoulos, G. 2023. Aedes aegypti Argonaute 2 controls arbovirus infection and host mortality. *Nature communications,* 14**,** 5773.

Dorigatti, I., Gaythorpe, K. A., Cox, V. M., Windram, F. A. & Cator, L. 2025. Priorities for modelling arbovirus transmission under climate change. *Trends in Molecular Medicine*.

Dummunee, K., Parry, R. H., Redecke, L., Varjak, M., Brennan, B.*, et al.* 2025. The catalytic tetrad of Aedes aegypti argonaute 2 is critical for the antiviral activity of the exogenous siRNA pathway. *Journal of Biological Chemistry,* 301.

Effler, P. V., Pang, L., Kitsutani, P., Vorndam, V., Nakata, M.*, et al.* 2005. Dengue fever, hawaii, 2001–2002. *Emerging infectious diseases,* 11**,** 742.

Ender, C. & Meister, G. 2010. Argonaute proteins at a glance. *J Cell Sci,* 123**,** 1819-23.

Enserink, M. 2007a. Chikungunya: no longer a third world disease. American Association for the Advancement of Science.

Enserink, M. 2007b. Tropical disease follows mosquitoes to Europe. *Science,* 317**,** 1485-1485.

Estevez-Castro, C. F., Rodrigues, M. F., Babarit, A., Ferreira, F. V., De Andrade, E. G.*, et al.* 2024. Neofunctionalization driven by positive selection led to the retention of the loqs2 gene encoding an Aedes specific dsRNA binding protein. *BMC biology,* 22**,** 14.

Fagegaltier, D., Bougé, A.-L., Berry, B., Poisot, É., Sismeiro, O.*, et al.* 2009. The endogenous siRNA pathway is involved in heterochromatin formation in Drosophila. *Proceedings of the National Academy of Sciences,* 106**,** 21258-21263.

Fazakerley, J. K. 2002. Pathogenesis of Semliki Forest virus encephalitis. *Journal of neurovirology,* 8.

Fazakerley, J. K. 2004. Semliki forest virus infection of laboratory mice: a model to study the pathogenesis of viral encephalitis. *Emergence and Control of Zoonotic Viral Encephalitides***,** 179-190.

Feng, X., Wu, W., Ren, X., Li, J., Zhang, X.*, et al.* 2018. MicroRNA-mediated regulation in plant-insect interactions. *Trends in Plant Science,* 23**,** 878-895.

Flynt, A. S., Greimann, J. C., Chung, W.-J., Lima, C. D. & Lai, E. C. 2009. MicroRNA biogenesis via splicing and exosome-mediated trimming in Drosophila. *Molecular Cell,* 38**,** 900-907.

Fontenille, D. & Toto, J. C. 2001. Aedes (Stegomyia) albopictus (Skuse), a potential new Dengue vector in southern Cameroon. *Emerging infectious diseases,* 7**,** 1066.

Forrester, N., Palacios, G., Tesh, R., Savji, N., Guzman, H., *et al.* 2012. Genome-scale phylogeny of the alphavirus genus suggests a marine origin. *Journal of virology,* 86**,** 2729-2738.

Forstemann, K., Horwich, M. D., Wee, L., Tomari, Y. & Zamore, P. D. 2007. Drosophila microRNAs are sorted into functionally distinct argonaute complexes after production by dicer-1. *Cell,* 130**,** 287-97.

Fragkoudis, R., Breakwell, L., Mckimmie, C., Boyd, A., Barry, G., *et al.* 2007. The type I interferon system protects mice from Semliki Forest virus by preventing widespread virus dissemination in extraneural tissues, but does not mediate the restricted replication of avirulent virus in central nervous system neurons. *Journal of general virology,* 88**,** 3373-3384.

Fragkoudis, R., Chi, Y., Siu, R., Barry, G., Attarzadeh-Yazdi, G., *et al.* 2008. Semliki Forest virus strongly reduces mosquito host defence signaling. *Insect molecular biology,* 17**,** 647-656.

Franz, A. W., Kantor, A. M., Passarelli, A. L. & Clem, R. J. 2015. Tissue barriers to arbovirus infection in mosquitoes. *Viruses,* 7**,** 3741-3767.

Fredericks, A. C., Russell, T. A., Wallace, L. E., Davidson, A. D., Fernandez-Sesma, A., *et al.* 2019. Aedes aegypti (Aag2)-derived clonal mosquito cell lines reveal the effects of pre-existing persistent infection with the insect-specific bunyavirus Phasi Charoen-like virus on arbovirus replication. *PLoS neglected tropical diseases,* 13**,** e0007346.

Frumence, E., Piorkowski, G., Traversier, N., Amaral, R., Vincent, M., *et al.* 2025. Genomic insights into the re-emergence of chikungunya virus on Réunion Island, France, 2024 to 2025. *Eurosurveillance,* 30**,** 2500344.

Fullam, A. & Schroder, M. 2013. DExD/H-box RNA helicases as mediators of anti-viral innate immunity and essential host factors for viral replication. *Biochim Biophys Acta,* 1829**,** 854-65.

Galiana-Arnoux, D., Dostert, C., Schneemann, A., Hoffmann, J. A. & Imler, J.-L. 2006. Essential function in vivo for Dicer-2 in host defense against RNA viruses in drosophila. *Nature Immunology,* 7**,** 590-597.

Gaunt, M. W., Sall, A. A., Lamballerie, X. D., Falconar, A. K., Dzhivanian, T. I., *et al.* 2001. Phylogenetic relationships of flaviviruses correlate with their epidemiology, disease association and biogeography. *Journal of General Virology,* 82**,** 1867-1876.

Gestuveo, R. J., Parry, R., Dickson, L. B., Lequime, S., Sreenu, V. B., *et al.* 2022a. Mutational analysis of Aedes aegypti Dicer 2 provides insights into the biogenesis of antiviral exogenous small interfering RNAs. *PLoS Pathog,* 18**,** e1010202.

Gestuveo, R. J., Royle, J., Donald, C. L., Lamont, D. J., Hutchinson, E. C.*, et al.* 2022b. Analysis of Semliki Forest virus produced in mosquito cells reveals novel RNA and protein components. *Journal of Virology,* 96**,** e00291-22.

Ghildiyal, M., Seitz, H., Horwich, M. D., Li, C., Du, T.*, et al.* 2008. Endogenous siRNAs derived from transposons and mRNAs in Drosophila somatic cells. *Science,* 320**,** 1077-1081.

Gould, E., Gallian, P., De Lamballerie, X. & Charrel, R. 2010. First cases of autochthonous dengue fever and chikungunya fever in France: from bad dream to reality! *Clinical microbiology and infection,* 16**,** 1702-1704.

Grandadam, M., Caro, V., Plumet, S., Thiberge, J.-M., Souarès, Y.*, et al.* 2011. Chikungunya virus, southeastern France. *Emerging infectious diseases,* 17**,** 910.

Gratz, N. 2004. Critical review of the vector status of Aedes albopictus. *Medical and veterinary entomology,* 18**,** 215-227.

Gritsun, T., Tuplin, A. & Gould, E. 2006. Origin, evolution and function of flavivirus RNA in untranslated and coding regions: implications for virus transmission. *Flaviviridae: Pathogenesis, Molecular Biology and Genetics. Horizon Scientific Press, Norwich, UK***,** 47-99.

Gubler, D. J.1998. Resurgent vector-borne diseases as a global health problem. *Emerging Infectious Diseases,* 4, 442-450.

Guillaumot, L., Ofanoa, R., Swillen, L., Singh, N., Bossin, H. C.*, et al.* 2012. Distribution of Aedes albopictus (Diptera, Culicidae) in southwestern Pacific countries, with a first report from the Kingdom of Tonga. *Parasites & vectors,* 5**,** 247.

Hammond, S. M., Bernstein, E., Beach, D. & Hannon, G. J. 2000. An RNA-directed nuclease mediates post-transcriptional gene silencing in Drosophila cells. *Nature,* 404**,** 293-296.

Handler, D., Olivieri, D., Novatchkova, M., Gruber, F. S., Meixner, K.*, et al.* 2013. A systematic analysis of Drosophila TUDOR domain-containing proteins identifies Vreteno and the Tdrd12 family as essential primary piRNA pathway factors. *EMBO Journal,* 32**,** 1869-1884.

Harris, E., Holden, K. L., Edgil, D., Polacek, C. & Clyde, K. Molecular biology of flaviviruses. New Treatment Strategies for Dengue and Other Flaviviral Diseases: Novartis Foundation Symposium 277, 2006. Wiley Online Library, 23-40.

Hartig, J. V., Esslinger, S., Bottcher, R., Saito, K. & Forstemann, K. 2009. Endo-siRNAs depend on a new isoform of loquacious and target artificially introduced, high-copy sequences. *EMBO J,* 28**,** 2932-44.

Hartman, A. L. & Myler, P. J. 2023. Bunyavirales: Scientific Gaps and Prototype Pathogens for a Large and Diverse Group of Zoonotic Viruses. *J Infect Dis,* 228**,** S376-S389.

Hauptmann, J., Dueck, A., Harlander, S., Pfaff, J., Merkl, R.*, et al.* 2013. Turning catalytically inactive human Argonaute proteins into active slicer enzymes. *Nature structural & molecular biology,* 20**,** 814-817.

Hemingway, J., Hawkes, N. J., Mccarroll, L. & Ranson, H. 2004. The molecular basis of insecticide resistance in mosquitoes. *Insect biochemistry and molecular biology,* 34**,** 653-665.

Hemingway, J., Ranson, H., Magill, A., Kolaczinski, J., Fornadel, C.*, et al.* 2016. Averting a malaria disaster: will insecticide resistance derail malaria control? *Lancet,* 387**,** 1785-8.

Hoffmann, A. A., Iturbe-Ormaetxe, I., Callahan, A. G., Phillips, B. L., Billington, K.*, et al.* 2014. Stability of the w Mel Wolbachia infection following invasion into Aedes aegypti populations. *PLoS neglected tropical diseases,* 8**,** e3115.

Hoffmann, A. A., Montgomery, B., Popovici, J., Iturbe-Ormaetxe, I., Johnson, P.*, et al.* 2011. Successful establishment of Wolbachia in Aedes populations to suppress dengue transmission. *Nature,* 476**,** 454-457.

Hoffmann, A. A., Ross, P. A. & Rašić, G. 2015. Wolbachia strains for disease control: ecological and evolutionary considerations. *Evolutionary applications,* 8**,** 751-768.

Hoffmann, M., Verzijl, D., Lundstrom, K., Simmen, U., Alewijnse, A. E.*, et al.* 2001. Recombinant Semliki Forest virus for over-expression and pharmacological characterisation of the histamine H2 receptor in mammalian cells. *European journal of pharmacology,* 427**,** 105-114.

Hotta, S. 1998. Dengue vector mosquitoes in Japan: the role of Aedes albopictus and Aedes aegypti in the 1942-1944 dengue epidemics of Japanese Main Islands.

Huang, Y.-J. S., Higgs, S. & Vanlandingham, D. L. 2019. Arbovirus-mosquito vector-host interactions and the impact on transmission and disease pathogenesis of arboviruses. *Frontiers in microbiology,* 10**,** 22.

Hussain, M., Frentiu, F. D., Moreira, L. A., O'neill, S. L. & Asgari, S. 2011. Wolbachia uses host microRNAs to manipulate host gene expression and facilitate colonization of the dengue vector Aedes aegypti. *Proc Natl Acad Sci U S A,* 108**,** 9250-5.

Hussain, M., Walker, T., O'neill, S. L. & Asgari, S. 2013. Blood meal induced microRNA regulates development and immune associated genes in the

Dengue mosquito vector, Aedes aegypti. *Insect Biochem Mol Biol,* 43**,** 146-52.

Iwakawa, H. O. & Tomari, Y. 2022. Life of RISC: Formation, action, and degradation of RNA-induced silencing complex. *Mol Cell,* 82**,** 30-43.

Jin, S., Zhan, J. & Zhou, Y. 2021. Argonaute proteins: structures and their endonuclease activity. *Molecular Biology Reports,* 48**,** 4837-4849.

Kääriäinen, L. & Ahola, T. 2002. Functions of alphavirus nonstructural proteins in RNA replication.

Kääriäinen, L., Takkinen, K., Keränen, S. & Söderlund, H. 1987. Replication of the genome of alphaviruses. *Journal of cell science,* 1987**,** 231-250.

Kawamura, Y., Saito, K., Kin, T., Ono, Y., Asai, K*., et al.* 2008. Drosophila endogenous small RNAs bind to Argonaute 2 in somatic cells. *Nature,* 453**,** 793-7.

Kemp, C. & Imler, J. L. 2009. Antiviral immunity in drosophila. *Curr Opin Immunol,* 21**,** 3-9.

Khvorova, A., Reynolds, A. & Jayasena, S. D. 2003. Functional siRNAs and miRNAs exhibit strand bias. *Cell,* 115**,** 209-16.

Kielian, M., Chanel-Vos, C. & Liao, M. 2010. Alphavirus entry and membrane fusion. *Viruses,* 2**,** 796-825.

Kiiver, K., Tagen, I., Zusinaite, E., Tamberg, N., Fazakerley, J. K*., et al.* 2008. Properties of non-structural protein 1 of Semliki Forest virus and its interference with virus replication. *J Gen Virol,* 89**,** 1457-1466.

Kim, K., Lee, Y. S., Harris, D., Nakahara, K. & Carthew, R. W. 2006. The RNAi machinery is essential for efficient gene silencing by artificial microRNAs in Drosophila. *Nucleic Acids Research,* 34**,** 6176-6187.

Kim, K., Siomi, M. C. & Siomi, H. 2009. Molecular mechanisms of microRNA biogenesis. *Trends in Biochemical Sciences,* 34**,** 226-233.

Kim, K. H., Rümenapf, T., Strauss, E. G. & Strauss, J. H. 2004. Regulation of Semliki Forest virus RNA replication: a model for the control of alphavirus pathogenesis in invertebrate hosts. *Virology,* 323**,** 153-163.

Klobučar, A., Merdić, E., Benić, N., BaklaiĆ, Ž. L. & KrČmar, S. A. 2006. First record of Aedes albopictus in Croatia. *Journal of the American Mosquito Control Association,* 22**,** 147-148.

Knudsen, A., Romi, R. & Majori, G. 1996. Occurrence and spread in Italy of Aedes albopictus, with implications for its introduction into other parts of Europe. *Journal of the American Mosquito Control Association,* 12**,** 177-183.

Kouri, G. P., Guzmán, M. G., Bravo, J. R. & Triana, C. 1989. Dengue haemorrhagic fever/dengue shock syndrome: lessons from the Cuban epidemic, 1981. *Bulletin of the World Health Organization,* 67**,** 375.

Kraemer, M. U., Sinka, M. E., Duda, K. A., Mylne, A. Q., Shearer, F. M.*, et al.* 2015. The global distribution of the arbovirus vectors Aedes aegypti and Ae. albopictus. *Elife,* 4**,** e08347.

Kuhn, J. H., Brown, K., Adkins, S., De La Torre, J. C., Digiaro, M.*, et al.* 2024. Promotion of order Bunyavirales to class Bunyaviricetes to accommodate a rapidly increasing number of related polyploviricotine viruses. *Journal of Virology,* 98**,** e01069-24.

Kuno, G. 2007. Research on dengue and dengue-like illness in East Asia and the Western Pacific during the first half of the 20th century. *Reviews in medical virology,* 17**,** 327-341.

Langmead, B. & Salzberg, S. L. 2012. Fast gapped-read alignment with Bowtie 2. *Nat Methods,* 9**,** 357-9.

Leake, C., Pudney, M. & Varma, M. 1980. Studies on arboviruses in established tick cell lines. *Invertebrate Systems In Vitro***,** 327-335.

Lee, Y. S., Nakahara, K., Pham, J. W., Kim, K., He, Z.*, et al.* 2004. Distinct roles for Drosophila Dicer-1 and Dicer-2 in the siRNA/miRNA silencing pathways. *Cell,* 117**,** 69-81.

Lello, L. S., Bartholomeeusen, K., Wang, S., Coppens, S., Fragkoudis, R.*, et al.* 2021. nsP4 is a major determinant of alphavirus replicase activity and template selectivity. *Journal of virology,* 95**,** 10.1128/jvi. 00355-21.

Leroy, E. M., Nkoghe, D., Ollomo, B., Nze-Nkogue, C., Becquart, P.*, et al.* 2009. Concurrent chikungunya and dengue virus infections during simultaneous outbreaks, Gabon, 2007. *Emerging infectious diseases,* 15**,** 591.

Li, H., Li, W. X. & Ding, S. W. 2002. Induction and suppression of RNA silencing by an animal virus. *Science,* 296**,** 1319-21.

Lim, A., Shearer, F. M., Sewalk, K., Pigott, D. M., Clarke, J.*, et al.* 2025. The overlapping global distribution of dengue, chikungunya, Zika and yellow fever. *Nature communications,* 16**,** 3418.

Lindenbach, B. D. & Rice, C. M. 2003. Molecular biology of flaviviruses. *Advances in virus research,* 59**,** 23-62.

Lingel, A., Simon, B., Izaurralde, E. & Sattler, M. 2003. Structure and nucleic-acid binding of the Drosophila Argonaute 2 PAZ domain. *Nature,* 426**,** 465-9.

Lingel, A., Simon, B., Izaurralde, E. & Sattler, M. 2004. Nucleic acid 3'-end recognition by the Argonaute2 PAZ domain. *Nat Struct Mol Biol,* 11**,** 576-7.

Liu, J., Swevers, L., Kolliopoulou, A. & Smagghe, G. 2019. Arboviruses and the challenge to establish systemic and persistent infections in competent mosquito vectors: the interaction with the RNAi mechanism. *Frontiers in physiology,* 10**,** 890.

Liu, Q., Rand, T. A., Kalidas, S., Du, F., Kim, H.-E.*, et al.* 2003. R2D2, a bridge between the initiation and effector steps of the Drosophila RNAi pathway. *Science,* 301**,** 1921-1925.

Liu, Y., Ye, X., Jiang, F., Liang, C., Chen, D.*, et al.* 2009. C3PO, an endoribonuclease that promotes RNAi by facilitating RISC activation. *Science,* 325**,** 750-3.

Liu-Helmersson, J., Stenlund, H., Wilder-Smith, A. & Rocklöv, J. 2014. Vectorial capacity of Aedes aegypti: effects of temperature and implications for global dengue epidemic potential. *PloS one,* 9**,** e89783.

Lundstrom, K. 2003. Semliki Forest virus vectors for gene therapy. *Expert opinion on biological therapy,* 3**,** 771-777.

Ma, J.-B., Yuan, Y.-R., Meister, G., Pei, Y., Tuschl, T.*, et al.* 2004. Structural basis for 5'-end-specific recognition of guide RNA by the A. fulgidus Piwi protein. *Nature,* 434**,** 666-670.

Mackenzie, J. S., Gubler, D. J. & Petersen, L. R. 2004. Emerging flaviviruses: the spread and resurgence of Japanese encephalitis, West Nile and dengue viruses. *Nature medicine,* 10**,** S98-S109.

Macrae, I. J., Zhou, K., Li, F., Repic, A., Brooks, A. N.*, et al.* 2006. Structural basis for double-stranded RNA processing by Dicer. *Science,* 311**,** 195-8.

Mandl, C. W., Heinz, F. X., Stöckl, E. & Kunz, C. 1989. Genome sequence of tick-borne encephalitis virus (Western subtype) and comparative analysis of nonstructural proteins with other flaviviruses. *Virology,* 173**,** 291-301.

Manore, C. A., Hickmann, K. S., Xu, S., Wearing, H. J. & Hyman, J. M. 2014. Comparing dengue and chikungunya emergence and endemic transmission in A. aegypti and A. albopictus. *Journal of theoretical biology,* 356**,** 174-191.

Marques, J. T., Kim, K., Wu, P. H., Alleyne, T. M., Jafari, N.*, et al.* 2010. Loqs and R2D2 act sequentially in the siRNA pathway in Drosophila. *Nat Struct Mol Biol,* 17**,** 24-30.

Marques, J. T., Wang, J. P., Wang, X., De Oliveira, K. P., Gao, C.*, et al.* 2013. Functional specialization of the small interfering RNA pathway in response to virus infection. *PLoS Pathog,* 9**,** e1003579.

Mathiot, C. C., Grimaud, G., Garry, P., Bouquety, J. C., Mada, A.*, et al.* 1990. An outbreak of human Semliki Forest virus infections in Central African Republic.

Matranga, C., Tomari, Y., Shin, C., Bartel, D. P. & Zamore, P. D. 2005. Passenger-strand cleavage facilitates assembly of siRNA into Ago2-containing RNAi enzyme complexes. *Cell,* 123**,** 607-20.

Mazzon, M., Castro, C., Thaa, B., Liu, L., Mutso, M.*, et al.* 2018. Alphavirus-induced hyperactivation of PI3K/AKT directs pro-viral metabolic changes. *PLoS Pathogens,* 14**,** e1006835.

Mcfarlane, M., Almire, F., Kean, J., Donald, C. L., Mcdonald, A.*, et al.* 2020. The Aedes aegypti domino ortholog p400 regulates antiviral exogenous small interfering RNA pathway activity and ago-2 expression. *Msphere,* 5**,** 10.1128/msphere. 00081-20.

Mcfarlane, M., Arias-Goeta, C., Martin, E., O'hara, Z., Lulla, A.*, et al.* 2014. Characterization of Aedes aegypti innate-immune pathways that limit Chikungunya virus replication. *PLoS neglected tropical diseases,* 8**,** e2994.

Mcloughlin, M. & Graham, D. 2007. Alphavirus infections in salmonids–a review. *Journal of fish diseases,* 30**,** 511-531.

Medlock, J. M., Hansford, K. M., Schaffner, F., Versteirt, V., Hendrickx, G.*, et al.* 2012. A review of the invasive mosquitoes in Europe: ecology, public health risks, and control options. *Vector-borne and zoonotic diseases,* 12**,** 435-447.

Meister, G., Landthaler, M., Patkaniowska, A., Dorsett, Y., Teng, G.*, et al.* 2004. Human Argonaute2 mediates RNA cleavage targeted by miRNAs and siRNAs. *Mol Cell,* 15**,** 185-97.

Merkling, S. H., Crist, A. B., Henrion-Lacritick, A., Frangeul, L., Couderc, E.*, et al.* 2023. Multifaceted contributions of Dicer2 to arbovirus transmission by Aedes aegypti. *Cell Reports,* 42.

Metz, S. W. & Pijlman, G. P. 2011. Arbovirus vaccines; opportunities for the baculovirus-insect cell expression system. *Journal of Invertebrate Pathology,* 107**,** S16-S30.

Miesen, P., Girardi, E. & Van Rij, R. P. 2016. Distinct sets of PIWI proteins produce arbovirus and transposon-derived piRNAs in Aedes aegypti mosquito cells. *Nucleic Acids Research,* 44**,** 6545-6556.

Minwuyelet, A., Petronio, G., Yewhalaw, D., Sciarretta, A., Magnifico, I.*, et al.* 2023. Symbiotic Wolbachia in mosquitoes and its role in reducing the transmission

of mosquito-borne diseases: updates and prospects. Front Microbiol. 2023 Oct 13; 14.

Miyoshi, H., Fujie, H., Shintani, Y., Tsutsumi, T., Shinzawa, S.*, et al.* 2005. Hepatitis C virus core protein exerts an inhibitory effect on suppressor of cytokine signaling (SOCS)-1 gene expression. *J Hepatol,* 43**,** 757-63.

Miyoshi, K., Tsukumo, H., Nagami, T., Siomi, H. & Siomi, M. C. 2005. Slicer function of Drosophila Argonautes and its involvement in RISC formation. *Genes & Development,* 19**,** 2837-2848.

Moore, C. G. 1999. Aedes albopictus in the United States: current status and prospects for further spread. *Journal of the American Mosquito Control Association,* 15**,** 221-227.

Morazzani, E. M., Wiley, M. R., Murreddu, M. G., Adelman, Z. N. & Myles, K. M. 2012. Production of virus-derived ping-pong-dependent piRNA-like small RNAs in the mosquito soma. *PLoS Pathog,* 8**,** e1002470.

Moreira, L. A., Iturbe-Ormaetxe, I., Jeffery, J. A., Lu, G., Pyke, A. T.*, et al.* 2009. A Wolbachia symbiont in Aedes aegypti limits infection with dengue, Chikungunya, and Plasmodium. *Cell,* 139**,** 1268-1278.

Mueller, S., Gausson, V., Vodovar, N., Deddouche, S., Troxler, L., Perot, J., *et al.* 2010. RNAi-mediated immunity provides strong protection against the negative-strand RNA vesicular stomatitis virus in Drosophila. *PNAS,* 107, 19390-19395.

Mukhopadhyay, S., Kuhn, R. J. & Rossmann, M. G. 2005. A structural perspective of the flavivirus life cycle. *Nature Reviews Microbiology,* 3**,** 13-22.

Müller, R., Weirick, T. & Uchida, S. 2020. Non-coding RNAs in cardiovascular disease. *Journal of Molecular and Cellular Cardiology,* 139**,** 89-98.

Myles, K. M., Wiley, M. R., Morazzani, E. M. & Adelman, Z. N. 2008. Alphavirus-derived small RNAs modulate pathogenesis in disease vector mosquitoes. *Proceedings of the National Academy of Sciences,* 105**,** 19938-19943.

Nakanishi, K. 2023. Anatomy of four human Argonaute proteins. *Nucleic Acids Research,* 51**,** 6606-6629.

Nandety, R. S., Kuo, Y.-W., Nouri, S. & Falk, B. W. 2015. Emerging strategies for RNA interference (RNAi) applications in insects. *Bioengineered,* 6**,** 8-19.

Nathan, M. B. & Knudsen, A. B. 1991. Aedes aegypti infestation characteristics in several Caribbean countries and implications for integrated community-based control. *Journal of the American Mosquito Control Association,* 7**,** 400-404.

Normile, D. 2013. Surprising new dengue virus throws a spanner in disease control efforts. American Association for the Advancement of Science.

Obbard, D. J., Jiggins, F. M., Halligan, D. L. & Little, T. J. 2006. Natural selection drives extremely rapid evolution in antiviral RNAi genes. *Curr Biol,* 16**,** 580-5.

Obbard, D. J., Welch, J. J., Kim, K. W. & Jiggins, F. M. 2009. Quantifying adaptive evolution in the Drosophila immune system. *PLoS Genet,* 5**,** e1000698.

Okamura, K., Ishizuka, A., Siomi, H. & Siomi, M. C. 2004. Distinct roles for Argonaute proteins in small RNA-directed RNA cleavage pathways. *Genes Dev,* 18**,** 1655-66.

Olina, A., Kulbachinskiy, A., Aravin, A. & Esyunina, D. 2018. Argonaute proteins and mechanisms of RNA interference in eukaryotes and prokaryotes. *Biochemistry (Moscow),* 83**,** 483-497.

Olmo, R. P., Ferreira, A. G., Izidoro-Toledo, T. C., Aguiar, E. R., De Faria, I. J.*, et al.* 2018. Control of dengue virus in the midgut of Aedes aegypti by ectopic expression of the dsRNA-binding protein Loqs2. *Nature microbiology,* 3**,** 1385-1393.

Olson, K. E. & Blair, C. D. 2015. Arbovirus-mosquito interactions: RNAi pathway. *Curr Opin Virol,* 15**,** 119-26.

Ooi, E.-E., Goh, K.-T. & Gubler, D. J. 2006. Dengue prevention and 35 years of vector control in Singapore. *Emerging infectious diseases,* 12**,** 887.

Pagès, F., Peyrefitte, C. N., Mve, M. T., Jarjaval, F., Brisse, S., Iteman, I., Gravier, P., Tolou, H. & Simon, F. 2009. Aedes albopictus mosquito: the main vector of the 2007 chikungunya outbreak in Gabon. *PLoS ONE*, 4, e4691.

Pant, C., Mount, G., Jatanasen, S. & Mathis, H. 1971. Ultra-low-volume ground aerosols of technical malathion for the control of Aedes aegypti L. *Bulletin of the World Health Organization,* 45**,** 805.

Paredes, A. M., Brown, D. T., Rothnagel, R., Chiu, W., Schoepp, R. J.*, et al.* 1993. Three-dimensional structure of a membrane-containing virus. *Proceedings of the National Academy of Sciences,* 90**,** 9095-9099.

Paupy, C., Delatte, H., Bagny, L., Corbel, V. & Fontenille, D. 2009. Aedes albopictus, an arbovirus vector: from the darkness to the light. *Microbes and infection,* 11**,** 1177-1185.

Paupy, C., Girod, R., Salvan, M., Rodhain, F. & Failloux, A.-B. 2001. Population structure of Aedes albopictus from La Reunion Island (Indian Ocean) with respect to susceptibility to a dengue virus. *Heredity,* 87**,** 273-283.

Paupy, C., Ollomo, B., Kamgang, B., Moutailler, S., Rousset, D.*, et al.* 2010. Comparative role of Aedes albopictus and Aedes aegypti in the emergence of Dengue and Chikungunya in central Africa. *Vector-Borne and Zoonotic Diseases,* 10**,** 259-266.

Pereira, C. a. D. M., Mendes, R. P. G., Silva, P. G. D., Chaves, E. J. F. & Pena, L. J. 2025. Vaccines against urban epidemic arboviruses: The state of the art. *Viruses,* 17**,** 382.

Peyrefitte, C. N., Rousset, D., Pastorino, B. A., Pouillot, R., Bessaud, M.*, et al.* 2007. Chikungunya virus, cameroon, 2006. *Emerging infectious diseases,* 13**,** 768.

Pierson, T. C. & Diamond, M. S. 2020. The continued threat of emerging flaviviruses. *Nature microbiology,* 5**,** 796-812.

Pietilä, M. K., Albulescu, I. C., Van Hemert, M. J. & Ahola, T. 2017. Polyprotein processing as a determinant for in vitro activity of semliki forest virus replicase. *Viruses,* 9**,** 292.

Powell, J. R. & Tabachnick, W. J. 2013. History of domestication and spread of Aedes aegypti-a review. *Memórias do Instituto Oswaldo Cruz,* 108**,** 11-17.

Pressman, S., Reinke, C. A., Wang, X. & Carthew, R. W. 2012. A Systematic Genetic Screen to Dissect the MicroRNA Pathway in Drosophila. *G3 (Bethesda),* 2**,** 437-48.

Quinlan, A. R. & Hall, I. M. 2010. BEDTools: a flexible suite of utilities for comparing genomic features. *Bioinformatics,* 26**,** 841-2.

Ramos-Nino, M. E., Clifton, M. E., Geraci, N. S., Sanguinetti, M., Stone, W. B.*, et al.* 2022. Transcriptomic analysis of larval zebrafish (Danio rerio) following embryonic atrazine exposure. *Chemosphere,* 287**,** 132174.

Rand, T. A., Ginalski, K., Grishin, N. V. & Wang, X. 2005. Biochemical identification of Argonaute 2 as the sole protein required for RNA-induced silencing complex activity. *Proceedings of the National Academy of Sciences,* 102**,** 17387-17392.

Rand, T. A., Petersen, S., Du, F. & Wang, X. 2004. Argonaute2 cleaves the anti-guide strand of siRNA during RISC activation. *Cell,* 123**,** 621-629.

Reiter, P., Fontenille, D. & Paupy, C. 2006. Aedes albopictus as an epidemic vector of chikungunya virus: another emerging problem? *The Lancet infectious diseases,* 6**,** 463-464.

Reuter, M., Parry, R. H., Mcfarlane, M., Gestuveo, R. J., Arif, R.*, et al.* 2025. The PAZ domain of Aedes aegypti Dicer 2 is critical for accurate and high-fidelity size determination of virus-derived small interfering RNAs. *RNA,* 31**,** 679-691.

Rezza, G., Nicoletti, L., Angelini, R., Romi, R., Finarelli, A.*, et al.* 2007. Infection with chikungunya virus in Italy: an outbreak in a temperate region. *The Lancet,* 370**,** 1840-1846.

Rodriguez-Andres, J., Rani, S., Varjak, M., Chase-Topping, M. E., Beck, M. H.*, et al.* 2012. Phenoloxidase activity acts as a mosquito innate immune response against infection with Semliki Forest virus. *PLoS pathogens,* 8**,** e1002977.

Roiz, D., Eritja, R., Molina, R., Melero-Alcibar, R. & Lucientes, J. 2014. Initial distribution assessment of Aedes albopictus (Diptera: Culicidae) in the Barcelona, Spain, area. *Journal of medical entomology,* 45**,** 347-352.

Rozhkov, N. V., Hammell, M. & Hannon, G. J. 2013. Multiple roles for Piwi in silencing Drosophila transposons. *Genes Dev,* 27**,** 400-12.

Rubio, M., Maestro, J. L., Piulachs, M.-D. & Belles, X. 2018. Conserved association of Argonaute 1 and 2 proteins with miRNA and siRNA pathways throughout insect evolution, from cockroaches to flies. *Biochimica et Biophysica Acta (BBA)-Gene Regulatory Mechanisms,* 1861**,** 554-560.

Russell, T. A., Ayaz, A., Davidson, A. D., Fernandez-Sesma, A. & Maringer, K. 2021. Imd pathway-specific immune assays reveal NF-κB stimulation by viral RNA PAMPs in Aedes aegypti Aag2 cells. *PLoS neglected tropical diseases,* 15**,** e0008524.

Rust, R. S. Human arboviral encephalitis. Seminars in pediatric neurology, 2012. Elsevier, 130-151.

Sabin, L. R., Zhou, R., Gruber, J. J., Lukinova, N., Bambina, S.*, et al.* 2009. Ars2 regulates both miRNA- and siRNA- dependent silencing and suppresses RNA virus infection in Drosophila. *Cell,* 138**,** 340-51.

Saito, K., Ishizuka, A., Siomi, H. & Siomi, M. C. 2005. Processing of pre-microRNAs by the Dicer-1-Loquacious complex in Drosophila cells. *PLoS Biol,* 3**,** e235.

Samuel, G. H., Adelman, Z. N. & Myles, K. M. 2018. Antiviral Immunity and Virus-Mediated Antagonism in Disease Vector Mosquitoes. *Trends Microbiol,* 26**,** 447-461.

Sánchez, M. D., Pierson, T. C., Mcallister, D., Hanna, S. L., Puffer, B. A.*, et al.* 2005. Characterization of neutralizing antibodies to West Nile virus. *Virology,* 336**,** 70-82.

Sánchez-Vargas, I., Scott, J. C., Poole-Smith, B. K., Franz, A. W., Barbosa-Solomieu, V.*, et al.* 2009. Dengue virus type 2 infections of Aedes aegypti are modulated by the mosquito's RNA interference pathway. *PLoS pathogens,* 5**,** e1000299.

Savage, H., Ezike, V., Nwankwo, A., Spiegel, R. & Miller, B. 1992. First record of breeding populations of Aedes albopictus in continental Africa: implications for arboviral transmission. *Med. Hyg,* 25**,** 318-325.

Schaffner, F., Van Bortel, W. & Coosemans, M. 2004. First record of Aedes (Stegomyia) albopictus in Belgium. *Journal of the American Mosquito Control Association,* 20**,** 201-203.

Scherer, C., Knowles, J., Sreenu, V. B., Fredericks, A. C., Fuss, J.*, et al.* 2021. An Aedes aegypti-aerived Ago2 knockout cell line to investigate arbovirus infections. *Viruses,* 13(6)**,** 1066.

Schnettler, E., Donald, C. L., Human, S., Watson, M., Siu, R. W.*, et al.* 2013. Knockdown of piRNA pathway proteins results in enhanced Semliki Forest virus production in mosquito cells. *Journal of General Virology,* 94**,** 1680-1689.

Schwarz, D. S., Hutvagner, G., Du, T., Xu, Z., Aronin, N.*, et al.* 2003. Asymmetry in the assembly of the RNAi enzyme complex. *Cell,* 115**,** 199-208.

Schweitzer, B. K., Chapman, N. M. & Iwen, P. C. 2009. Overview of the Flaviviridae with an emphasis on the Japanese encephalitis group viruses. *Laboratory medicine,* 40**,** 493-499.

Seamer, J., Randles, W. & Fitzgeorge, R. 1967. The course of Semliki Forest virus infection in mice. *British Journal of Experimental Pathology,* 48**,** 395.

Silver, K., Cooper, A. M. & Zhu, K. Y. 2021. Strategies for enhancing the efficiency of RNA interference in insects. *Pest Management Science,* 77**,** 2645-2658.

Siu, R. W., Fragkoudis, R., Simmonds, P., Donald, C. L., Chase-Topping, M. E.*, et al.* 2011. Antiviral RNA interference responses induced by Semliki Forest virus infection of mosquito cells: characterization, origin, and frequency-dependent functions of virus-derived small interfering RNAs. *Journal of virology,* 85**,** 2907-2917.

Skidmore, A. M. & Bradfute, S. B. 2023. The life cycle of the alphaviruses: From an antiviral perspective. *Antiviral Res,* 209**,** 105476.

Smith, C. G. 1956. The history of dengue in tropical Asia and its probable relationship to the mosquito Aedes aegypti.

Smithburn, K. & Haddow, A. 1944. Semliki Forest virus: I. Isolation and pathogenic properties. *The Journal of Immunology,* 49**,** 141-157.

Song, J.-J., Smith, S. K., Hannon, G. J. & Joshua-Tor, L. 2004. Crystal structure of Argonaute and its implications for RISC slicer activity. *science,* 305**,** 1434-1437.

Soper, F. L. 1967. Aedes aegypti and yellow fever. *Bulletin of the World Health Organization,* 36**,** 521.

Soumahoro, M.-K., Fontenille, D., Turbelin, C., Pelat, C., Boyd, A.*, et al.* 2010. Imported chikungunya virus infection. *Emerging infectious diseases,* 16**,** 162.

Specchia, V., Piacentini, L., Tritto, P., Fanti, L., D'alessandro, R.*, et al.* 2008. Hsp90 prevents phenotypic variation by suppressing the mutagenic activity of transposons. *Nature,* 463**,** 662-665.

Strauss, E. G., Rice, C. M. & Strauss, J. H. 1983. Sequence coding for the alphavirus nonstructural proteins is interrupted by an opal termination codon. *Proceedings of the National Academy of Sciences,* 80**,** 5271-5275.

Strauss, J. H. & Strauss, E. G. 1994. The alphaviruses: gene expression, replication, and evolution. *Microbiol Rev,* 58**,** 491-562.

Takeuchi, O. & Akira, S. 2008. Pattern recognition receptors and inflammation. *Cell,* 140**,** 805-820.

Tamberg, N., Lulla, V., Fragkoudis, R., Lulla, A., Fazakerley, J. K.*, et al.* 2007. Insertion of EGFP into the replicase gene of Semliki Forest virus results in a novel, genetically stable marker virus. *Journal of General Virology,* 88**,** 1225-1230.

Tian, B., Bevilacqua, P. C., Diegelman-Parente, A. & Mathews, M. B. 2011. The double-stranded-RNA-binding motif: interference and much more. *Nature Reviews Molecular Cell Biology,* 12**,** 399-411.

Tolia, N. H. & Joshua-Tor, L. 2007. Slicer and the argonautes. *Nature chemical biology,* 3**,** 36-43.

Tomari, Y., Du, T., Haley, B., Schwarz, D. S., Bennett, R.*, et al.* 2004. RISC assembly defects in the Drosophila RNAi mutant armitage. *Cell,* 116**,** 831-841.

Tomari, Y., Du, T. & Zamore, P. D. 2007. Sorting of Drosophila small silencing RNAs. *Cell,* 130**,** 299-308.

Tran, A., L'ambert, G., Lacour, G., Benoît, R., Demarchi, M.*, et al.* 2013. A rainfall- and temperature-driven abundance model for Aedes albopictus populations. *International journal of environmental research and public health,* 10**,** 1698-1719.

Turelli, M. & Hoffmann, A. A. 1995. Cytoplasmic incompatibility in Drosophila simulans: dynamics and parameter estimates from natural populations. *Genetics,* 140**,** 1319-1338.

Ülper, L., Sarand, I., Rausalu, K. & Merits, A. 2008. Construction, properties, and potential application of infectious plasmids containing Semliki Forest virus full-length cDNA with an inserted intron. *Journal of virological methods,* 148**,** 265-270.

Utarini, A., Indriani, C., Ahmad, R. A., Tantowijoyo, W., Arguni, E.*, et al.* 2021. Efficacy of Wolbachia-infected mosquito deployments for the control of dengue. *New England Journal of Medicine,* 384**,** 2177-2186.

Vanblargan, L. A., Mukherjee, S., Dowd, K. A., Durbin, A. P., Whitehead, S. S.*, et al.* 2013. The type-specific neutralizing antibody response elicited by a dengue vaccine candidate is focused on two amino acids of the envelope protein. *PLoS pathogens,* 9**,** e1003761.

Varjak, M., Donald, C. L., Mottram, T. J., Sreenu, V. B., Merits, A.*, et al.* 2017a. Characterization of the Zika virus induced small RNA response in Aedes aegypti cells. *PLoS Negl Trop Dis,* 11**,** e0006010.

Varjak, M., Gestuveo, R. J., Burchmore, R., Schnettler, E. & Kohl, A. 2020. aBravo Is a Novel Aedes aegypti Antiviral Protein That Interacts with, but Acts Independently of, the Exogenous siRNA Pathway Effector Dicer 2. *Viruses,* 12**,** 748.

Varjak, M., Leggewie, M. & Schnettler, E. 2018. The antiviral piRNA response in mosquitoes? *Journal of General Virology,* 99**,** 1551-1562.

Varjak, M., Maringer, K., Watson, M., Sreenu, V. B., Fredericks, A. C.*, et al.* 2017b. Aedes aegypti Piwi4 is a noncanonical PIWI protein involved in antiviral responses. *MSphere,* 2**,** 10.1128/msphere. 00144-17.

Vasiljeva, L., Merits, A., Golubtsov, A., Sizemskaja, V., Kääriäinen, L.*, et al.* 2003. Regulation of the sequential processing of Semliki Forest virus replicase polyprotein. *Journal of Biological Chemistry,* 278**,** 41636-41645.

Vaux, D. J., Helenius, A. & Mellman, I. 1988. Spike—nucleocapsid interaction in Semliki Forest virus reconstructed using network antibodies. *Nature,* 336**,** 36-42.

Vazeille, M., Moutailler, S., Coudrier, D., Rousseaux, C., Khun, H.*, et al.* 2007. Two Chikungunya isolates from the outbreak of La Reunion (Indian Ocean) exhibit different patterns of infection in the mosquito, Aedes albopictus. *PloS one,* 2**,** e1168.

Vega-Rua, A., Zouache, K., Caro, V., Diancourt, L., Delaunay, P.*, et al.* 2013. High efficiency of temperate Aedes albopictus to transmit chikungunya and dengue viruses in the Southeast of France. *PloS one,* 8**,** e59716.

Voss, J. E., Vaney, M. C., Duquerroy, S., Vonrhein, C., Girard-Blanc, C.*, et al.* 2010. Glycoprotein organization of Chikungunya virus particles revealed by X-ray crystallography. *Nature,* 468**,** 709-12.

Walker, T., Jeffries, C. L., Mansfield, K. L. & Johnson, N. 2014. Mosquito cell lines: history, isolation, availability and application to assess the threat of arboviral transmission in the United Kingdom. *Parasites & vectors,* 7**,** 382.

Wang, S. H. & Elgin, S. C. R. 2011. Drosophila Piwi functions downstream of piRNA production mediating a chromatin-based transposon silencing mechanism in female germ line. *Proceedings of the National Academy of Sciences,* 108**,** 21164-21169.

Wang, X.-H., Aliyari, R., Li, W.-X., Li, H.-W., Kim, K.*, et al.* 2006. RNA interference directs innate immunity against viruses in adult Drosophila. *Science,* 312**,** 452-454.

Watanabe, T., Imai, H. & Minami, N. 2008. Identification and expression analysis of small RNAs during development. *RNAi: Design and Application.* Springer.

Weaver, S. C. & Barrett A. D. 2004. Transmission cycles, host range, evolution and emergence of arboviral disease. *Nature Reviews,* 2, 789-801.

Weaver, S. C., Charlier, C., Vasilakis, N. & Lecuit, M. 2018. Zika, chikungunya, and other emerging vector-borne viral diseases. *Annual review of medicine,* 69**,** 395-408.

Weaver, S. C. & Reisen, W. K. 2010. Present and future arboviral threats. *Antiviral research,* 85**,** 328-345.

Welker, N. C., Habig, J. W. & Bass, B. L. 2011. Genes misregulated in C. elegans deficient in Dicer, RDE-4, or RDE-1 are enriched for innate immunity genes. *RNA,* 17**,** 1090-1102.

Wilson, A. L., Courtenay, O., Kelly-Hope, L. A., Scott, T. W., Takken, W.*, et al.* 2020. The importance of vector control for the control and elimination of vector-borne diseases. *PLoS Negl Trop Dis,* 14**,** e0007831.

Yamaguchi, S., Naganuma, M., Nishizawa, T., Kusakizako, T., Tomari, Y.*, et al.* 2022. Structure of the Dicer-2–R2D2 heterodimer bound to a small RNA duplex. *Nature,* 607**,** 393-398.

Ye, Y. H., Carrasco, A. M., Frentiu, F. D., Chenoweth, S. F., Beebe, N. W.*, et al.* 2015. Wolbachia reduces the transmission potential of dengue-infected Aedes aegypti. *PLoS neglected tropical diseases,* 9**,** e0003894.

Zacks, M. A. & Paessler, S. 2010. Encephalitic alphaviruses. *Veterinary microbiology,* 140**,** 281-286.

Zanotto, P. D., Gould, E. A., Gao, G. F., Harvey, P. H. & Holmes, E. C. 1996. Population dynamics of flaviviruses revealed by molecular phylogenies. *Proceedings of the National Academy of Sciences,* 93**,** 548-553.

Zhang, G., Hussain, M., O'neill, S. L. & Asgari, S. 2013. Wolbachia-regulated microRNAs and host immunity in Aedes aegypti. *PLoS Neglected Tropical Diseases,* 7**,** e2397.

Zhang, H., Kolb, F. A., Jaskiewicz, L., Westhof, E. & Filipowicz, W. 2004. Single processing center models for human Dicer and bacterial RNase III. *Cell,* 118**,** 57-68.

Zhang, X., Li, X., Jiang, T. & Fu, J. 2026. A brief review of chikungunya fever: From molecular virology to countermeasures. *Infect Med (Beijing),* 5**,** 100231.

Zhou, R., Czech, B., Brennecke, J., Sachidanandam, R., Wohlschlegel, J. A.*, et al.* 2009. Processing of Drosophila endo-siRNAs depends on a specific Loquacious isoform. *RNA,* 15**,** 1886-95.

Ziemiecki, A. & Garoff, H. 1978. Subunit composition of the membrane glycoprotein complex of Semliki Forest virus. *Journal of molecular biology,* 122**,** 259-269.

Zimmerman, O., Holmes, A. C., Kafai, N. M., Adams, L. J. & Diamond, M. S. 2023. Entry receptors - the gateway to alphavirus infection. *J Clin Invest,* 133.